

Development of Activity-based Reporter Gene Technology (AbRGT) for Imaging of Protease Activity and its Applications

A thesis

submitted in the partial fulfillment of the requirements
of the degree of

Doctor of Philosophy

By

Punita Bathla

20142003



Indian Institute of Science Education and Research, Pune

May 2021

Dedicated to my parents,

Mr. Anil Bathla and Ms. Sunita Bathla



INDIAN INSTITUTE OF SCIENCE EDUCATION AND RESEARCH,
PUNE,
Dr. Homi Bhabha Road, Pune - 411008

Certificate

This is to certify that the work incorporated in this thesis entitled “**Development of Activity-based Reporter Gene Technology (AbRGT) and its Applications**” submitted by **Ms. Punita Bathla** was carried out by the candidate under my supervision. The work presented here or any part of it has not been included in any other thesis submitted previously for the award of any degree or diploma from any other University and Institution.

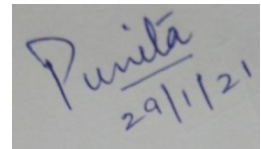
A handwritten signature in blue ink, appearing to read "J. Bathla", is shown within a rectangular frame.

Date: 29-01-21

Dr. Britto S. Sandanaraj
(Supervisor)

Declaration

I declare that this written submission represents my ideas in my own words, and wherever other's ideas have been included, I have adequately cited and referenced the original sources. I also declare that I have adhered to all principles of academic honesty and integrity and have not misrepresented or fabricated, or falsified any idea/data/fact/source in my submission. I understand that violation of the above will cause disciplinary action by the Institute and can also evoke penal action from the sources which have thus not been appropriately cited or from whom proper permission has not been taken when needed.

A rectangular box containing a handwritten signature in blue ink. The signature reads "Punita" above a horizontal line, with "29/1/21" written below the line.

Date: 29-01-21

Ms. Punita Bathla

20142003

Acknowledgments

Foremost, I would like to express my sincere gratitude towards my advisor Dr. Britto S. Sandanaraj, for providing me an opportunity to work in his laboratory as a Ph.D. student. His guidance and feedback throughout my Ph.D. has helped me to work better on my research projects. He gave me the freedom to design and execute the experiments that allowed me to develop my thinking abilities.

I would like to extend my gratitude towards my research advisory committee (RAC) members, Dr. Mayurika Lahiri and Prof. Gopal Kundu, for their time and valuable suggestions they have given in my RAC meetings.

I would like to thank Dr. Abhijit De and Aaiyas Mujawar for helping me out in the cloning and BRET part of my thesis.

I am thankful to all the past and present lab members of Dr. Britto's lab. I would specially like to thank Mohan and Pavan for their help, support, and friendship.

I would specially like to thank Prof. LS. Shasidhara for his kind support of providing us the lab space in the biology department and allowed us to access the common biology instruments. I also thank Prof. Sanjeev Galande for providing us the financial support for the completion of the project at a crucial time. I also express my deepest gratitude to Dr. Thomas Pucadiyl for his support. He has always been a great inspiration for me.

I also like to thank IISER Pune for the great facilities and infrastructure. I thank the Biology department management team (Mrinalini Virkar, Rupali Jadhav, Shabnam Patil, Mahesh Rote, Piyush Gadekar, Kalpesh Thakare) and the Chemistry department management team (Mahesh Jhadav, Ganesh Dimber, Mayuresh Kulkarni, Bhagyashri Kolapkar, Yathish, Megha Paygude). I thank the IISER Pune microscopy facility team (Vijay Vittal, Dr. Santosh Poddar, Rahul, Aditi) for their help. I also thank Rafeeqe from the science media center (SMC), IISER Pune, for helping me out with the illustrations. I thank IISER Pune for funding my fellowship and Infosys India for the travel fellowship.

I would also like to thank my integrated Ph.D. 2014 batchmates for giving me a bundle of memories. I really enjoyed my time at IISER Pune because of such helpful and fun people around me. I specially like to thank Shikha and Nilam for their support and guidance. I would also like to thank Prashant for the help and discussions about my project.

Finally, I would like to thank my family for their constant support, motivation, and encouragement throughout my Ph.D. I would like to thank my mother, Sunita Bathla, for believing in me. Her unconditional love and support helped me always to be strong. I would also to thank my father, Anil Bathla, for always cheering me up. I thank my biggest motivation and inspiration, my sister Srishti Bathla who has always imbibed positivity in me, and my lovely brother, Anand Bathla, for all the fun moments we spent together. It could only become possible with the love and support of the incredible family I have.

Table of contents

Synopsis.....	i
List of abbreviations	iv
Chapter 1: Methods to study protease function	
1.1 Introduction to protease	2
1.2 Traditional proteomics approach.....	3
1.3 Fluorescence imaging methods	6
1.3.1 Substrate-based reporters	6
1.3.1.1 Fluorogenic substrate-based probes.....	7
1.3.1.2 FRET-based probes	9
1.3.1.2.1 Synthetic FRET-based probes.....	9
1.3.1.2.1.1 Fluorochrome as a FRET acceptor	9
1.3.1.2.1.2 Quencher as a FRET acceptor	10
1.3.1.2.1.3 Self-quenching based FRET probes.....	12
1.3.1.2.1.4 Quantum dots as FRET donors.....	13
1.3.1.2.2 Protein-based FRET probes	15
1.3.1.3 BRET-based probes	17
1.3.2 Pros and cons of substrate-based probes	19
1.3.3 Activity-based probes	19
1.3.3.1 Activity-based fluorescent probes (ABFPs)	21
1.3.3.2 Quenched-activity based probes.....	22
1.3.4 Pros and cons of ABPs.....	24
1.3.5 Activity-dependent proximity ligation method.....	24
1.4 Current challenges and aim of the thesis	26
1.5 References	27
Chapter 2: Development of Activity-based Reporter Gene Technology (AbRGT) for imaging of protease activity	
2.1 Introduction	39
2.2 Concept of AbRGT	40
2.3 Choice of the system to demonstrate the AbRGT.....	42

2.4	Choice of the protease of interest (PoI) to demonstrate AbRGT.....	44
2.5	Results and Discussion.....	45
2.5.1	Development of AbRGT using caspase-3 as a PoI	45
2.5.1.1	In vitro labeling of recombinant caspase-3	46
2.5.1.1.1	Expression and purification of recombinant caspase-3.....	46
2.5.1.1.2	Michaelis-Menton kinetic assay and Lineweaver Burk plot	47
2.5.1.1.3	Determination of the kcat of recombinant caspase-3	48
2.5.1.1.4	Labeling of recombinant caspase-3 by Rh-VAD-FMK probe	49
2.5.1.2	FRET standardization.....	50
2.5.1.3	Imaging caspase-3 activation using AbRGT approach	52
2.5.1.4	Validation of the off-target labeling of other protease by the Rh-VAD-FMK-probe	55
2.5.1.5	Acceptor photo-bleaching method to confirm the FRET occurrence.....	56
2.5.1.6	Imaging caspase-3 activation at different time points.....	59
2.5.1.7	Imaging caspase-3 activation using Rh-DEVD-FMK probe	62
2.5.1.8	Imaging caspase-3 activation in HeLa and HEK-293 cells	63
2.5.1.9	Optimization of time window of caspase-3 or -7 activation in HeLa cells	65
2.5.1.10	Confirmation of cleaved caspase-3 by western blotting.....	65
2.6	Conclusion	67
2.7	Materials and methods	68
2.7.1	Reagents	68
2.7.2	Expression and purification of recombinant human caspase-3	68
2.7.3	MALDI- ToF analysis.....	69
2.7.4	Michaelis-Menton kinetics assay	69
2.7.5	Determination of kcat of caspase-3	70
2.7.6	Recombinant caspase-3 labeling by Rh-VAD-FMK probe	70
2.7.7	In-gel fluorescence assay	71
2.7.8	Cell culture methods	71
2.7.9	Plasmids and transient transfection	71
2.7.10	Labeling of active caspases in apoptotic cells by Rh-VAD-FMK probe.....	72
2.7.11	Fluorescence imaging studies and FRET procedure	72
2.7.12	Acceptor photobleaching method.....	73

2.7.13	Live-cell microscopy and image analysis	73
2.7.14	Quantitative analysis	73
2.7.15	STED imaging	74
2.7.16	Immunoblotting	74
2.7.17	Plasmid information	75
2.8	References	76

Chapter 3: Applications of Activity-based Reporter Gene Technology

3.1	Introduction	80
3.2	Results	80
3.2.1	Utilization of AbRGT for inhibitors screening	80
3.2.2	Specific imaging of other caspases by AbRGT.....	83
3.2.2.1	Specific imaging of caspase-7 activation in the apoptosis pathway	83
3.2.2.2	Specific imaging of caspase-9 activation in apoptosis pathway	89
3.2.2.3	Specific activation of caspase-8 activation in apoptosis pathway	93
3.2.3	Direct imaging of cathepsin-B activation in the apoptosis pathway using AbRGT	95
3.2.3.1	Validation of cathepsin B localization in the lysosome	97
3.2.3.2	Cathepsin B activation in the apoptosis pathway.....	98
3.3	Conclusion	102
3.4	Material and Methods	103
3.4.1	Reagents	103
3.4.2	Inhibitor Assay	103
3.4.3	Plasmid information.....	104
3.4.4	Caspase inhibitors structures.....	105
3.5	References	106

Chapter 4: Development of BRET-approach of Activity-based Reporter Gene Technology (AbRGT)

4.1	Introduction	110
4.2	Results	111
4.2.1	The concept of BRET-approach of AbRGT	111
4.2.2	Choice of the BRET donor and acceptor	112
4.2.3	Development of BRET-approach of AbRGT	114

4.2.3.1 Cloning of caspase-3 into RLuc 8.6 vector	114
4.2.3.2 Expression of caspase-3 RLuc 8.6 vector in MCF-7 cells.....	114
4.2.3.3 Quantification of caspase-3 activation using BRET-approach of AbRGT	116
4.2.3.4 Screening protease inhibitors in a high-throughput assay using BRET- approach of AbRGT	117
4.2.3.5. Quantification of caspase-3 activation in Caspase-3 RLuc expressing stable MCF-7 clones	119
4.3 Materials and methods	121
4.3.1 Reagents	122
4.3.2 Cloning	122
4.3.3 Transient transfections	122
4.3.4 Luciferase assay	123
4.3.4 Caspase-3 activity measurement	123
4.3.5 Inhibitors screening in a high-throughput format	123
4.3.6 Stable clone	123
4.3.7 BRET measurements.....	124
4.3.8 Plasmids and primers information.....	125
4.3.9 Inhibitors structure.....	126
4.4 References	127
Chapter 5: Conclusions and future directions	
5.1 Summary of the thesis.....	130
5.1.1 Advantages of AbRGT	132
5.1.2 Limitations of AbRGT	132
5.2 Future directions	133
5.2.1 In vivo imaging of protease function.....	133
5.2.3 Imaging the function of the uncharacterized protease	134
5.3 References	136
5.4 List of publications and patent	137

Synopsis

Fluorescence imaging methods integrated with substrate-based reporter assays (both genetic and synthetic substrate) are routinely used to study the function of “active protease” in the (patho) physiological processes. However, most of the substrate-based reporters lack target specificity in the in vivo conditions. Recently, the activity-based fluorescent probe (ABFP) method is used for monitoring protease function in vivo. This method provides an opportunity to back-track the signal produced by the target enzyme and other proteases. However, this is achieved through post-processing of cell or tissue lysate followed by in-gel fluorescence studies. ABFP method is labor-intensive and cannot be translated to high-throughput imaging studies. To address the drawbacks of existing techniques, herein, we disclose the design and development of a new technology called “Activity-based Reporter Gene Technology” (AbRGT). It uses a reporter protein-tagged protease of interest (PoI) and an activity-based fluorescent probe (ABFP). The specific activation of PoI is determined by measuring the fluorescence resonance energy transfer (FRET) signal that occurs only upon labeling of ABFP to the reporter protein-tagged PoI. In this manner, the method allows the imaging of an active protease with an exquisite specificity in the presence of highly homogenous proteins within a cell. As a proof-of-concept, we have applied this method to study the function of individual caspase protease in both intrinsic and extrinsic apoptosis signaling pathways. We demonstrate that the same method can be used for profiling of compounds that can inhibit caspases activity. We have also shown the design and potential use of the BRET approach of AbRGT in the high-throughput screening of protease inhibitors. Altogether, this method holds huge potential for applications in the area of diagnostics, screening of drugs, and other discovery efforts.

Chapter-1 of my thesis focuses on introducing protease, protease regulation, and the methodologies used to study protease function. Proteases play a fundamental role in patho (physiological) processes. The activation of protease from its zymogen state is tightly regulated at multiple levels. The conventional proteomics approach provides information on the global expression of the protease. The expression profile of the protease does not always correlate with its functional state as most of the proteases are post-translationally modified or bound by endogenous inhibitors. Recently, fluorescent imaging methods such

as substrate-based reporter and ABFP technologies have been developed to study protease function. However, both these methods lack target specificity in the native cellular environment. To address these limitations, we have developed a novel approach called Activity-based Reporter Gene Technology (AbRGT)

Chapter-2 of my thesis discusses the design and development of AbRGT. This method image specific protease activation with unprecedented specificity. We demonstrated AbRGT by imaging the specific activation of caspase-3 in the apoptosis signaling pathway. The method integrates two labeling motifs; a reporter protein tagged to the protease of interest and an activity-based fluorescent probe (ABFP) that targets the active site of a protease. FRET between the reporter protein (donor) and the fluorophore (acceptor) of ABFP occurs upon the labeling of ABFP to the GFP-tagged PoI. The nonspecific labeling of the probe creates a highly specific FRET pair that reports only the target protease activity but not the other proteases in the cell.

In **Chapter-3**, we have validated our method by demonstrating its applicability by specifically imaging the function of five different target proteases (caspase-3, -7, -8, and -9 and cathepsin-B), independently in three different cell lines (HeLa, HEK-293, and MCF-7). We have shown the potential of the method for the screening of protease inhibitors. As another potential application, we have demonstrated the method can be used for validating the activation of a protease in a signaling pathway by studying the direct activation of cathepsin B in the apoptosis pathway.

FRET approach of AbRGT is a method of choice for performing the single-cell assays. It is not suitable for performing population-based assays due to the autofluorescence from cells. In addition, the FRET approach requires direct excitation of the fluorophore resulting in photobleaching. To overcome these limitations, we have demonstrated the development of the bioluminescence resonance energy transfer (BRET)-approach of AbRGT in **Chapter-4**. The BRET approach of AbRGT combines the use of luciferase to the protease of interest (PoI) and an ABFP targeting PoI and other protease resulting in the generation of *in situ* BRET pair. We have also shown the potential of the BRET-approach of AbRGT for high-throughput screening of caspase-3 inhibitors.

Chapter-5 discusses the summary and future directions of the thesis. In the future, the method can be used for the *in vivo* imaging of protease function by using the BRET-approach of AbRGT. Alternatively, the FRET approach of AbRGT can also be used for *in vivo* imaging by choosing RFP (donor) and a near-infrared fluorophore (NIRF, acceptor). The method can also be applied for imaging the function of uncharacterized protease. We have identified, HtrA2, a serine protease, as an interesting target protease to study its function in the apoptosis pathway as it is known to induce apoptosis via both caspase-dependent and independent pathway and is also not widely explored.

List of abbreviations

A

AbRGT	Activity-based reporter gene technology
ABFPs	Activity-based fluorescent probes
ABPs	Activity-based probes
ADPL	Activity-dependent proximity ligation
Apaf1	Apoptotic protease activating factor 1
AOMK	Acyloxymethyl-ketone

B

BFP	Blue fluorescent protein
BHQ-3	Black-hole quencher-3
BODIPY	Borondipyrromethane
BRET	Bioluminescence resonance energy transfer
BSA	Bovine serum albumin

C

CARD	Caspase activation and recruitment domains
CBG	Click beetle green
CDCF	6-carboxy-2', 7'-dichlorofluorescein hydrazine
CFP	Cyan fluorescent protein
CTCF	Corrected total cell fluorescence
CTMR	5-carboxytetramethylrhodamine

D

DAHC	1, 2 - diamino cyclohexane
dATP	Deoxyadenosine triphosphate
DEDs	Death effector domains
DHAP	Dihydroxyacetone phosphate
DISC	Death-inducing signaling complex
DMEM	Dulbecco's modified eagle's medium
DMSO	Dimethyl sulfoxide
DTT	Dithiothreitol

E

EBFP	Enhanced blue fluorescent protein
EDTA	Ethylenediamine tetraacetic acid

EGFP Enhanced green fluorescent protein
ESI Electrospray ionization

F

FACS Fluorescence-activated cell sorting
FBS Fetal bovine serum
FP Forward primer
FRET Fluorescence resonance energy transfer

G

GPCR G-protein coupled receptor
GFP Green fluorescent protein

H

HRP Horseradish peroxidase
HTS High-throughput studies
HtrA2 High temperature requirement A2

I

pI Isoelectric point
IEX Ion-exchange chromatography
IAPs Inhibitor of apoptotic proteins

L

LSCD Large subunit catalytic domain
LD Linker domain
LB Luria-Bertani
LP-1 Legumain probe-1

M

MOMP Mitochondrial outer membrane permeabilization
mBRET Milli-BRET
MS Mass spectrometry
(m/z) Mass-to-charge
MALDI Matrix-assisted laser desorption ionization
MMP-13 Matrix metalloproteinase-13

MPEG	Methoxypolyethylene glycol
N	
NCEH1	Neutral cholesterol ester hydrolase-1
NIR	Near-infrared
NIRF	Near-infrared fluorescence
NMR	Nuclear magnetic resonance
O	
OA	Osteoarthritis
P	
PBS	Phosphate buffer saline
PCR	Polymerase chain reaction
PIPES	Piperazine-N,N'-bis (2-ethanesulfonic acid)
PL	Poly-L-lysine
PMK	Phenoxymethyl ketone
PoI	Protease-of-interest
PTMs	Post-translational modifications
PVDF	Polyvinylidene difluoride
Q	
qABPs	Quenched-activity based probes
QDs	Quantum dots
R	
RCA	Rolling circle amplification
RER	Rough endoplasmic reticulum
Rh-FP	Rhodamine-fluorophosphate
RFP	Red fluorescent protein
ROI	Region of interest
RP	Reverse primer
Rh-VAD-FMK	Rhodamine-VAD-fluoromethyl ketone

S

SDS-PAGE	Sodium dodecyl sulfate-polyacrylamide gel electrophoresis
SEC	Size exclusion chromatography
SELDI	Surface-enhanced laser desorption/ionization
SGDD	Structure-guided drug design
SP	Signal sequence
SSCD	Small subunit catalytic domain
STED	Stimulated emission depletion
STS	Staurosporine

T

3D	Three dimensional
2D-PAGE	Two dimensional-polyacrylamide gel electrophoresis
TFA	Trifluoroacetic acid
TMR	Tetramethyl rhodamine
TOPO	Trioctylphosphine oxide
TRAIL	TNF-related tumor-inducing ligand

U

UV	Ultraviolet
----	-------------

Y

YFP	Yellow fluorescent protein
-----	----------------------------

Chapter 1

Methods to study protease function

1.1 Introduction to protease

Proteases are the enzymes that catalyze the hydrolysis of the amide bond between two amino acids in a polypeptide chain of a protein. Proteases constitute the largest class of enzymes, representing nearly 2% of the human genome.^{1,2} Based on the catalytic mechanism, proteases are classified into five different protease families, *i.e.*, aspartyl, cysteine, metallo-, serine, and threonine proteases.¹ Protease function is central in various physiological processes, including development³, tissue remodeling⁴, programmed cell death^{5,6}, immune response⁷, etc., and it also plays a crucial role in pathological conditions such as cancer^{8,9} and allergic diseases¹⁰, etc. Proteases serve as a biomarker in diseases such as cardiovascular diseases.¹¹ This close association between protease and diseases makes it a great target in the area of drug discovery, diagnosis, and therapeutics, etc.¹²

Proteases are translated as inactive enzymes such as zymogens that undergo post-translational modifications (PTMs) to become active proteases. The proteolytic cleavage of the inhibitory prodomain from the zymogen form is required for the activation of protease. Proteolytic cleavage in the activation process is an irreversible event, leading to the tight regulation of protease activity in the cellular system. The activity of protease is limited by the interaction with endogenous protease inhibitors and by degradation by the proteasomal compartment via the ubiquitination pathway (Figure 1.1).¹³ Due to this multilevel regulation, protease abundance may not always correlate to its activity levels. Essentially, it is the protease activity rather than its abundance that plays a significant function in biological processes.¹⁴ Emergence of the field of proteomics led to the study of protease structure and function. Since then, several technologies, including conventional proteomics approach and optical imaging methods, have been developed to detect protease function.

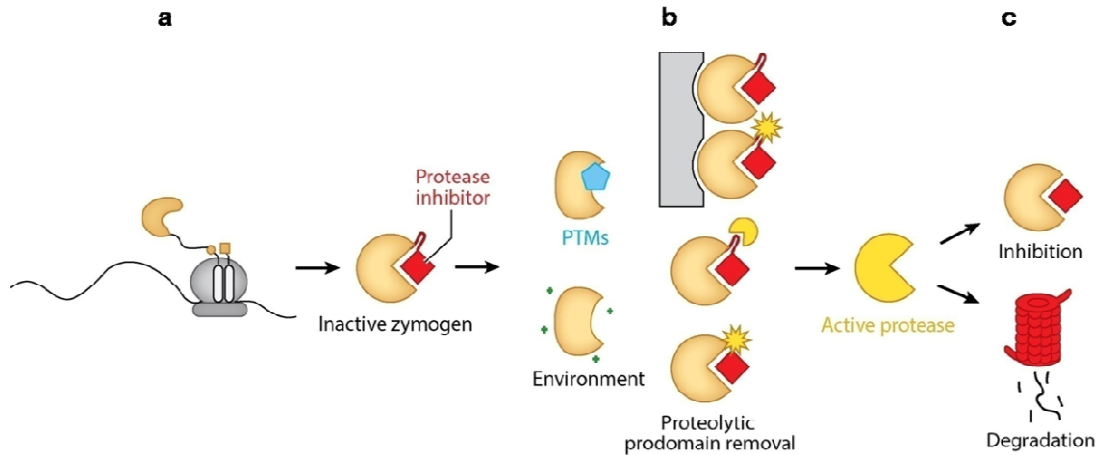


Figure 1.1 Schematic representation of the regulation of protease activity. (a) Proteases are synthesized as an inactive zymogen by ribosomes. (b) Proteases are activated via several different mechanisms such as post-translational modifications (PTMs) or other environmental factors like pH change, cofactor binding, etc., and also by the proteolytic cleavage of prodomain. Prodomain cleavage can occur by the action of another individual protease or the same protease (autocatalysis). (c) Protease activity is further restricted by the binding of an endogenous protease inhibitor or by proteasomal degradation. Adapted with permission from reference (15). Copyright © 2014, Annual Reviews.

1.2 Traditional proteomics approach

The conventional proteomics methodologies take into account the overall expression level of a protease in a cell, tissue, or organism level.¹⁴ This proteomics approach recognizes the presence of a particular protease, *i.e.*, protease-of-interest (PoI) and its relative quantity at a given time.^{16,17}

Traditionally, the study of protease has been a “top-down” approach, *i.e.*, the PoI is expressed in a suitable host, extracted, purified, biochemically and structurally characterized to decipher its possible role in the living system. The advent of gel-based approaches as a principle separation technique is considered as a significant boon in the area of proteomics. Examples of gel-based methods such as sodium dodecyl sulfate-polyacrylamide gel electrophoresis (SDS-PAGE) facilitates resolving different protease from a mixture based on its molecular size. It also gives information on the estimated molecular size of a PoI.¹⁸ A step forward to SDS-PAGE is the invention of two dimensional-polyacrylamide gel electrophoresis (2D-PAGE) that can resolve different

proteins in two dimensions. In the first dimension, proteins are separated based on its isoelectric point (pI), whereas, in the second dimension, proteins are resolved depending on its molecular weight. This gel-based approach has proved to be very useful as a qualitative tool as it has been applied to evaluate the PTMs of a protein, mutant protein analysis, etc.¹⁹

To obtain a pure protein fraction, various chromatographic methods such as ion-exchange chromatography (IEC), size exclusion chromatography (SEC), and affinity chromatography, etc., have been developed as classical protein purification techniques. IEC separates the protein based on the net positive or negative charge carried by a protein at its physiological pH, while SEC resolves the proteins based on the difference in their sizes.^{20,21} However, affinity chromatography takes advantage of the differential non-covalent interaction strength between biomolecules. It uses the specific interactions that exist in the biomolecules, such as antigen-antibody interactions.²² In addition to its applications in isolating specific biomolecules, it also serves several applications in the area of drug discovery.²³

Thereafter, to study the structure of a protein, techniques like X-ray crystallography have been widely used. X-ray crystallography is a breakthrough technique that elucidates the three dimensional (3D) structural details of a protein crystal at an atomic resolution of 0.83 Å.²⁴ This technique has helped in identifying molecular interactions between different molecules, such as discovering inhibitors for protease utilizing a structure-guided drug design (SGDD) approach.²⁵

Subsequently, for the characterization of multiple different proteins at a time, techniques like mass spectrometry (MS) has been developed. MS is a high-throughput, analytical technique that determines the molecular weight of a purified protein or mixture of different proteins. Protein samples are transformed into charged species by an ionization source, and the mass analyzer then measures the mass-to-charge (m/z) ratio of the charged proteins. Depending on the ionization source, different MS techniques like matrix-assisted laser desorption ionization (MALDI), surface-enhanced laser desorption/ionization (SELDI), and electrospray ionization (ESI), etc.^{26,27} have been developed (Figure 1.2). MS serves vast

biochemical applications in drug discovery, e.g., identification of the protein biomarkers associated with pathological conditions²⁸, etc.

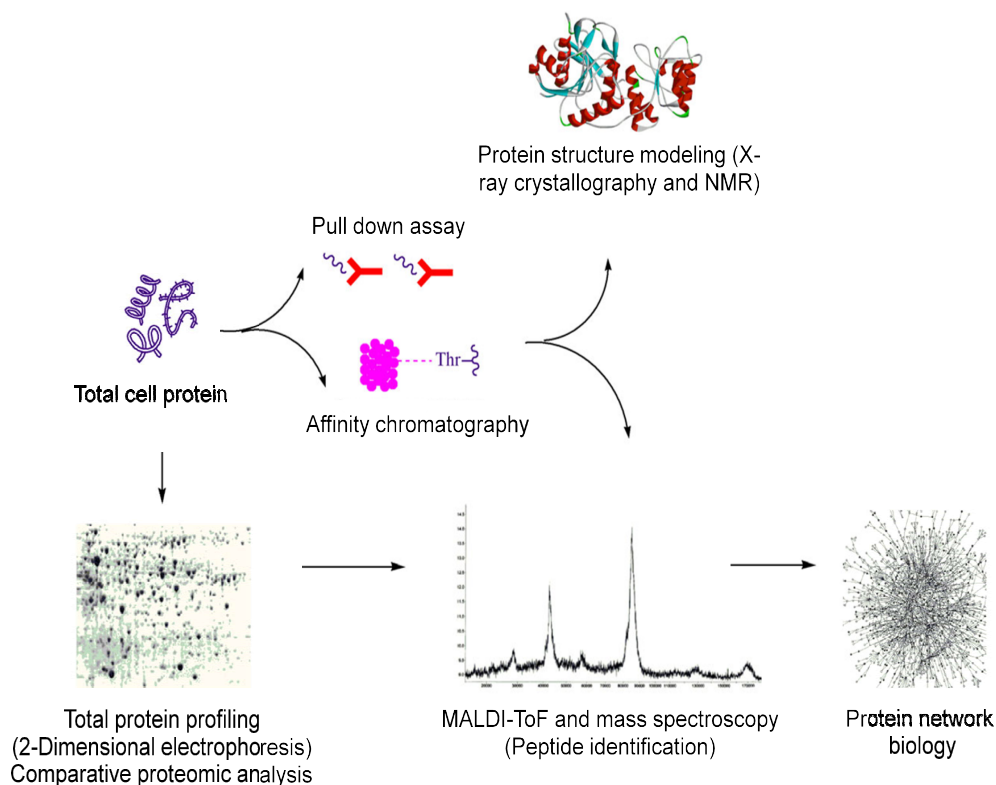


Figure 1.2 Schematic representation for detecting protein function by conventional proteomics methodologies. It involves protein extraction, purification, and structural studies. The total protein is extracted from the cells or tissue sample via sonication or treatment with detergents. The protein of interest can be isolated by utilizing various chromatographic techniques depending on the biochemical nature of polypeptides. For the structural and functional characterization of protein, various methods like X-ray crystallography, NMR, and MALDI-TOF are extensively used. The MALDI-ToF is also used in high-throughput studies, including total proteome analysis that enables the study of protein network biology. Adapted with permission from reference (29). Copyright © 2017, Oxford University Press.

The standard proteomics methods proved useful in providing information on protease presence, abundance, PTMs, protein-protein interaction, etc. However, these methods are also not very selective and are often biased towards the protease present in high abundance.³⁰ These methods also involve the homogenization of cell/tissue resulting in the loss of the spatial information of the protease and hence, unable to detect protease function in its native cellular environment. The protease function is highly influenced by its

microenvironment, spatial localization, and dynamic interactions with other biomolecules; the conventional proteomics approach does not offer details about the “functional state” of a protease.³¹ The fluorescence imaging probes addresses some of the limitations posed by the traditional proteomics approach by deciphering the “functional state,” *i.e.*, the active state of protease rather than just abundance.

1.3 Fluorescence imaging methods

Optical imaging methods is a robust approach to non-invasively study the biochemical processes in the living system. The fluorescence imaging uses fluorophores that are excited by laser diodes at a wavelength specific to the fluorophore. The emitted light from the fluorophore is further detected by the detector. Since it is a non-invasive approach, it is safe and straightforward to use.³² It also offers the advantage of imaging the function of a protease in real-time in the living system. The methods are broadly classified into substrate-based reporter assays and activity-based fluorescent probes (ABFP).

1.3.1 Substrate-based reporters

Substrate-based reporters are the small molecules probes that dissect the function of the protease family in an *in vitro* and an *in vivo* system. It constitutes of two primary chemical moieties (i) a peptide substrate and (ii) a reporter molecule. (i) The peptide substrate is the recognition and cleavage sequence of the protease. It also drives the selectivity towards the target protease family. (ii) The reporter molecule, such as a fluorophore for visualization and detection. Substrate-based reporters consist of a peptide substrate coupled to the reporter molecule resulting in the quenching of the fluorescence of the fluorophore. The cleavage in the peptide recognition sequence by an active protease leads to the changes in the spectral properties of the fluorophore. The alteration in the fluorophore's spectral properties is measured, which acts as a direct readout of the protease activity (Figure 1.3).^{33,34}

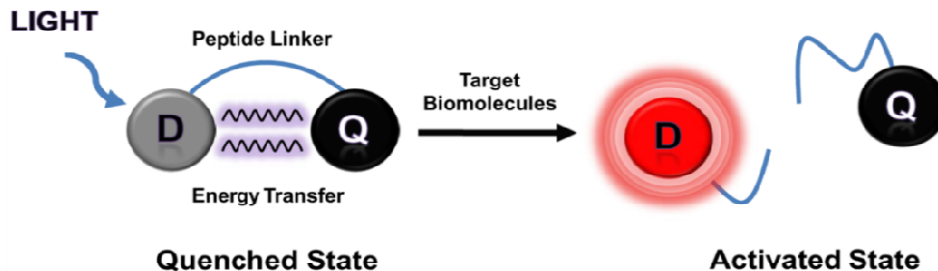


Figure 1.3 Schematic representation of a typical substrate-based probe. A substrate-based probe composed of a recognition element called peptide linker bound to a fluorophore and a quencher at opposite ends. The donor molecule is excited, which transfers the energy to the quencher via fluorescence resonance energy transfer (FRET), bioluminescence resonance energy transfer (BRET), or nanosurface energy transfer (NSET) phenomenon. The cleavage of the peptide linker by the target molecule (protease) results in the loss of energy transfer, indicative of protease activity. D: Fluorophore, Q: Quencher. Adapted with permission from reference (35). Copyright © 2012, World Scientific.

1.3.1.1 Fluorogenic substrate-based probes

Fluorogenic substrate-based probes are the prototype of the substrate-based probes. The probe is designed by coupling a fluorophore to the peptide substrate resulting in quenching of the fluorescence signal of the fluorophore. Cleavage by the protease releases the free fluorophore that restores the original fluorescence signal of the fluorophore. Gurtu *et al.* designed fluorogenic substrates Ac-DEVD-AFC/*p*NA for the detection of caspase activity in 32D cell lysate. The probe utilizes the DEVD tetrapeptide as the recognition sequence for caspases.³⁶ Active caspases cleave the DEVD peptide sequence after the second aspartate. The DEVD peptide is labeled to a fluorophore, 7-amino-4-trifluoromethyl coumarin (AFC), or a chromophore, *p*-nitroanilide (*p*NA). The presence of active caspase in the apoptotic 32D cells is determined by the release of free AFC or *p*NA molecule upon the cleavage of the DEVD-AFC/*p*NA substrate by active caspases (Figure 1.4). Using this assay, they found that the DEVD-dependent protease activity is co-related to the apoptotic events of the cells.³⁷

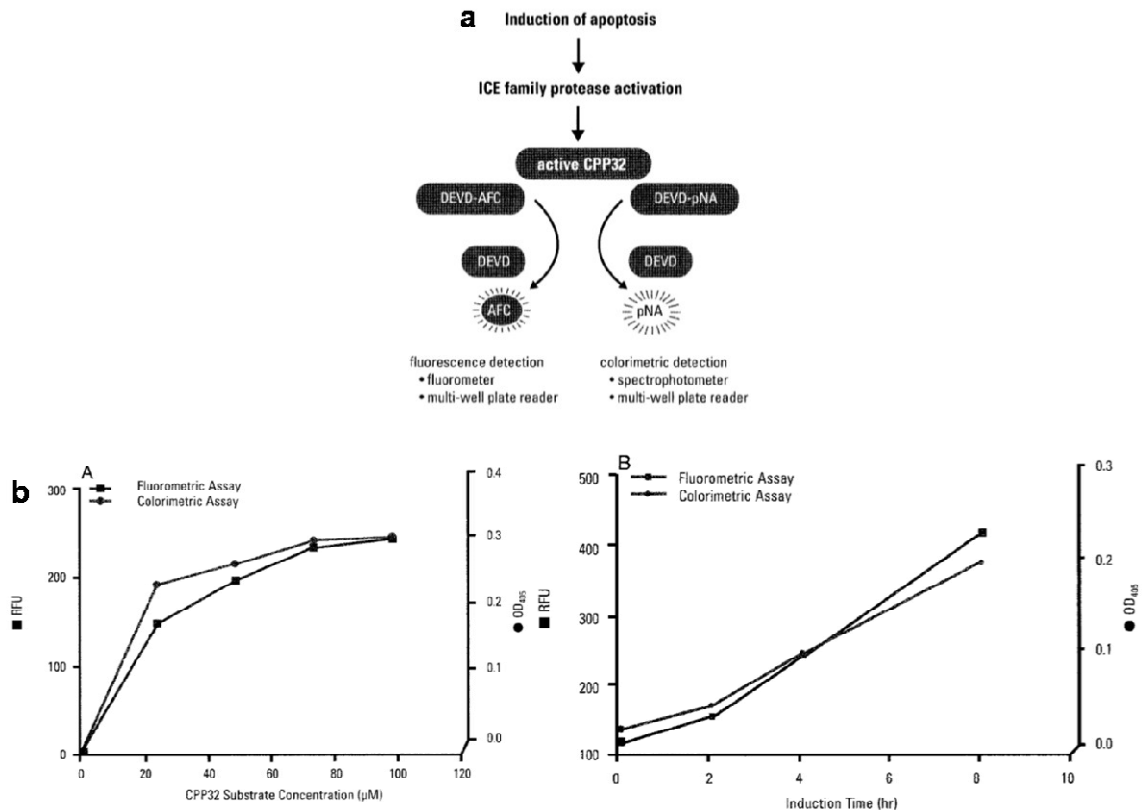


Figure 1.4 Schematic representation of the fluorogenic substrate-based probe used for detecting caspase activity in the apoptosis pathway. (a) Detection of DEVD-dependent protease activity utilizing fluorometric and colorimetric assays. The release of AFC from DEVD-AFC after cleavage by the caspase results in the shift of the AFC fluorescence emission to 508 nm that is detected using a fluorometric assay. Similarly, the release of pNA from the DEVD-pNA is detected using a colorimetric assay. (b) Right, 32D cells were induced to undergo apoptosis by treatment with etoposide, an apoptosis-inducing drug (100 μM) for 8 h. The cells are lysed, and DEVD-dependent proteolytic activity was analyzed at varying substrate concentrations of DEVD-AFC and DEVD-pNA, respectively. Left, 32D cells were induced to undergo apoptosis by treatment with etoposide (100 μM) at varying time-points as indicated. DEVD-dependent proteolytic activity was detected using the ApoAlert CPP32 assay kit according to the manufacturer's instructions. Substrates DEVD-AFC and DEVD-pNA (50 μM) were added to the lysed cells. RFU, relative fluorescence unit. Adapted with permission from reference (37). Copyright © 1997 Academic Press.

One of the significant advantages of these probes is that it requires minimal modifications to the natural peptide recognition sequence of the protease.³⁸ However, these probes are generally utilized for *in vitro* studies. Another major caveat of using fluorophores like AFC for cell imaging is that the absorption maxima of AFC is ~375 nm, *i.e.*, excites in the ultraviolet (UV) region, and hence contributes to the high background due to auto-fluorescence of the cells with UV light.³⁹ Also, these probes are intensity-based fluorescent

probes that can add to artifacts caused by probe concentration, and hence limiting the sensitivity. In order to enhance the sensitivity of these probes, another class of ratiometric substrate-based probes such as FRET-based probes has been developed.

1.3.1.2 FRET-based probes

FRET-based probes work on the fluorescence resonance energy transfer (FRET) phenomenon. It constitutes of a donor and an acceptor molecule attached to either end of the peptide recognition sequence cleavable by the protease. The distance between the donor and acceptor molecule can be regulated by adjusting the peptide linker length and is kept less than 10 nm for the efficient FRET process. FRET pair, *i.e.*, donor and the acceptor molecule, is chosen such that the emission spectra of the donor overlap the excitation spectra of the acceptor. The donor molecule non-radiatively transfers the energy to the acceptor molecule upon excitation.^{40,41} However, cleavage in the peptide linker sequence by the active protease leads to the spatial separation of the donor and the acceptor molecule eliminating the FRET effect. The loss of FRET causes an increase in the donor molecule intensity and a simultaneous decrease in the acceptor molecule intensity. The changes in the spectral properties of the FRET pair can be measured and co-related with the protease activity. Since the FRET-based probes are based on the ratiometric measurements of emission intensities at two different wavelengths, donor and acceptor, it significantly enhances the signal/noise ratio. These probes are also more sensitive as compared to the intensity-based fluorogenic substrate-based probes. FRET-based probes are further classified as synthetic FRET-based probes and protein-based FRET probes.

1.3.1.2.1 Synthetic FRET-based probes

1.3.1.2.1.1 Fluorochrome as a FRET acceptor: Nagano *et al.* developed a synthetic FRET-based probe for measuring caspase-3 activity in apoptotic HeLa-S3 cells. They chose 6-carboxy-2', 7'-dichlorofluorescein hydrazine (CDCF) as a donor fluorochrome, and 5-carboxytetramethylrhodamine (CTMR) as an acceptor fluorochrome. CDCF and CTMR are conjugated via the peptide sequence, GDEVDGVD. CDCF and CTMR exhibit the FRET phenomenon in the intact probe. To detect the caspases-3 activity in the apoptosis pathway, cells are treated with etoposide (apoptosis inducer). The active caspase-3 cleaves the

peptide linker and eliminates the FRET effect. FRET loss causes an increase in the fluorescence signal of the donor CDCF after etoposide treatment, indicative of the caspase-3 activity in apoptotic HeLa-S3 cells (Figure 1.5).⁴²

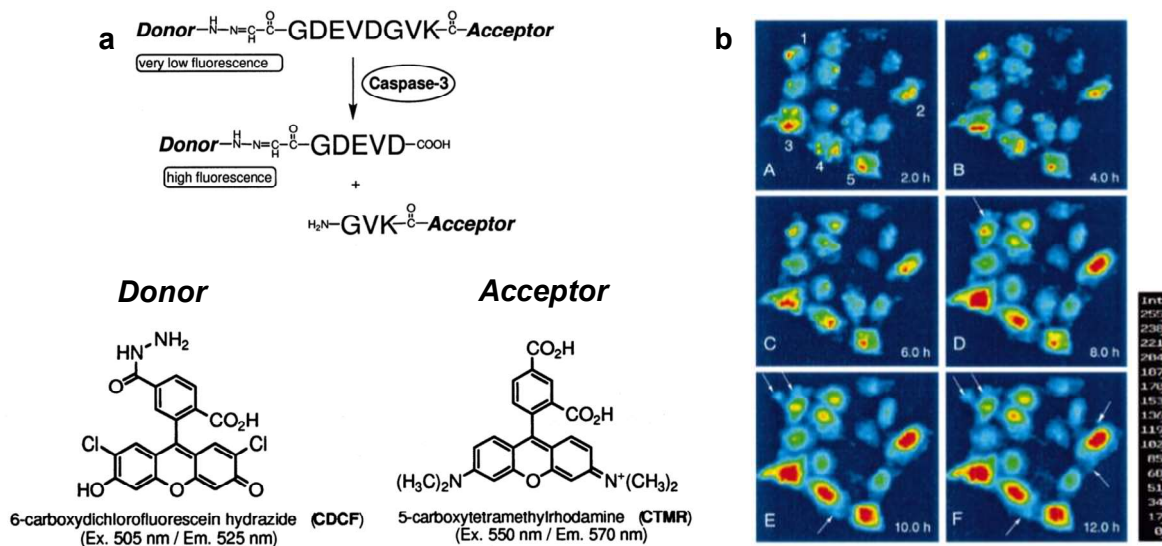


Figure 1.5 Schematic representation of synthetic FRET-based probe and its utility in detecting apoptosis. (a) Top, design of the synthetic fluorometric probe for measuring caspase-3 activation. Probe constituting of a donor and an acceptor linked via GDEVDGVK peptide. The acceptor molecule diffuses away from the donor molecule upon cleavage by the caspase-3, resulting in FRET loss, indicative of caspase-3 activity. Bottom, the chemical structure of donor molecule CTMR and the acceptor molecule CDCF. (b) HeLa-S3 cells are microinjected with the CDCF-GDEVDGVK-CTMR probe. After 12 h, cells are treated with 10 Wg/ml etoposide. Fluorescence microscopy images are taken A: 2 h, B: 4 h, C: 6 h, D: 8 h, E: 10 h, and F: 12 h of etoposide treatment. Arrows indicate the cell membrane blebs. Numbering from 1-5 is designated for five cells, as shown in A. The fluorescence signal strength is indicated in the color spectrum scale, where the color blue and red represents the lowest and the highest signal strength respectively. Adapted with permission from reference (42). Copyright © 1999 Federation of European Biochemical Societies.

1.3.1.2.1.2 Quencher as a FRET acceptor: A quencher molecule absorbs light emitted from the donor fluorochrome and re-emits the energy in the form of visible light (fluorescence quencher) or as heat (dark quenchers). The use of a quencher molecule in the FRET pair as an acceptor molecule enhances the sensitivity of the probe as a quencher molecule absorbs light from the donor molecule more efficiently than the acceptor fluorochrome. Also, the quencher molecule in the FRET pair reduces the background fluorescence caused by the direct excitation of acceptor fluorochrome.⁴³ Kuiwon Choi and

co-workers demonstrated the application of a fluorochrome-quencher FRET-based probe in detecting matrix metalloproteinase-13 (MMP-13) activity in osteoarthritis (OA) induced rat models. MMPs are known to be an accessible biomarker to study OA. Low expression levels of MMP-13 is observed in normal cartilages while it is shown to be upregulated in OA.⁴⁴ To image MMP-13 activity, a fluorochrome-quencher FRET-based probe is designed. The probe uses (i) a near-infrared (NIR) dye, *i.e.*, Cy5.5 (blue circle), that emits light above 650 nm. These NIR dyes are widely used *in vivo* studies as it is least scattered or absorbed by the tissue due to its long wavelength and hence minimizes the auto-fluorescence. (ii) A NIR dark quencher, black-hole quencher-3 (BHQ-3, black circle) which makes a suitable FRET pair with Cy5.5 dye and (iii) an MMP-13 cleavable peptide, GPLGMRGLGK. The intact probe is non-fluorescent due to the quenching of Cy5.5 fluorescence by BHQ-3 quencher; however, the cleavage by MMP-13 restores the fluorescence of Cy5.5 fluorescence. The fluorescence readout is a direct measurement of MMP-13 activity. Using this probe, they detected the early and late stages of OA by imaging MMP-13 activity (Figure 1.6).⁴⁵

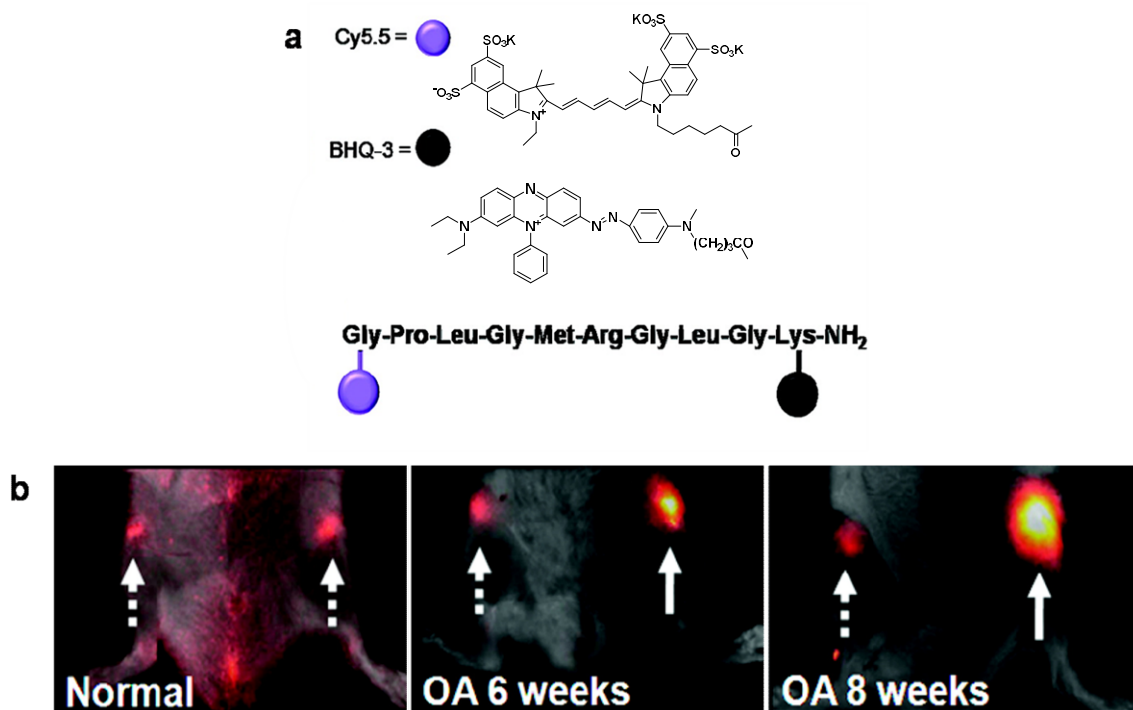


Figure 1.6 Schematic representation of a fluorochrome-quencher FRET-based probe and its

applications *in vivo* imaging of MMP-13 activity in OA-induced rat model. (a) Design of the MMP-13 probe that utilizes near-infrared (NIR) dye, Cy5.5 (blue circle), and NIR dark quencher BHQ-3 (black circle) separated by the MMP-13 peptide substrate. The MMP-13 probe is non-fluorescent due to fluorescence quenching of Cy5.5 by BHQ-3 as a result of the close proximity of Cy5.5 and BHQ-3. Cleavage by the MMP-13 between Gly and Leu in the peptide substrate restores the fluorescence of Cy5.5. (b) *In vivo* imaging of the MMP-13 activity in osteoarthritis (OA) induced rat model of six weeks and eight weeks, intermediate and late-stage OA, respectively. OA induced cartilages generated a strong NIR signal as compared to the normal cartilages indicative of MMP-13 activity. Adapted with permission from reference (45). Copyright © 2008, American Chemical Society.

1.3.1.2.1.3 Self-quenching based FRET probes: Self-quenching or homo-FRET refers to a phenomenon that occurs between two identical fluorophores in close proximity and suppresses the fluorescence of each other by cross-relaxation. Self-quenching FRET-based probes are designed by attaching the identical fluorophores to the opposite ends of the peptide substrate that exhibit self-quenching FRET mechanism. Cleavage by the protease at the peptide linker restores the fluorescence of each fluorochrome molecule.^{46,47} Weissleder *et al.* developed a FRET-based probe based on a self-quenching mechanism to detect the activity of cathepsin-like protease in a mouse tumor model. They have used synthetic graft copolymer incorporating poly-L-lysine (PL) that is used as a backbone, methoxy polyethylene glycol (MPEG) as a delivery vehicle, and Cy5.5 dye as a fluorochrome. The resulting probe, *i.e.* (Cy5.5)₁₁-PL-(MPEG)₉₂, abbreviated as (C-PGC), uses 92 MPEG molecules and 11 Cy5.5 molecules for each PL backbone. The PL backbone contains 44 unmodified lysines for the protease that uses lysine-lysine specificity as its cleavage site (Figure 1.7). The probe treated with trypsin showed a 12 fold increase in NIR fluorescence intensity versus untreated ones. *In vivo* studies showed an intense NIRF signal in tumor implanted nude mice, indicating the cleavage of the probe by cathepsin-like proteases. They successfully imaged tumors in mouse xenograft by developing a self-quenched near-infrared fluorescence (NIRF) probe.⁴⁸

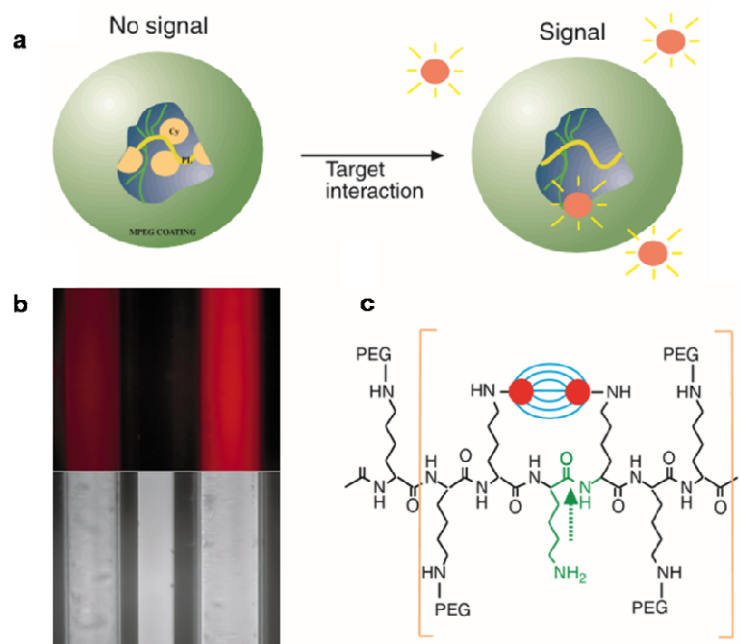


Figure 1.7 Schematic representation of a self-quenching near-infrared fluorescent (NIRF) probe. (a) The identical fluorochromes in close proximity diminish the fluorescence signal of each fluorochrome by a self-quenching phenomenon. The interaction by the target proteases releases the fluorochromes and restores the original fluorescence. The amount of fluorescence generated is a direct measure of the target protease's activity. (b) A (Cy5.5)₁₁-PL-MPEG92 (abbreviated as C-PGC) probe containing capillary phantom untreated or treated with trypsin. Fluorescence intensity difference of 12 fold was observed in trypsin inactivated versus activated probe. (c) Chemical structure of the repeating unit of the C-PGC graft copolymer showing self-quenching by Cy5.5 fluorescent dye and the cleavage site for trypsin (green arrow). Adapted with permission from reference (48). Copyright © 1999, Springer Nature.

1.3.1.2.1.4 Quantum dots as FRET donors: Quantum dots (QDs) are nanometer-sized semiconductor nanocrystals. Upon excitation, QDs emit in the wide range of fluorescence emission spectrum, depending on its size. The QD-FRET based protease sensors are designed such that the peptide substrate labeled fluorescent dye binds to QDs, resulting in the quenching of the fluorescence of QDs. Cleavage of the peptide substrate by protease restores the fluorescence of the QDs.⁴⁹⁻⁵¹ The article by Lifang Shi *et al.* has demonstrated the synthesis and development of QD FRET-based protease sensors for measuring the MMPs, *i.e.*, collagenase activity in the breast cancer cells. They utilized CdSe/ZnS quantum dots with trioctylphosphine oxide (TOPO) ligands. TOPO ligands are replaced by tetrapeptide RGDC labeled to rhodamine dye. Here, Cd/Se ZnS acts as a FRET donor,

rhodamine as the FRET acceptor, and RGDC peptide as collagenase substrate. Cleavage of the RGDC peptide by collagenase results in FRET loss, indicative of collagenase activity. Based on the FRET readout, they measured the MMP activity and differentiated normal versus cancerous tissue (Figure 1.8).⁵² Owing to its unique characteristics, such as high photostability, brightness, tight emission spectra, high molar absorption coefficient, longer lifetime, QDs have been extensively used as fluorescent probes in bioimaging.^{53,54} Since QDs are made of heavy metal ions such as Cd^{2+} and Hg^{2+} , toxicity is one of the major concerns while using QDs based probes *in vivo* systems.⁵⁵

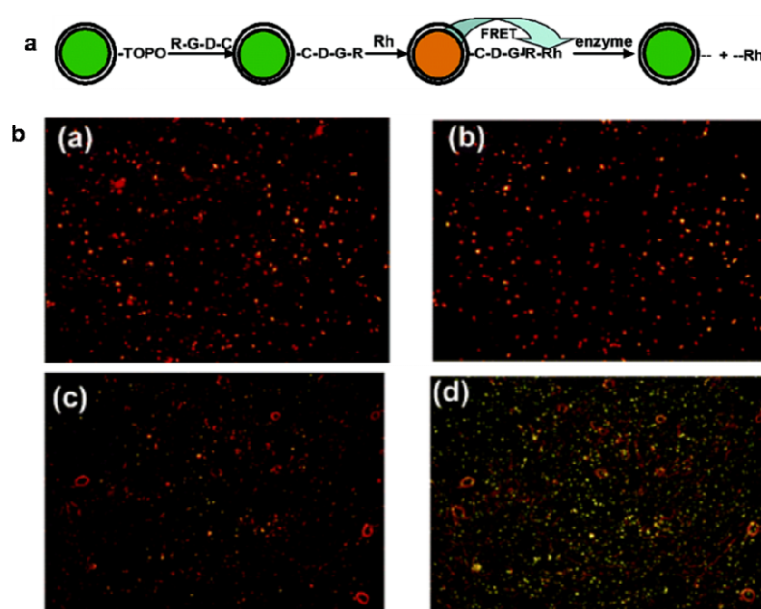


Figure 1.8 Schematic representation of quantum dots (QD)-fluorochrome FRET-based probes for imaging of collagenase activity in normal versus cancerous cells. (a) The probe is composed of CdSe/ZnS quantum dots with trioctylphosphine oxide (TOPO) ligands. Tetrapeptide RGDC conjugated to rhodamine dye replaces TOPO ligands leads to the formation of rhodamine-labeled peptide-coated CdSe/ZnS quantum dots. Cleavage by the collagenase at the peptide substrate RGDC restores QD fluorescence, indicative of collagenase activity. (b) Fluorescence microscopy images of rhodamine-labeled peptide-coated quantum dots incubated in HTB 126 cell line (breast cancer cells) for [top panel (a)] 0 min, [top panel (b)] 15 mins and in HTB 125 cell line (normal breast cells), for [bottom panel (c)] 0 min, and for [bottom panel (d)] 15 mins. Adapted with permission from reference (52). Copyright © 2006, American Chemical Society.

The synthetic FRET-based probes have served tremendous applications in imaging protease activation and the diagnosis of diseases. The limitation of these probes is that it is sometimes impermeable to the cells and requires microinjection to perform cellular studies.

Microinjection makes the process tedious to be translated into high-throughput studies (HTS).⁵⁶

1.3.1.2.2 Protein-based FRET probes

The Discovery and development of green fluorescent protein (GFP) from the jellyfish *Aequorea victoria* by Osamu Shimomura, Martin Chalfie, and Roger Tsien brought a revolution in the biosciences. The three shared a Nobel Prize in Chemistry in 2008 for this remarkable discovery.⁵⁷ Wild-type GFP molecule absorbs light at 395 nm with a minor peak at 470 nm and emits light in the green region with an emission maximum of 509 nm.⁵⁸ The introduction of the recombinant gene technology expanded the utility of GFP as a gene expression marker and *in situ* tagging of proteins.⁵⁹ Further, Roger Tsien and co-workers successfully developed spectral variants of wild-type GFP by performing site-directed mutagenesis. The resultant color variants are cyan fluorescent protein (CFP), a yellow fluorescent protein (YFP), a blue fluorescent protein (BFP), a red fluorescent protein (RFP).⁶⁰

The color variants are utilized to make a protein-based FRET probe for protease activity detection. The two-color variants of GFP molecules that make a suitable FRET pair are genetically encoded at opposite ends of the cleavable peptide substrate. Cleavage of the peptide substrate linker by protease activity causes the FRET loss, an increase in donor protein intensity, and a simultaneous increase in acceptor protein intensity.⁶¹ The article by Ying Luo and co-workers has demonstrated the use of the protein-based FRET probe named GDB. GDB encodes for an enhanced green fluorescent protein (EGFP) and enhanced blue fluorescent protein (EBFP) conjugated via the 18 amino acid linker containing the DEVD recognition sequence. EGFP acts as a fluorescence donor, EBFP as a fluorescence acceptor, and DEVD as the substrate recognition sequence for caspases. The probe is utilized to measure caspase-3 activity in apoptotic HeLa cells. Apoptosis was induced by transfecting the cells with pCMV-Rip vector construct expressing protein kinase Rip. Rip is known to be involved in the TNF-induced apoptosis pathway.⁶² Co-expression of the cells with pCMV-Rip and pGDB eliminates the FRET signal between EGFP and EBFP due to the cleavage at the DEVD peptide recognition site. Loss in the FRET signal

observed in apoptotic cells indicating the presence of active caspase-like protease (Figure 1.9).⁶³

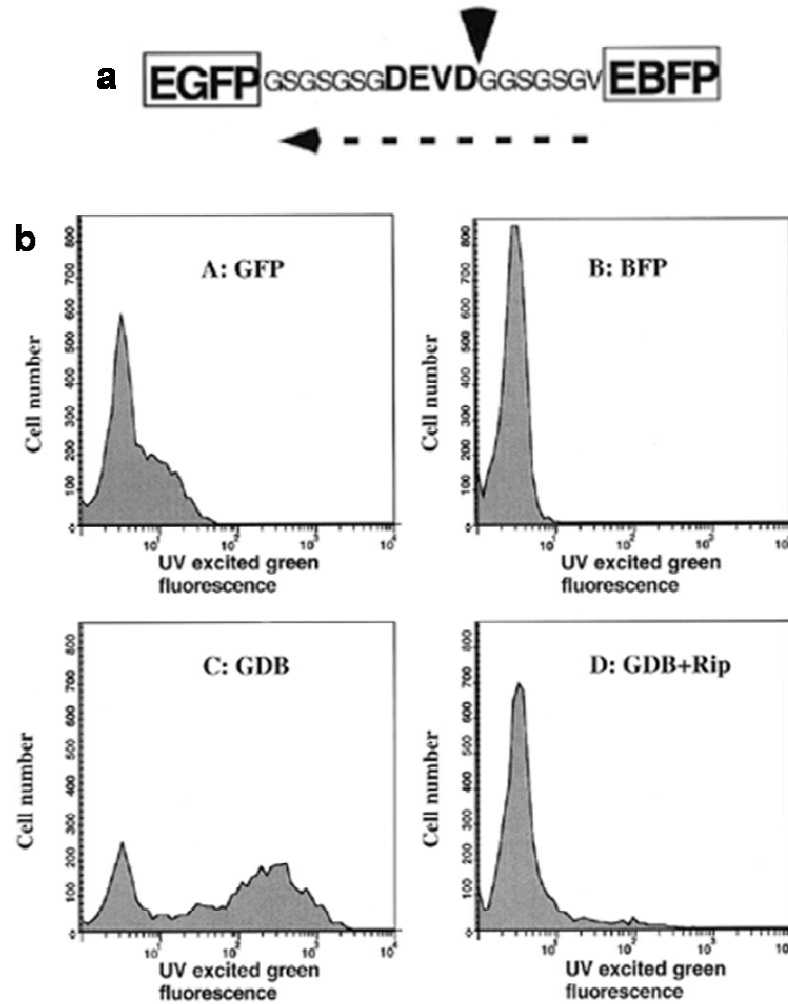


Figure 1.9 Schematic representation of a protein-based FRET probe for measuring caspase-3 activity in apoptotic cells. (a) Structure of GDB protein-based FRET probe constituting of EGFP, EBFP, and peptide linker incorporating DEVD peptide recognition sequence. FRET direction is represented by a dashed arrow. The arrow at the peptide sequence represents the caspase cleavage site. Cleavage at the peptide sequence by caspase-like protease results in FRET loss indicative of caspase activity. (b) Analysis of the FRET effect by utilizing fluorescence-activated cell sorting (FACS) analysis. HEK-293 cells were transfected with pGDB or/and Rip, pEGFP, and pEBFP were harvested 24–36 h after transfection. Laser 1, used for triggering and scatter detection, 488 nm excitation line; laser 2, used for fluorescence detection in two channels using 450/65 and 530/40 bandpass filters, 351 excitation line. Only 530/40 detection channel data is shown. **A:** Cells expressing EGFP only. **B:** Cells expressing EBFP only. **C:** Cells transfected by pGDB. **D:** Cells co-transfected by pGDB and pCMV-Rip. Adapted with permission from reference (63). Copyright ©

1998, Oxford University Press.

The advantage of using protein-based FRET probes is that it is genetically encoded that uses the natural substrate for protease, and can mimic the native environment for a protease action. It also eliminates the problems associated with cell permeability since the probe is encoded by the genetic material. Unlike synthetic FRET-based probes, it does not require *in vitro* modifications of the substrate. The caveat is that the GFP and its spectral variants have a broad spectrum and cause bleed-through issues, e.g., FRET pair like ECFP and EYFP show spectral bleeding and hence decrease the sensitivity of FRET readout.³⁹

1.3.1.3 BRET-based probes

Bioluminescence resonance energy transfer (BRET) refers to the energy transfer between a bioluminescent molecule that acts as an energy donor and a fluorescent molecule that acts as an energy acceptor. Like FRET, BRET also requires spectral overlapping between the donor and the acceptor molecules and a minimum distance of (< 10 nm) for the energy transfer. The luciferase enzyme utilizes a substrate; the catalysis of the luciferase substrate emits light that gets absorbed by a fluorescent acceptor to re-emit the light as a longer wavelength.⁶⁴ BRET-based probes are developed by attaching a protease-cleavable peptide linker with a bioluminescent donor and a fluorophore acceptor to opposite ends. The absence of active protease shows a higher BRET signal, while the presence of active protease shows the reduction in the BRET signal. The protease activity can be measured by calculating the milli-BRET (mBRET) values.^{65,66} Piwnica-Worms and co-workers constructed a BRET-biosensor to detect the executioner caspase activity *in cellulo*. The BRET-based probe pCBG-DEVD-tdTomato; encodes for the DEVD peptide sequence, *i.e.*, recognition sequence for executioner caspases, with click beetle green (CBG) and tdTomato at opposite ends. Here, CBG is the bioluminescent protein donor, and tdTomato is the fluorescence acceptor molecule. The executioner caspases activity was tested in apoptotic HepG2 cells by monitoring the changes in the BRET ratio due to the cleavage of the pCBG-DEVD-tdTomato probe (Figure 1.10).⁶⁷

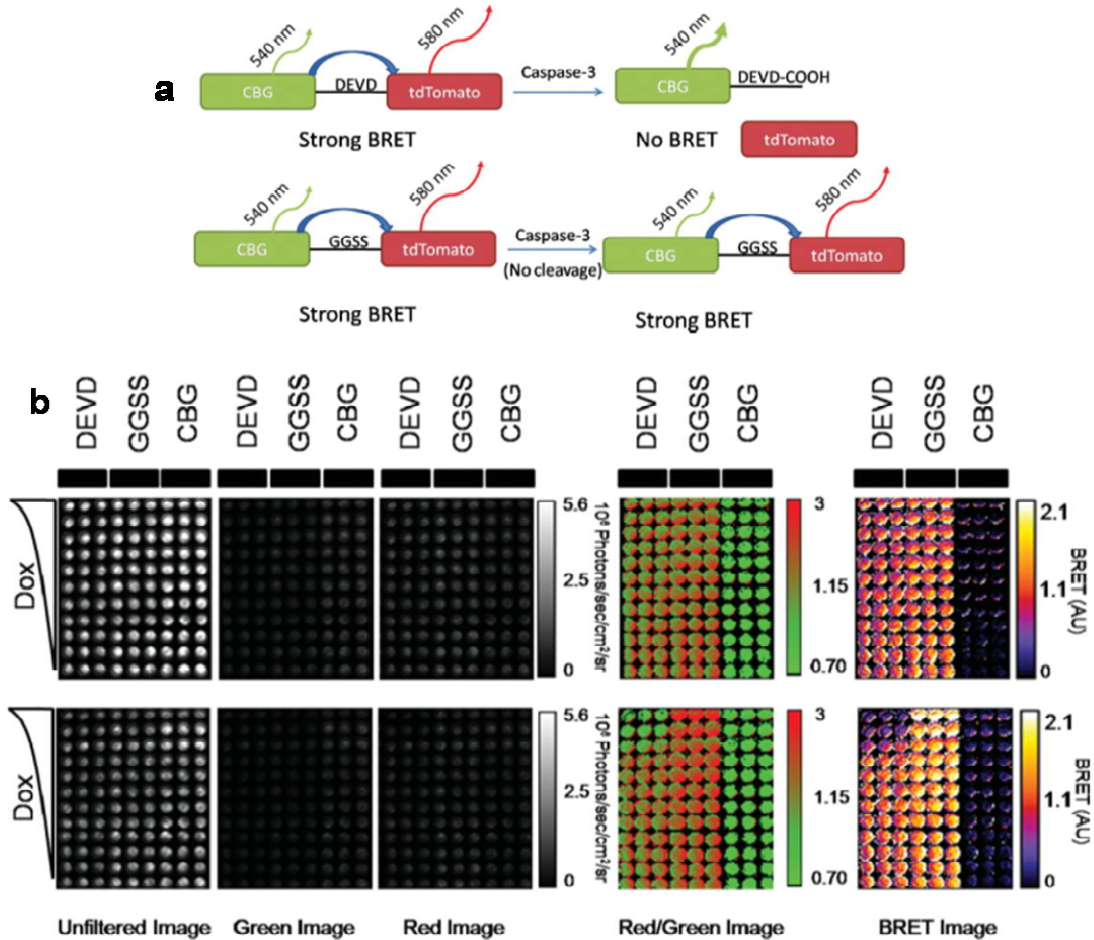


Figure 1.10 Schematic representation of a BRET-based probe and its function in detecting caspase activity in a 96-well plate format. (a) The function of CBG-DEVD-tdTomato BRET-based probe in detecting caspase-3 activity. Upon addition of the CBG substrate, it transfers the energy to tdTomato which emits energy at 580 nm wavelength and is detected by a long pass filter > 590 nm. The tdTomato diffuses away from the CBG after the cleavage at the DEVD peptide sequence resulting in BRET loss resulting in the light emission at the peak of the luciferase emission wavelength (540 nm). A control probe is also designed with an uncleavable linker GGSS yielding CBG-GGSS-DEVD probe. The BRET value for the control probe, CBG-GGSS-DEVD, is maintained even in the presence of active caspase-3. (b) Utilization of CBG-DEVD-tdTomato BRET-based probe to detect caspase activation induced by doxorubicin. HeLa cells were transiently transfected with a vector encoding for either pCBG-DEVD-tdTomato, pCBG-GGSS-tdTomato, or pCBG alone and then plated in triplicates columns in black-walled 96-well plates. After 24 hours, doxorubicin was added to the cells in decreasing concentrations (10 to 0 μ M) from the top to the bottom of the plate and then imaged at 5 time-points. Images shown are from 1.5 h time-point (top panel) or 12 h time-point (bottom panel) (peak induction). The images are, from left to right, the average radiance acquired from an unfiltered acquisition, a green filter (540AF20 nm), or a red filter (>590 nm long pass). After thresholding out the detector noise, the red/green ratio of the filtered images was calculated and false-colored. Finally, a BRET image was obtained by subtracting from the red/green pixel ratio to the average value of the red/green ratio from doxorubicin untreated CBG

wells. Adapted with permission from reference (67). Copyright © 2009 American Institute of Chemical Engineers (AIChE).

Since the FRET system requires the external light source for the donor molecule excitation, it leads to autofluorescence, photobleaching, and light scattering, etc., which hampers the sensitivity. Whereas BRET is a naturally occurring phenomenon where the donor molecule generates light upon the catalysis of the luciferase (donor) substrate; hence, it is suitable for imaging in living subjects and also in light-sensitive cells. However, FRET is a robust technique that provides a high spatial resolution for imaging of the interacting protein partners in living cells. It is well suited for single-cell assays, where the background can be differentiated by taking unlabeled regions of the cell as a reference. On the contrary, BRET is not very suitable for imaging purposes or single-cell assays because of the low output of the emitted light. It is, however, superior to FRET to perform population-based cell assays since it offers a high signal to noise ratio as compared to FRET.⁶⁸

1.3.2 Pros and cons of substrate-based probes

There are several advantages of using substrate-based probes. (i) The probe design is simple and straightforward and can be encoded genetically or synthesized chemically (ii) can measure the turnover number of a protease. The enzyme kinetics parameters such as K_M , V_{max} , k_{cat} for a protease can be calculated using these probes. (iii) Signal amplification, *i.e.*, one single protease, can hydrolyze multiple substrate molecules. The drawbacks of using substrate-based probes are; (i) it lacks specificity, *i.e.*, the peptide sequence of the probe can be cleaved off by multiple proteases of the same family and is not specific for one particular protease. (ii) The signal produced by a specific protease can not be back-tracked as the probe does not remain bound to the target protease after getting cleaved. Due to this, the exact subcellular location of the protease activity can not be identified.¹⁵ Another option for substrate-based probes is the activity-based probes (ABPs). However, the mechanism of action by which the two methods detect protease activity is different.

1.3.3 Activity-based probes

ABPs measure the activity of a class of protease by covalently modifying the active-site of the protease by forming a covalent bond. The amount of active-site modification by the

ABP is indirectly correlated to its activity. ABP is composed of three core structural elements called warhead or the reactive group, linker or peptide recognition sequence, and the tag (Figure 1.11).^{15,31,69}

Warhead: Warhead is the reactive functional group that forms a covalent bond by reacting with the catalytic active-site residue of the protease. Various warhead groups have been designed and successfully applied to target a specific class of protease. For instance, the fluorophosphonate functional group is designed as a warhead for targeting serine proteases like trypsin or chymotrypsin.⁷⁰ The range of different proteases targeted by the ABP depends on the warhead since it drives the reactivity of the probe towards the target protease.

Linker: A linker connects the warhead to the tag. It serves two purposes, (i) linker helps in reducing the steric hindrance between the warhead and the tag. (ii) It also enhances the selectivity of the probe towards specific proteases; by the incorporation peptide sequence that mimics the binding pocket of the cellular substrate of the protease. For example, the DEVD peptide sequence is incorporated in the linker region for probes that target executioner caspases, i.e., cysteine protease.

Tag: The purpose of the tag is to visualize or purify the protease labeled by ABP. Radiolabeled, fluorescent, and biotin tags, in combination with SDS-PAGE and mass spectrometry, have been used to analyze, identify, and purify the labeled protease by ABP.

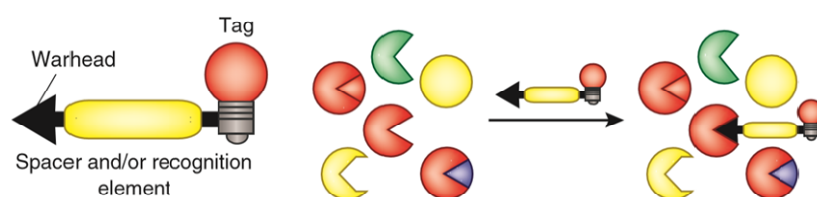


Figure 1.11 Schematic representation of an activity-based probe (ABP) and its function in labeling active protease. ABP is made up of three main components: warhead, spacer or recognition element, and tag. Warhead is the reactive group that targets the active site of a protease. A spacer or recognition element drives the selectivity of the probe towards the target protease and the tag for visualization or detection, e.g., fluorescent dye or an affinity handle like biotin. The electrophilic warhead of the ABP reacts with the nucleophilic active site of the protease and makes a covalent bond resulting in the labeling of protease by an ABP. Adapted with permission from reference (69). Copyright © 2012, Springer Nature.

1.3.3.1 Activity-based fluorescent probes (ABFPs)

The development of activity-based fluorescent probes (ABFPs) is a significant boon to ABP technology. ABFP utilizes a fluorescence molecule as a tag that allows the direct visualization of the target protease activity *in vivo* studies. It also enables the characterization of the ABFP labeled active proteases by using additional biochemical techniques like SDS-PAGE. The article by Matthew Bogoy and co-workers demonstrated the development of an ABFP, LP-1 (Legumain probe-1), for *in vivo* imaging of legumain activity. LP-1 consists of aza-Asn epoxide as a warhead, selective inhibitor for cysteine protease⁷¹, linker sequence incorporating proline for recognition by legumain⁷², and Cy5 as the fluorescent tag. They were able to track the legumain activity in both normal tissues and solid tumors (Figure 1.12).⁷³ Also, ABFP has been successfully applied to directly image proteases like caspase-3⁷⁴, caspase-6⁷⁵, cathepsin X⁷⁶, etc. However, the major drawback of using an ABFP is its inherent fluorescence, i.e., it emits fluorescence signal both when bound to the target protease or in the unbound form in the solution. To overcome this limitation, a new class of ABFP is developed called quenched-activity based probes (qABPs).

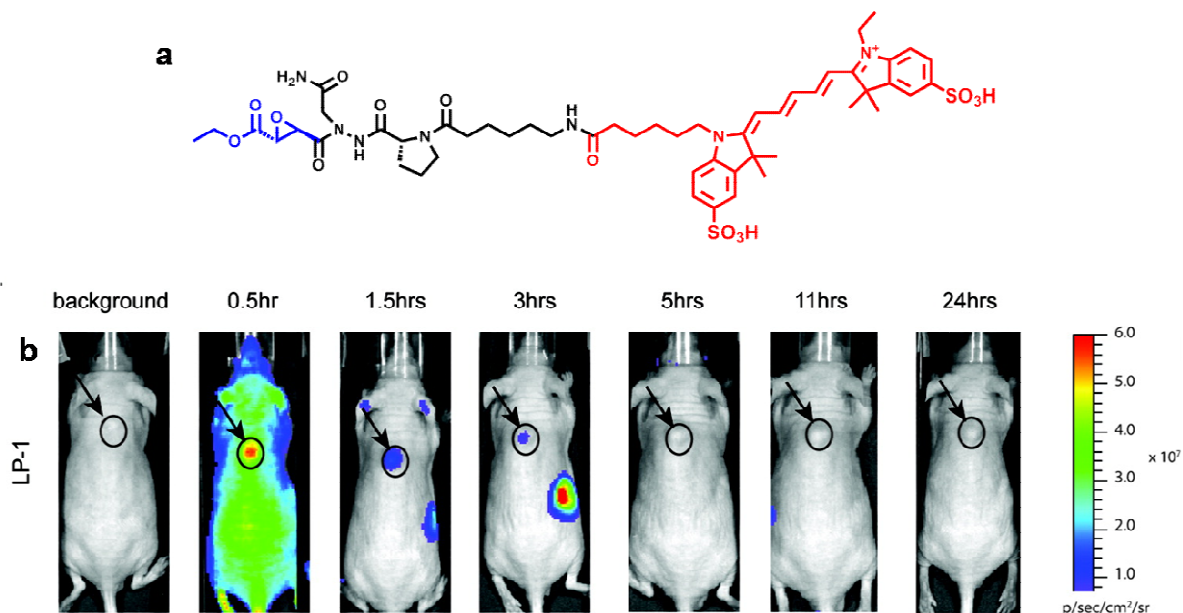


Figure 1.12 Schematic representation of activity-based fluorescent probe (ABFP), legumain probe-1 (LP-1), and its function *in vivo* imaging of legumain. (a) Chemical structure of LP-1 constituting of aza-Asn epoxide as a warhead (blue), proline containing linker sequence (black), and Cy5 dye as a fluorescent tag (red). (b) Images obtained from the *in vivo* imaging experiments performed in mice

bearing C2C12/ras xenograft tumors. Mice were intravenously injected with an LP-1 probe, and images were collected at indicated points to detect the presence of active legumain. A colorimetric scale is used to represent the images based on photons per second per centimeter square per steradian ($\text{p s}^{-1} \text{ cm}^{-2} \text{ sr}^{-1}$) overlaid on bright light images. Adapted with permission from reference (72). Copyright © 2010, American Chemical Society.

1.3.3.2 Quenched-activity based probes

qABPs are the ABFPs with an added quencher molecule. The quencher molecule is attached to the warhead group quenching the fluorescence of the fluorophore of the ABFP. The removal of the quencher group by the proteolytic cleavage results in the covalent attachment of the ABFP to the target protease and simultaneous emission of the fluorescence signal. In this way, qABPs emits the fluorescence signal only when it is bound to the target. The article by Matthew Bogoy and co-workers demonstrates the development and synthesis of GB117, a qABP for imaging active cysteine cathepsin-B proteases. GB117 consists of acyloxymethyl-ketone (AOMK) as a reactive warhead group that targets cysteine protease. AOMK is coupled to the QSY7 quencher molecule and the dipeptide phenylalanine lysine on each end. Cathepsin-B shows selectivity towards amino acid residue phenylalanine.^{77,78} The dipeptide is conjugated to borondipyrromethane-tetramethyl rhodamine-X (BODIPY-TMR-X) dye as a fluorophore. They have synthesized the GB111 probe that is without the quencher molecule as a control. Quenched probe GB117 and the nonquenched probe GB111 were used to image cathepsin-B activity in live NIH-3T3 cells and the MCF-10A 3D cultured cells. The more specific staining pattern was observed in the case of GB117 as compared to GB111 before the washing step (Figure 1.13).⁷⁹ Another example of a qABPs developed by Martijn Verdoes *et al.* is used for the *in vivo* imaging of cysteine protease activity. The probe uses phenoxyethyl ketone (PMK) as a reactive warhead, sulfo-QSY21 as a quenching group, and Cy5 dye for visualization. The probe is utilized for the non-invasive imaging of tumor-bearing mice.⁸⁰ The significant advantage of qABP is qABPs are more sensitive probes than ABFPs for imaging of active protease. Since qABPs generates fluorescence signal only upon binding to the active protease, also it is well suitable for real-time imaging of protease activity in live cells.

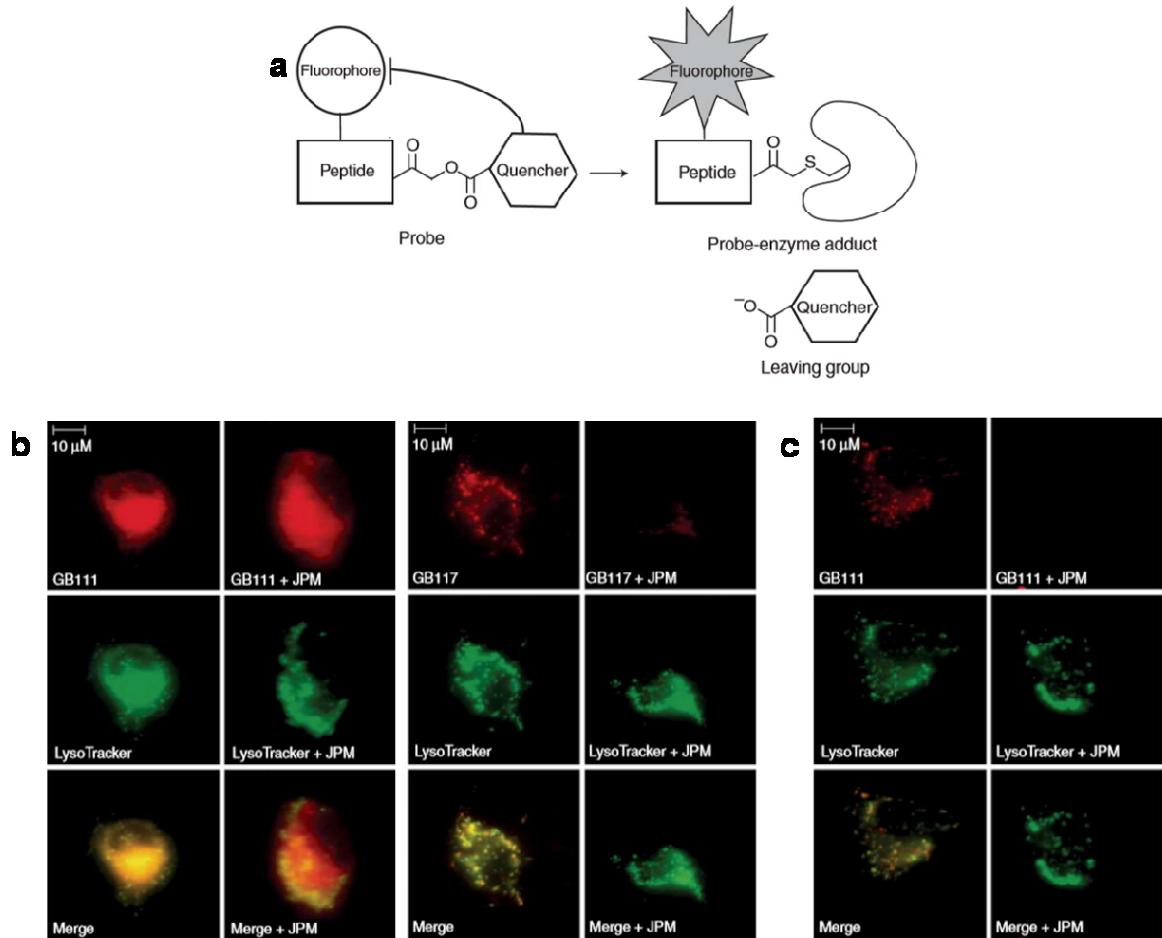


Figure 1.13 Schematic representation of a qABP and its function in imaging protease activity in live cells. (a) Covalent labeling of active protease by qABP. The labeling of the active protease results in the elimination of the quencher group and the formation of the fluorescently label protease. (b) NIH 3T3 cells were pretreated with JPM-OEt inhibitor ($50 \mu\text{M}$), a general papain family protease inhibitor, or vehicle DMSO (0.1%) for 1 h, and then subsequently labeled with GB111, an ABP or GB117, a qABP ($1 \mu\text{M}$) for 4-5 h. Cells were then stained with LysoTracker, an acidotropic lysosomal marker, and were imaged in an inverted fluorescent microscope. (c) Cells were labeled as in b but washed for 3 h in the JPM-OEt added culture medium before imaging. Red staining depicts the protease activity; green staining depicts the lysosomal compartments, while yellow staining represents the overlap in red and green fluorescence signals. Adapted with permission from reference (78). Copyright © 2005, Springer Nature.

1.3.4 Pros and cons of ABPs

Unlike substrate-based probes, the signal produced by a particular protease can be traced back, identified, and quantified by performing additional biochemical assays like SDS-PAGE. The disadvantages associated with ABPs are (i) Lacks signal amplification: one molecule of ABP covalently binds to one molecule of active proteases resulting in the inactivation of the protease, which hampers signal amplification. (ii) Off-target labeling: ABPs are not specific for one particular protease of interest; it always shows some cross-reactivity in the members of the same protease family. However, the specificity of the ABP towards the target protease can be enhanced by modulating the warhead through the traditional chemistry approach and screening for the peptide recognition sequence library with better selectivity towards the target protease.⁷⁶ Edgington *et al.* demonstrated that it is possible to minimize the cross-labeling of the ABFP by comprehensive probe engineering. They designed an ABFP for in vivo imaging of caspases in the apoptosis pathway. The probe is shown to target caspases with high selectivity; however, the cross-reactivity of the probe towards legumain could not be eliminated. It concludes that it is very challenging to design an ABFP that is entirely selective towards a protease.⁷⁴

1.3.5 Activity-dependent proximity ligation method

Moellering and co-workers developed a novel platform called activity-dependent proximity ligation (ADPL) that can image the protease activity with absolute specificity and selectivity in a single cell. The approach combines the use of family-wide ABP with biotin as an affinity tag³¹ and the proximity-dependent DNA ligation assays.⁸¹ The following steps are required to perform ADPL for active protease detection. (i) The live cells are incubated with family-wide ABP with a biotin affinity tag for the labeling of PoI. (ii) Fixed cells are then incubated with primary antibodies specific to the PoI and the biotin tag of the ABP. (iii) Subsequently, cells are then incubated with secondary antibody-oligonucleotide conjugates specific for each primary antibody. The close proximity of the ABP and PoI allows the hybridization and ligation of the two bridging complementary oligonucleotides. (iv) The signal is amplified by ligation and rolling circle amplification (RCA). (v) Hybridization of the complementary oligonucleotides conjugated to a fluorophore enabled the detection by the emission of the fluorescence signal (Figure 1.14). The ADPL platform

is used to image the specific activation of enzymes like neutral cholesterol ester hydrolase-1 (NCEH1), a serine hydrolase, activity in cancer cell lines from ovarian and prostate cancer.⁸² The platform is further extended to soluble-ADPL (sADPL) that can measure the activity of multiple enzymes from the same or different families using barcoded reagents and a multiplexing scheme.⁸³

ADPL offers several unique advantages like (i) In principle, cross-reactivity and off-target labeling are eliminated, and the signal is narrowed down to the detection of a specific PoI. (ii) It allows signal amplification, which is achieved by the proximity-dependent barcoded oligonucleotides. (iii) It enables the detection of the low abundance and low activity protease in a single cell with high resolution. However, ADPL is a multi-step process that also requires the need of specific antibodies against the PoI. Also, it is difficult to translate the method to *in vivo* imaging of protease activity.

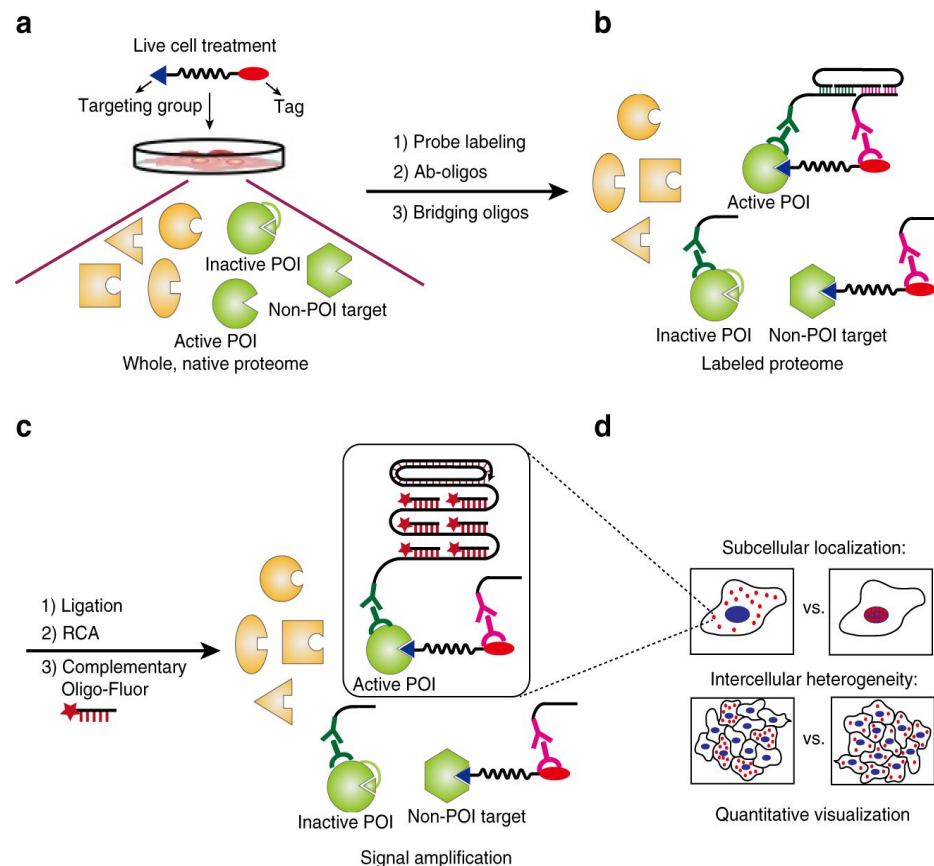


Figure 1.14 Schematic representation of the workflow of activity-dependent proximity ligation (ADPL) platform. (a) Live cells are incubated with an activity-based probe (ABP) that labels active proteins within the cells. (b) To detect the presence of ABP labeled protein-of-interest (PoI), fixed cells are incubated with primary antibodies specific for PoI and probe detection handle (biotin). Cells are further incubated with secondary antibody-oligonucleotide conjugates specific for each primary antibody. When the probe and PoI are on the same protein, it will allow the hybridization and ligation of two bridging complementary oligonucleotides. (c) The signal is amplified through ligation, rolling circle amplification, and detection is achieved by subsequent hybridization of complementary oligonucleotides conjugated to a fluorophore. (d) PoI activity is visualized and quantified using fluorescence microscopy. Adapted with permission from reference (81). Copyright @ 2017, Springer Nature.

1.4 Current challenges and aim of the thesis

Several imaging methods for imaging protease function have been developed with some advantages and disadvantages. Protein-based⁸³⁻⁸⁵ and synthetic^{87,88} substrates-based reporter assays and activity-based fluorescent probes (ABFPs) are the two methods that are frequently used to detect the function of "active proteases" in the (patho) physiological processes. However, the substrate-based reporters lack target specificity in the *in vivo*

conditions. Also, the signal generated by a particular protease can not be traced back, while an activity-based fluorescent probe (ABFP) method targets a class of protease and hence induces non-specificity in the system. However, the absolute specificity of the ABFP towards the target protease can be achieved by engineering the warhead, the reactive functional group, and the peptide scaffold of the ABFP. By extensive probe engineering, Bogyo and co-workers enhanced the specificity of an ABFP to the target protease using the medicinal chemistry approach. However, the results of that study showed it is nearly impossible to design an ABFP with exclusive specificity towards a target protease.⁷⁴ To achieve absolute specificity, probe engineering alone may not be beneficial. Towards that end, Moellering and co-workers developed an activity-dependent proximity ligation platform (ADPL) that can measure the protease activity with absolute specificity.⁸¹ However, ADPL requires the specific antibody against PoI, and also, it is difficult to translate the method to *in vivo* studies.

To overcome some of the limitations posed by the existing technologies, we aim to develop a novel approach for imaging of protease function with unprecedented specificity. Our goal is to design and develop a simple, straightforward, and yet robust method that can be readily applied to any protease of interest (PoI). The purpose is not to provide a substitute for existing current proteomics methods as the ABFP approach in combination with mass spectrometry is a robust technology that enables the detection of active protease with unknown targets.⁸⁹ The objective is to offer an alternative platform for existing tools with some unique features. The development of novel imaging tools that can image the function of active protease with absolute specificity serves enormous potential for applications in the area of high-throughput screening, *in vivo* imaging, target validation, diagnostic, and drug screening.^{33, 90, 91}

1.5 References:

- 1 Rawlings, N. D., Tolle, D. P. & Barrett, A. J. MEROPS: the peptidase database. *Nucleic Acids Res.* **32**, D160-D164 (2004).
- 2 Puente, X. S., Sánchez, L. M., Overall, C. M. & López-Otín, C. Human and mouse proteases: a comparative genomic approach. *Nat. Rev. Genet.* **4**, 544-558 (2003).

- 3 Matrisian, L. M. & Hogan, B. L. 8 Growth Factor-Regulated Proteases and
Extracellular Matrix Remodeling during Mammalian Development. *Curr. Top. Dev.*
24, 219-259 (1990).
- 4 Chen, W.-T. Membrane proteases: roles in tissue remodeling and tumour invasion.
Curr. Opin. Cell Biol. **4**, 802-809 (1992).
- 5 Solomon, M., Belenghi, B., Delledonne, M., Menachem, E. & Levine, A. The
involvement of cysteine proteases and protease inhibitor genes in the regulation of
programmed cell death in plants. *The Plant Cell* **11**, 431-443 (1999).
- 6 Alnemri, E. S. Mammalian cell death proteases: a family of highly conserved
aspartate specific cysteine proteases. *J. Cell. Biochem.* **64**, 33-42 (1997).
- 7 Heutinck, K. M., ten Berge, I. J., Hack, C. E., Hamann, J. & Rowshani, A. T. Serine
proteases of the human immune system in health and disease. *Mol. Immunol.* **47**,
1943-1955 (2010).
- 8 Koblinski, J. E., Ahram, M. & Sloane, B. F. Unraveling the role of proteases in
cancer. *Clin. Chim. Acta* **291**, 113-135 (2000).
- 9 López-Otín, C. & Matrisian, L. M. Emerging roles of proteases in tumour
suppression. *Nat. Rev. Cancer* **7**, 800-808 (2007).
- 10 Reed, C. E. & Kita, H. The role of protease activation of inflammation in allergic
respiratory diseases. *J. Allergy Clin. Immunol.* **114**, 997-1008 (2004).
- 11 Liu, Y. *et al.* Usefulness of serum cathepsin L as an independent biomarker in
patients with coronary heart disease. *Am. J. Cardiol.* **103**, 476-481 (2009).
- 12 Drag, M. & Salvesen, G. S. Emerging principles in protease-based drug discovery.
Nat. Rev. Drug Discov. **9**, 690-701 (2010).
- 13 Turk, B. Targeting proteases: successes, failures and future prospects. *Nat. Rev.*
Drug Discov. **5**, 785-799 (2006).
- 14 Pandey, A. & Mann, M. Proteomics to study genes and genomes. *Nature* **405**, 837-
846 (2000).
- 15 Sanman, L. E. & Bogyo, M. Activity-based profiling of proteases. *Annu. Rev.*
Biochem. **83**, 249-273 (2014).
- 16 Blackstock, W. P. & Weir, M. P. Proteomics: quantitative and physical mapping of
cellular proteins. *Trends Biotechnol.* **17**, 121-127 (1999).
- 17 Anderson, N. L. & Anderson, N. G. Proteome and proteomics: new technologies,
new concepts, and new words. *Electrophoresis* **19**, 1853-1861 (1998).
- 18 Brunelle, J. L. & Green, R. in *Meth. Enzymol.* Vol. 541 151-159 (Elsevier, 2014).
- 19 Magdeldin, S. *et al.* Basics and recent advances of two dimensional-polyacrylamide
gel electrophoresis. *Clin. Proteomics* **11**, 16 (2014).
- 20 Acikara, Ö. B. Ion exchange chromatography and its applications. *Column*
chromatography, 31-58 (2013).
- 21 Mori, S. & Barth, H. G. *Size exclusion chromatography.* (Springer Science &
Business Media, 2013).

- 22 Hage, D. S. Affinity chromatography: a review of clinical applications. *Clin. Chem.* **45**, 593-615 (1999).
- 23 Hage, D. S. *et al.* Pharmaceutical and biomedical applications of affinity chromatography: recent trends and developments. *J. Pharm. Biomed.* **69**, 93-105 (2012).
- 24 Durbin, S. & Feher, G. Protein crystallization. *Annu. Rev. Phys. Chem.* **47**, 171-204 (1996).
- 25 Williams, S. P., Kuyper, L. F. & Pearce, K. H. Recent applications of protein crystallography and structure-guided drug design. *Curr Opin Chem Biol* **9**, 371-380 (2005).
- 26 Aebersold, R. & Mann, M. Mass spectrometry-based proteomics. *Nature* **422**, 198-207 (2003).
- 27 Issaq, H. J., Veenstra, T. D., Conrads, T. P. & Felschow, D. The SELDI-TOF MS approach to proteomics: protein profiling and biomarker identification. *Biochem. Biophys. Res. Commun.* **292**, 587-592 (2002).
- 28 Geoghegan, K. F. & Kelly, M. A. Biochemical applications of mass spectrometry in pharmaceutical drug discovery. *Mass Spectrom. Rev.* **24**, 347-366 (2005).
- 29 Aslam, B., Basit, M., Nisar, M. A., Khurshid, M. & Rasool, M. H. Proteomics: technologies and their applications. *J. Chromatogr. Sci.* **55**, 182-196 (2017).
- 30 Garbis, S., Lubec, G. & Fountoulakis, M. Limitations of current proteomics technologies. *J. Chromatogr. A* **1077**, 1-18 (2005).
- 31 Cravatt, B. F., Wright, A. T. & Kozarich, J. W. Activity-based protein profiling: from enzyme chemistry to proteomic chemistry. *Annu. Rev. Biochem.* **77**, 383-414 (2008).
- 32 Lichtman, J. W. & Conchello, J.-A. Fluorescence microscopy. *Nature methods* **2**, 910-919 (2005).
- 33 Neefjes, J. & Dantuma, N. P. Fluorescent probes for proteolysis: tools for drug discovery. *Nat. Rev. Drug Discov.* **3**, 58-69 (2004).
- 34 R Drake, C., C Miller, D. & F Jones, E. Activatable optical probes for the detection of enzymes. *Curr. Org. Synth.* **8**, 498-520 (2011).
- 35 Lee, S. & Chen, X. Molecular imaging probes for cancer research. *World Scientific*, 519-543 (2012).
- 36 Talanian, R. V. *et al.* Substrate specificities of caspase family proteases. *J. Biol. Chem.* **272**, 9677-9682 (1997).
- 37 Gurtu, V., Kain, S. R. & Zhang, G. Fluorometric and colorimetric detection of caspase activity associated with apoptosis. *Anal. Biochem.* **251**, 98-102 (1997).
- 38 Sandanaraj, B. S., Kneuer, R. & Beckmann, N. Optical and magnetic resonance imaging as complementary modalities in drug discovery. *Future Med. Chem.* **2**, 317-337 (2010).

- 39 Baruch, A., Jeffery, D. A. & Bogyo, M. Enzyme activity—it's all about image. *Trends Cell Biol.* **14**, 29-35 (2004).
- 40 Jares-Erijman, E. A. & Jovin, T. M. FRET imaging. *Nat. Biotechnol.* **21**, 1387-1395 (2003).
- 41 Sekar, R. B. & Periasamy, A. Fluorescence resonance energy transfer (FRET) microscopy imaging of live cell protein localizations. *J. Cell Biol.* **160**, 629-633 (2003).
- 42 Mizukami, S. *et al.* Imaging of caspase-3 activation in HeLa cells stimulated with etoposide using a novel fluorescent probe. *FEBS Lett.* **453**, 356-360 (1999).
- 43 Sapsford, K. E., Berti, L. & Medintz, I. L. Materials for fluorescence resonance energy transfer analysis: beyond traditional donor–acceptor combinations. *Angew. Chem. Int. Ed.* **45**, 4562-4589 (2006).
- 44 Rousseau, J.-C. & Delmas, P. D. Biological markers in osteoarthritis. *Nat. Rev. Rheumatol.* **3**, 346-356 (2007).
- 45 Lee, S. *et al.*
- 46 Yeow, E. K. & Clayton, A. H. Enumeration of oligomerization states of membrane proteins in living cells by homo-FRET spectroscopy and microscopy: theory and application. *Biophys. J.* **92**, 3098-3104 (2007).
- 47 Tramier, M. *et al.* in *Meth. Enzymol.* Vol. 360 580-597 (Elsevier, 2003).
- 48 Weissleder, R., Tung, C.-H., Mahmood, U. & Bogdanov, A. In vivo imaging of tumors with protease-activated near-infrared fluorescent probes. *Nat. Biotechnol.* **17**, 375-378 (1999).
- 49 Alivisatos, A. P., Gu, W. & Larabell, C. Quantum dots as cellular probes. *Annu. Rev. Biomed. Eng.* **7**, 55-76 (2005).
- 50 Kim, G. B. & Kim, Y.-P. Analysis of protease activity using quantum dots and resonance energy transfer. *Theranostics* **2**, 127 (2012).
- 51 Zhou, M. & Ghosh, I. Quantum dots and peptides: a bright future together. *Biomolecules* **88**, 325-339 (2007).
- 52 Shi, L., De Paoli, V., Rosenzweig, N. & Rosenzweig, Z. Synthesis and application of quantum dots FRET-based protease sensors. *J. Am. Chem. Soc.* **128**, 10378-10379 (2006).
- 53 Wegner, K. D. & Hildebrandt, N. Quantum dots: bright and versatile in vitro and in vivo fluorescence imaging biosensors. *Chem. Soc. Rev.* **44**, 4792-4834 (2015).
- 54 Jaiswal, J. K. & Simon, S. M. Potentials and pitfalls of fluorescent quantum dots for biological imaging. *Trends Cell Biol.* **14**, 497-504 (2004).
- 55 Hardman, R. A toxicologic review of quantum dots: toxicity depends on physicochemical and environmental factors. *Environ. Health Perspect.* **114**, 165-172 (2006).
- 56 Rowland, C. E., Brown III, C. W., Medintz, I. L. & Delehanty, J. B. Intracellular FRET-based probes: a review. *Methods Appl. Fluoresc.* **3**, 042006 (2015).

- 57 Zimmer, M. GFP: from jellyfish to the Nobel prize and beyond. *Chem. Soc. Rev.* **38**, 2823-2832 (2009).
- 58 Tsien, R.Y. The green fluorescent protein. *Annu. Rev. Biochem.* **67**, 509-544 (1998).
- 59 Chalfie, M., Tu, Y., Euskirchen, G., Ward, W. W. & Prasher, D. C. Green fluorescent protein as a marker for gene expression. *Science* **263**, 802-805 (1994).
- 60 Heim, R. & Tsien, R. Y. Engineering green fluorescent protein for improved brightness, longer wavelengths and fluorescence resonance energy transfer. *Curr. Biol.* **6**, 178-182 (1996).
- 61 Zhang, J., Campbell, R. E., Ting, A. Y. & Tsien, R. Y. Creating new fluorescent probes for cell biology. *Nat. Rev. Mol. Cell Biol.* **3**, 906-918 (2002).
- 62 Hsu, H., Huang, J., Shu, H.-B., Baichwal, V. & Goeddel, D. V. TNF-dependent recruitment of the protein kinase RIP to the TNF receptor-1 signaling complex. *Immunity* **4**, 387-396 (1996).
- 63 Xu, X. *et al.* Detection of programmed cell death using fluorescence energy transfer. *Nucleic Acids Res.* **26**, 2034-2035 (1998).
- 64 Xu, Y., Piston, D. W. & Johnson, C. H. A bioluminescence resonance energy transfer (BRET) system: application to interacting circadian clock proteins. *Proc. Natl. Acad. Sci. U.S.A.* **96**, 151-156 (1999).
- 65 Bacart, J., Corbel, C., Jockers, R., Bach, S. & Couturier, C. The BRET technology and its application to screening assays. *Biotechnol. J.* **3**, 311-324 (2008).
- 66 Ong, I. L. H. & Yang, K.-L. Recent developments in protease activity assays and sensors. *Analyst* **142**, 1867-1881 (2017).
- 67 Gammon, S. T., Villalobos, V. M., Roshal, M., Samrakandi, M. & Piwnicka-Worms, D. Rational design of novel red-shifted BRET pairs: Platforms for real-time single-chain protease biosensors. *Biotechnol. Prog.* **25**, 559-569 (2009).
- 68 Boute, N., Jockers, R. & Issad, T. The use of resonance energy transfer in high-throughput screening: BRET versus FRET. *Trends Pharmacol. Sci.* **23**, 351-354 (2002).
- 69 Deu, E., Verdoes, M. & Bogyo, M. New approaches for dissecting protease functions to improve probe development and drug discovery. *Nat. Struct. Mol. Biol.* **19**, 9 (2012).
- 70 1 Rawlings, N. D., Tolle, D. P. & Barrett, A. J. MEROPS: the peptidase database. *Nucleic Acids Res.* **32**, D160-D164 (2004).
- 2 Puente, X. S., Sánchez, L. M., Overall, C. M. & López-Otín, C. Human and mouse proteases: a comparative genomic approach. *Nat. Rev. Genet.* **4**, 544-558 (2003).
- 3 Matrisian, L. M. & Hogan, B. L. 8 Growth Factor-Regulated Proteases and Extracellular Matrix Remodeling during Mammalian Development. *Curr. Top. Dev.* **24**, 219-259 (1990).
- 4 Chen, W.-T. Membrane proteases: roles in tissue remodeling and tumour invasion. *Curr. Opin. Cell Biol.* **4**, 802-809 (1992).

- 5 Solomon, M., Belenghi, B., Delledonne, M., Menachem, E. & Levine, A. The involvement of cysteine proteases and protease inhibitor genes in the regulation of programmed cell death in plants. *The Plant Cell* **11**, 431-443 (1999).
- 6 Alnemri, E. S. Mammalian cell death proteases: a family of highly conserved aspartate specific cysteine proteases. *J. Cell. Biochem.* **64**, 33-42 (1997).
- 7 Heutinck, K. M., ten Berge, I. J., Hack, C. E., Hamann, J. & Rowshani, A. T. Serine proteases of the human immune system in health and disease. *Mol. Immunol.* **47**, 1943-1955 (2010).
- 8 Koblinski, J. E., Ahram, M. & Sloane, B. F. Unraveling the role of proteases in cancer. *Clin. Chim. Acta* **291**, 113-135 (2000).
- 9 López-Otín, C. & Matrisian, L. M. Emerging roles of proteases in tumour suppression. *Nat. Rev. Cancer* **7**, 800-808 (2007).
- 10 Reed, C. E. & Kita, H. The role of protease activation of inflammation in allergic respiratory diseases. *J. Allergy Clin. Immunol.* **114**, 997-1008 (2004).
- 11 Liu, Y. *et al.* Usefulness of serum cathepsin L as an independent biomarker in patients with coronary heart disease. *Am. J. Cardiol.* **103**, 476-481 (2009).
- 12 Drag, M. & Salvesen, G. S. Emerging principles in protease-based drug discovery. *Nat. Rev. Drug Discov.* **9**, 690-701 (2010).
- 13 Turk, B. Targeting proteases: successes, failures and future prospects. *Nat. Rev. Drug Discov.* **5**, 785-799 (2006).
- 14 Pandey, A. & Mann, M. Proteomics to study genes and genomes. *Nature* **405**, 837-846 (2000).
- 15 Sanman, L. E. & Bogyo, M. Activity-based profiling of proteases. *Annu. Rev. Biochem.* **83**, 249-273 (2014).
- 16 Blackstock, W. P. & Weir, M. P. Proteomics: quantitative and physical mapping of cellular proteins. *Trends Biotechnol.* **17**, 121-127 (1999).
- 17 Anderson, N. L. & Anderson, N. G. Proteome and proteomics: new technologies, new concepts, and new words. *Electrophoresis* **19**, 1853-1861 (1998).
- 18 Brunelle, J. L. & Green, R. in *Meth. Enzymol.* Vol. 541 151-159 (Elsevier, 2014).
- 19 Magdeldin, S. *et al.* Basics and recent advances of two dimensional-polyacrylamide gel electrophoresis. *Clin. Proteomics* **11**, 16 (2014).
- 20 Acikara, Ö. B. Ion exchange chromatography and its applications. *Column chromatography*, 31-58 (2013).
- 21 Mori, S. & Barth, H. G. *Size exclusion chromatography.* (Springer Science & Business Media, 2013).
- 22 Hage, D. S. Affinity chromatography: a review of clinical applications. *Clin. Chem.* **45**, 593-615 (1999).
- 23 Hage, D. S. *et al.* Pharmaceutical and biomedical applications of affinity chromatography: recent trends and developments. *J. Pharm. Biomed.* **69**, 93-105 (2012).

- 24 Durbin, S. & Feher, G. Protein crystallization. *Annu. Rev. Phys. Chem.* **47**, 171-204 (1996).
- 25 Williams, S. P., Kuyper, L. F. & Pearce, K. H. Recent applications of protein crystallography and structure-guided drug design. *Curr Opin Chem Biol* **9**, 371-380 (2005).
- 26 Aebersold, R. & Mann, M. Mass spectrometry-based proteomics. *Nature* **422**, 198-207 (2003).
- 27 Issaq, H. J., Veenstra, T. D., Conrads, T. P. & Felschow, D. The SELDI-TOF MS approach to proteomics: protein profiling and biomarker identification. *Biochem. Biophys. Res. Commun.* **292**, 587-592 (2002).
- 28 Geoghegan, K. F. & Kelly, M. A. Biochemical applications of mass spectrometry in pharmaceutical drug discovery. *Mass Spectrom. Rev.* **24**, 347-366 (2005).
- 29 Aslam, B., Basit, M., Nisar, M. A., Khurshid, M. & Rasool, M. H. Proteomics: technologies and their applications. *J. Chromatogr. Sci.* **55**, 182-196 (2017).
- 30 Garbis, S., Lubec, G. & Fountoulakis, M. Limitations of current proteomics technologies. *J. Chromatogr. A* **1077**, 1-18 (2005).
- 31 Cravatt, B. F., Wright, A. T. & Kozarich, J. W. Activity-based protein profiling: from enzyme chemistry to proteomic chemistry. *Annu. Rev. Biochem.* **77**, 383-414 (2008).
- 32 Lichtman, J. W. & Conchello, J.-A. Fluorescence microscopy. *Nature methods* **2**, 910-919 (2005).
- 33 Neefjes, J. & Dantuma, N. P. Fluorescent probes for proteolysis: tools for drug discovery. *Nat. Rev. Drug Discov.* **3**, 58-69 (2004).
- 34 R Drake, C., C Miller, D. & F Jones, E. Activatable optical probes for the detection of enzymes. *Curr. Org. Synth.* **8**, 498-520 (2011).
- 35 Lee, S. & Chen, X. in *Molecular Imaging Probes For Cancer Research* 519-543 (World Scientific, 2012).
- 36 Talanian, R. V. *et al.* Substrate specificities of caspase family proteases. *J. Biol. Chem.* **272**, 9677-9682 (1997).
- 37 Gurtu, V., Kain, S. R. & Zhang, G. Fluorometric and colorimetric detection of caspase activity associated with apoptosis. *Anal. Biochem.* **251**, 98-102 (1997).
- 38 Sandanaraj, B. S., Kneuer, R. & Beckmann, N. Optical and magnetic resonance imaging as complementary modalities in drug discovery. *Future Med. Chem.* **2**, 317-337 (2010).
- 39 Baruch, A., Jeffery, D. A. & Bogoyo, M. Enzyme activity—it's all about image. *Trends Cell Biol.* **14**, 29-35 (2004).
- 40 Jares-Erijman, E. A. & Jovin, T. M. FRET imaging. *Nat. Biotechnol.* **21**, 1387-1395 (2003).

- 41 Sekar, R. B. & Periasamy, A. Fluorescence resonance energy transfer (FRET) microscopy imaging of live cell protein localizations. *J. Cell Biol.* **160**, 629-633 (2003).
- 42 Mizukami, S. *et al.* Imaging of caspase-3 activation in HeLa cells stimulated with etoposide using a novel fluorescent probe. *FEBS Lett.* **453**, 356-360 (1999).
- 43 Sapsford, K. E., Berti, L. & Medintz, I. L. Materials for fluorescence resonance energy transfer analysis: beyond traditional donor–acceptor combinations. *Angew. Chem. Int. Ed.* **45**, 4562-4589 (2006).
- 44 Rousseau, J.-C. & Delmas, P. D. Biological markers in osteoarthritis. *Nat. Rev. Rheumatol.* **3**, 346-356 (2007).
- 45 Lee, S. *et al.* Dark quenched matrix metalloproteinase fluorogenic probe for imaging osteoarthritis development in vivo. *Bioconjug. Chem.* **19**, 1743-1747 (2008).
- 46 Yeow, E. K. & Clayton, A. H. Enumeration of oligomerization states of membrane proteins in living cells by homo-FRET spectroscopy and microscopy: theory and application. *Biophys. J.* **92**, 3098-3104 (2007).
- 47 Tramier, M. *et al.* in *Meth. Enzymol.* Vol. 360 580-597 (Elsevier, 2003).
- 48 Weissleder, R., Tung, C.-H., Mahmood, U. & Bogdanov, A. In vivo imaging of tumors with protease-activated near-infrared fluorescent probes. *Nat. Biotechnol.* **17**, 375-378 (1999).
- 49 Alivisatos, A. P., Gu, W. & Larabell, C. Quantum dots as cellular probes. *Annu. Rev. Biomed. Eng.* **7**, 55-76 (2005).
- 50 Kim, G. B. & Kim, Y.-P. Analysis of protease activity using quantum dots and resonance energy transfer. *Theranostics* **2**, 127 (2012).
- 51 Zhou, M. & Ghosh, I. Quantum dots and peptides: a bright future together. *Biomolecules* **88**, 325-339 (2007).
- 52 Shi, L., De Paoli, V., Rosenzweig, N. & Rosenzweig, Z. Synthesis and application of quantum dots FRET-based protease sensors. *J. Am. Chem. Soc.* **128**, 10378-10379 (2006).
- 53 Wegner, K. D. & Hildebrandt, N. Quantum dots: bright and versatile in vitro and in vivo fluorescence imaging biosensors. *Chem. Soc. Rev.* **44**, 4792-4834 (2015).
- 54 Jaiswal, J. K. & Simon, S. M. Potentials and pitfalls of fluorescent quantum dots for biological imaging. *Trends Cell Biol.* **14**, 497-504 (2004).
- 55 Hardman, R. A toxicologic review of quantum dots: toxicity depends on physicochemical and environmental factors. *Environ. Health Perspect.* **114**, 165-172 (2006).
- 56 Rowland, C. E., Brown III, C. W., Medintz, I. L. & Delehanty, J. B. Intracellular FRET-based probes: a review. *Methods Appl. Fluoresc.* **3**, 042006 (2015).
- 57 Zimmer, M. GFP: from jellyfish to the Nobel prize and beyond. *Chem. Soc. Rev.* **38**, 2823-2832 (2009).

- 58 Tsien, R.Y. The green fluorescent protein. *Annu. Rev. Biochem.* 67, 509-544 (1998).
- 59 Chalfie, M., Tu, Y., Euskirchen, G., Ward, W. W. & Prasher, D. C. Green fluorescent protein as a marker for gene expression. *Science* **263**, 802-805 (1994).
- 60 Heim, R. & Tsien, R. Y. Engineering green fluorescent protein for improved brightness, longer wavelengths and fluorescence resonance energy transfer. *Curr. Biol.* **6**, 178-182 (1996).
- 61 Zhang, J., Campbell, R. E., Ting, A. Y. & Tsien, R. Y. Creating new fluorescent probes for cell biology. *Nat. Rev. Mol. Cell Biol.* **3**, 906-918 (2002).
- 62 Hsu, H., Huang, J., Shu, H.-B., Baichwal, V. & Goeddel, D. V. TNF-dependent recruitment of the protein kinase RIP to the TNF receptor-1 signaling complex. *Immunity* **4**, 387-396 (1996).
- 63 Xu, X. *et al.* Detection of programmed cell death using fluorescence energy transfer. *Nucleic Acids Res.* **26**, 2034-2035 (1998).
- 64 Xu, Y., Piston, D. W. & Johnson, C. H. A bioluminescence resonance energy transfer (BRET) system: application to interacting circadian clock proteins. *Proc. Natl. Acad. Sci. U.S.A.* **96**, 151-156 (1999).
- 65 Bacart, J., Corbel, C., Jockers, R., Bach, S. & Couturier, C. The BRET technology and its application to screening assays. *Biotechnol. J.* **3**, 311-324 (2008).
- 66 Ong, I. L. H. & Yang, K.-L. Recent developments in protease activity assays and sensors. *Analyst* **142**, 1867-1881 (2017).
- 67 Gammon, S. T., Villalobos, V. M., Roshal, M., Samrakandi, M. & Piwnicka-Worms, D. Rational design of novel red-shifted BRET pairs: Platforms for real-time single-chain protease biosensors. *Biotechnol. Prog.* **25**, 559-569 (2009).
- 68 Boute, N., Jockers, R. & Issad, T. The use of resonance energy transfer in high-throughput screening: BRET versus FRET. *Trends Pharmacol. Sci.* **23**, 351-354 (2002).
- 69 Deu, E., Verdoes, M. and Bogyo, M. New approaches for dissecting protease functions to improve probe development and drug discovery. *Nat. Struct. Mol. Biol.* **19**, 9 (2012).
- 70 Liu, Y., Patricelli M. P, and Cravatt, B. F. Activity-based protein profiling: the serine hydrolases. *Proc. Natl. Acad. Sci. U.S.A.* **96**, 14694-14699, (1999)
- 71 James, K. E. *et al.* Aza-peptide epoxides: potent and selective inhibitors of *Schistosoma mansoni* and pig kidney legumains (asparaginyl endopeptidases). *Biol. Chem.* **384**, 1613-1618 (2003).
- 72 Sexton, K. B., Witte, M. D., Blum, G. & Bogyo, M. Design of cell-permeable, fluorescent activity-based probes for the lysosomal cysteine protease asparaginyl endopeptidase (AEP)/legumain. *Bioorganic Med. Chem. Lett.* **17**, 649-653 (2007).

- 73 Lee, J. & Bogoy, M. Development of near-infrared fluorophore (NIRF)-labeled activity-based probes for in vivo imaging of legumain. *ACS Chem. Biol.* **5**, 233-243 (2010).
- 74 Edgington, L. E. *et al.* Noninvasive optical imaging of apoptosis by caspase-targeted activity-based probes. *Nat. Med.* **15**, 967 (2009).
- 75 Edgington, L. E. *et al.* An optimized activity-based probe for the study of caspase-6 activation. *Chem. Biol.* **19**, 340-352 (2012).
- 76 Paulick, M. G. & Bogoy, M. Development of activity-based probes for cathepsin X. *ACS Chem. Biol.* **6**, 563-572 (2011).
- 77 Cezari, M. H. S., Puzer, L., Juliano, M. A., Carmona, A. K. & Juliano, L. Cathepsin B carboxydipeptidase specificity analysis using internally quenched fluorescent peptides. *Biochem. J.* **368**, 365-369 (2002).
- 78 Cotrin, S. S. *et al.* Positional-scanning combinatorial libraries of fluorescence resonance energy transfer peptides to define substrate specificity of carboxydipeptidases: assays with human cathepsin B. *Anal. Biochem.* **335**, 244-252 (2004).
- 79 Blum, G. *et al.* Dynamic imaging of protease activity with fluorescently quenched activity-based probes. *Nat. Chem. Biol.* **1**, 203-209 (2005).
- 80 Verdoes, M. *et al.* Improved quenched fluorescent probe for imaging of cysteine cathepsin activity. *J. Am. Chem. Soc.* **135**, 14726-14730 (2013).
- 81 Fredriksson, S. *et al.* Protein detection using proximity-dependent DNA ligation assays. *Nat. Biotechnol.* **20**, 473-477 (2002).
- 82 Li, G. *et al.* An activity-dependent proximity ligation platform for spatially resolved quantification of active enzymes in single cells. *Nat. Commun.* **8**, 1-12 (2017).
- 83 Li, G. *et al.* Ultrasensitive, multiplexed chemoproteomic profiling with soluble activity-dependent proximity ligation. *Proc. Natl. Acad. Sci. U.S.A.* **116**, 21493-21500 (2019).
- 84 Fernández-Fernández, Á. D. *et al.*, Caught green-handed: methods for *in vivo* detection and visualization of protease activity. *J. Exp. Bot.*, **70**, 2125–2141 (2019).
- 85 Mitra, R. D., Silva, C. M. & Youvan, D. C. Fluorescence resonance energy transfer between blue-emitting and red-shifted excitation derivatives of the green fluorescent protein. *Gene* **173**, 13-17 (1996).
- 86 Onuki, R. *et al.* Confirmation by FRET in individual living cells of the absence of significant amyloid β -mediated caspase 8 activation. *Proc. Natl. Acad. Sci. U.S.A.* **99**, 14716-14721 (2002).
- 87 Bullok, K. E. *et al.* Biochemical and in vivo characterization of a small, membrane-permeant, caspase-activatable far-red fluorescent peptide for imaging apoptosis. *Biochemistry* **46**, 4055-4065 (2007).

- 88 Bullok, K. & Piwnica-Worms, D. Synthesis and characterization of a small, membrane-permeant, caspase-activatable far-red fluorescent peptide for imaging apoptosis. *J. Med. Chem.* **48**, 5404-5407 (2005).
- 89 Nomura, D. K., Dix, M. M. & Cravatt, B. F. Activity-based protein profiling for biochemical pathway discovery in cancer. *Nat. Rev. Cancer* **10**, 630-638 (2010).
- 90 Krucker, T. & Sandanaraj, B. S. Optical imaging for the new grammar of drug discovery. *Philos. Trans. Royal Soc. A* **369**, 4651-4665 (2011).
91. Oliveira-Silva, R. *et al.* Monitoring Proteolytic Activity in Real Time: A new world of opportunities for biosensors. *Trends Biochem. Sci.* **45**, 604-618 (2020).

Chapter 2

Development of Activity-based Reporter Gene Technology (AbRGT) for imaging of protease activity

2.1 Introduction

Proteases play an essential role in many physiological processes, including development,¹ blood coagulation,² and programmed cell death,³ and also in pathological conditions such as cancer⁴ and infectious disease.⁵ The conventional proteomics approach provides information on the global expression level of the enzyme.⁶ However, those readouts do not always correlate with the functional state, as most of the proteases are post-translationally modified or bound by endogenous inhibitors.⁷ In spite of decades of research on protease function, imaging of “active protease” with an exquisite specificity is still a significant technical challenge.⁸ Although the role of active proteases has been studied at the physiological concentration in cell/tissue lysates,^{6,7} very few techniques are available to monitor its function in their native biological conditions in living cells.^{9,10} Imaging of active protease in live cells with an absolute specificity will have applications in understanding various diseases and in testing the efficacy of targeted drugs.¹¹

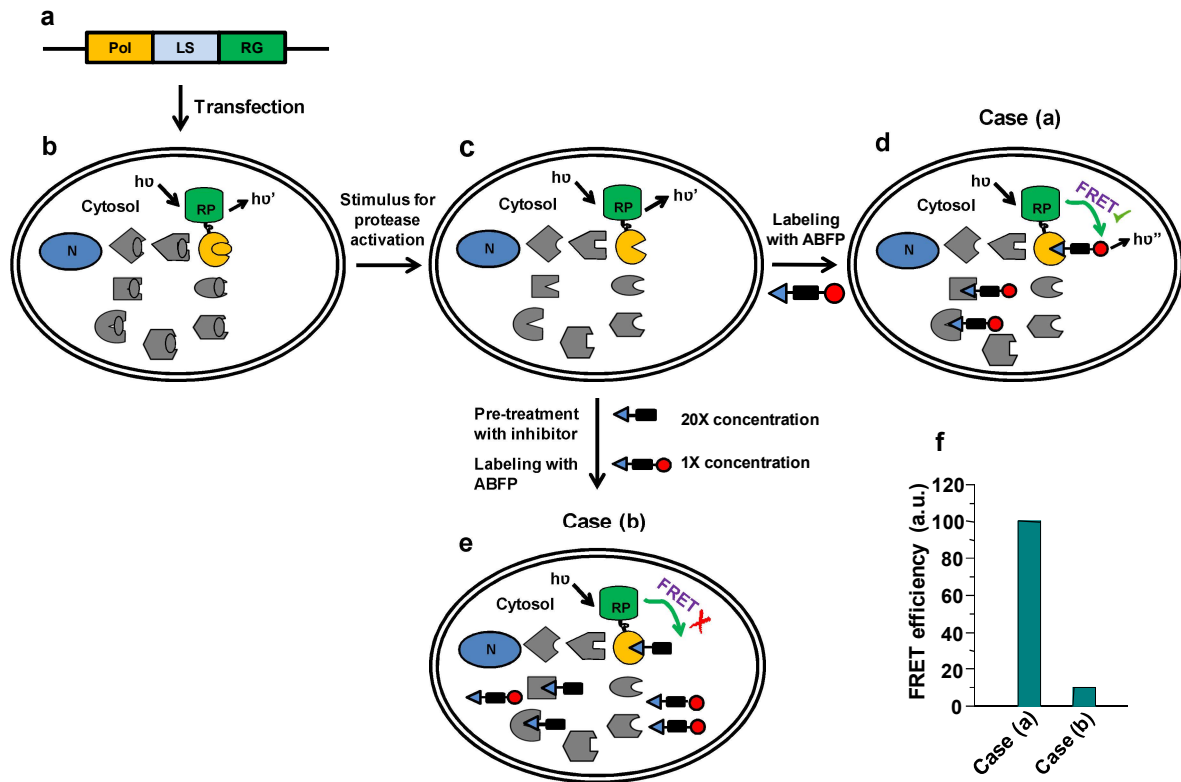
Substrate-based reporter assays^{12,13} and the activity-based fluorescent probe (ABFP) method^{14,15} are two major techniques used to monitor the function of active proteases. In the substrate-based reporter assay, absolute specificity is the main challenge as substrates can be cleaved by other proteases present in native biological conditions. Also, this method lacks provision to trace back the fluorescence signal produced by the target enzyme. ABFPs covalently modify the active site of an enzyme. Hence, the fluorescence signal generated by the target enzyme and another off-target labeling can be traced back by performing in-gel fluorescence assays of cell or tissue lysates.^{13,16} However, the ABFP method cannot be employed to follow the biological processes in intact cells with an absolute specificity because of cross-reactivity of the probe toward other enzymes.

To address the drawbacks of existing techniques, herein, we demonstrate the design and development of a new method called activity-based reporter gene technology (AbRGT). AbRGT is a hybrid of the reporter gene and ABFP technologies. Here, the enzyme tagged to the fluorescent reporter protein is labeled by an ABFP creating a FRET pair. The readout of this technology is based on the FRET effect, which is a very accurate, sensitive method

and can be performed in a live cell. In situ generation of a FRET pair in a living cell has been previously demonstrated by covalent labeling of the fusion protein by the synthetic fluorophore. Hoffmann *et al.* have shown the activation of GPCR (G-protein coupled receptor) tagged to CFP (cyan fluorescent protein) can be studied by labeling it with a synthetic FLAsH probe resulting in the FRET effect.¹⁷ Nevertheless, to the best of our knowledge, the detection of “active enzyme” by *in situ* generation of a FRET pair has not been previously reported. This method discloses an innovative way to image the function of the active protease with an exquisite specificity in a living cell.

2.2 Concept of AbRGT

The concept of our technology is diagrammatically depicted in (Figure 2.1) Here, the plasmid encoding protease-of-interest (PoI) tagged to a reporter protein (RP; FRET donor) (Figure 2.1a) is expressed in the cell line of interest (Figure 2.1b). An appropriate stimulus is given to cells for the activation of PoI (Figure 2.1c), followed by incubation of cells with a cell-permeable ABFP carrying an appropriate fluorophore (FRET acceptor). Labeling of PoI by an ABFP instantaneously creates a FRET pair in situ (Figure 2.1d). Upon RP excitation, the emission of RP is absorbed by fluorophore of ABFP, resulting in quenching of RP fluorescence and simultaneous excitation and emission of ABFP at a longer wavelength resulting in the FRET effect (case a). Since the FRET effect heavily depends on the distance between donor and acceptor, the labeling of other proteases by an ABFP will not contribute to the FRET signal.



Pol = Protease of Interest; LS = Linker Sequence; RG = Reporter Gene; RP = Reporter Protein; N = Nucleus; ABFP = Activity-based Fluorescent Probe

Figure 2.1 Schematic representation of AbRGT. (a) Plasmid DNA encoding protease-of-interest (PoI) (yellow) tagged to a reporter gene (green). (b) Cell expressing PoI tagged to a reporter protein along with other proteases with the same or different protease family (gray). (c) Conversion of the active protease from inactive zymogen form upon the application of an appropriate stimulus. (d) Case a, PoI tagged to RP, labeled with ABFP (1x concentration), showing the FRET effect. (e) Case b, cells are pretreated with the active-site protease inhibitor (20x concentrations) and then labeled by ABFP, abolishing the FRET effect. (f) Hypothetical graphical representation of FRET efficiency comparison between cases a and b.

Additionally, this technology can be used for inhibitor profiling of protease as labeling of PoI by an inhibitor would abolish the in situ generation of a FRET pair (Figure 2.1e) and hence no FRET effect (case b). FRET efficiency comparison between “case a” (without inhibitor) versus “case b” (with inhibitor) is represented in a hypothetical bar graph (Figure 2.1f). There would be a significant loss in the FRET efficiency of the cells pretreated with an inhibitor versus untreated ones.

2.3 Choice of the system to demonstrate the AbRGT

To validate our method, we chose to study the function of caspases in the apoptosis signaling pathway. Apoptosis is the programmed cell death that plays a significant role in tissue homeostasis and development in the biological system. The regulation of apoptosis is tightly controlled, and any dysregulation can result in various diseases such as cancer and autoimmune diseases. Apoptosis can occur via two pathways, *i.e.*, mitochondrial mediated (or intrinsic)¹⁸ and death-receptor mediated (or extrinsic)¹⁹ pathways.

The extrinsic pathway is initiated upon the binding of ligands to the death receptors present on the cell surface leading to the formation of a death-inducing signaling complex (DISC) that subsequently activates initiator caspases (caspase-8 or caspase-10). The initiator caspases then activate the effector caspases by the site-specific proteolytic cleavage. The effector caspase further dismantles the cell by degrading key intracellular molecules. However, the intrinsic pathway is initiated by the release of specific death promoting molecules from mitochondria that is triggered by several chemotherapeutic agents, radiation, etc. The main event in the intrinsic pathway includes mitochondrial outer membrane permeabilization (MOMP) that is considered to be an irreversible event in apoptosis. MOMP leads to the release of certain proteins from the mitochondria. The released proteins trigger a cascade of the caspase activation events resulting in apoptosis. However, both the intrinsic and extrinsic pathways converge at the activation of effector caspases (caspase-3 or caspase-7), leading to the destruction of crucial proteins and eventually results in apoptosis (Figure 2.2).²⁰

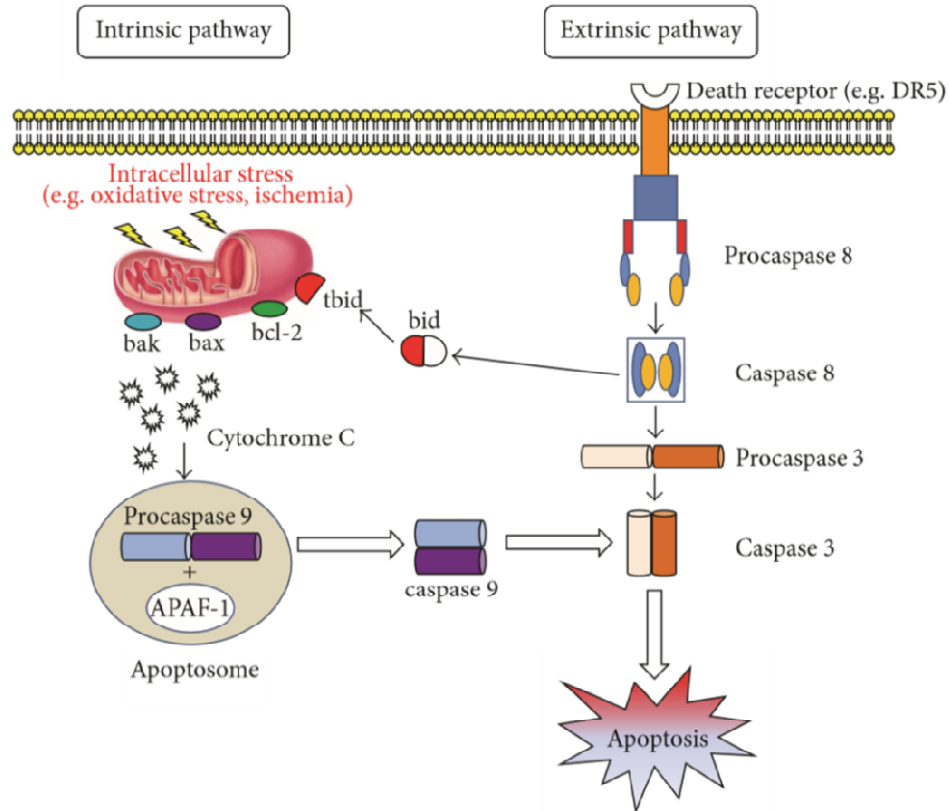


Figure 2.2 Apoptosis can occur through two alternative pathways: mitochondria-dependent (or intrinsic) and death receptor-mediated (or extrinsic). The former pathway is shown on the left side, and the latter is on the right side. The extrinsic pathway initiated by the binding of the ligands to specific death receptors, e.g., Fas and tumor necrosis factor- (TNF-) related apoptosis-inducing ligand (TRAIL) receptors DR4, and DR5 induce cell death upon binding with Fas ligand (FasL) or TRAIL, respectively. This process activates caspase 8. However, the intrinsic pathway induces apoptosis by bid (BH3 interacting domain death agonist) cleavage, causing mitochondrial outer membrane permeabilization (MOMP) and releasing cytochrome C and subsequent activation of caspases-9 and -3. The intrinsic pathway is partly regulated by bcl family members bound to the mitochondrial membrane, including bax (pro-apoptotic) and bcl-2 (anti-apoptotic). The cytochrome c release from the mitochondria is inhibited by the anti-apoptotic proteins bcl-2 and bcl-XL. However, all pro-apoptotic proteins, bcl-2—associated X protein(bax), bcl-2 homologous antagonist/killer (bak), and bid promote cytochrome C release from mitochondria. The cytochrome C and deoxyadenosine triphosphate (dATP) bind to apoptotic protease activating factor (APAF-1) and forms a multimeric complex. The complex recruits and activates procaspase-9, an executioner protease. Active caspase-9 subsequently activates caspase-3. Caspase-3 activation leads to DNA fragmentation and cell death. Adapted with permission from reference (21) Copyright © 2014 Carla Loreto *et al.*

2.4 Choice of the protease of interest (PoI) to demonstrate AbRGT

To demonstrate the work-flow of AbRGT, we chose to monitor the function of caspase-3 in the apoptosis signaling pathway. The caspase-3 protease is chosen because it is the main executioner caspase in the apoptosis signaling pathway. Caspase-3 is synthesized as a 32 kDa inactive zymogen consisting of a prodomain, a larger subunit (p17), and a smaller subunit (p12). The procaspase-3 is activated upon proteolytic cleavage by the effector caspase-6 or -7. The proteolytic cleavage occurs after an aspartate (D) residue in 32 kDa procaspase-3 in amino acid sequences, ESMDS (amino acids 25–29), and IETDS (amino acids 172–176), yielding two subunits p17 and p12. The two subunits (p17 and p12) forms a homodimer of heterodimer exhibiting two independent, active sites. The active site involves the elements from both p17 and p12 subunits. The catalysis is performed by amino acids Cys163 and His121 from the p17 subunit (Figure 2.3).²²

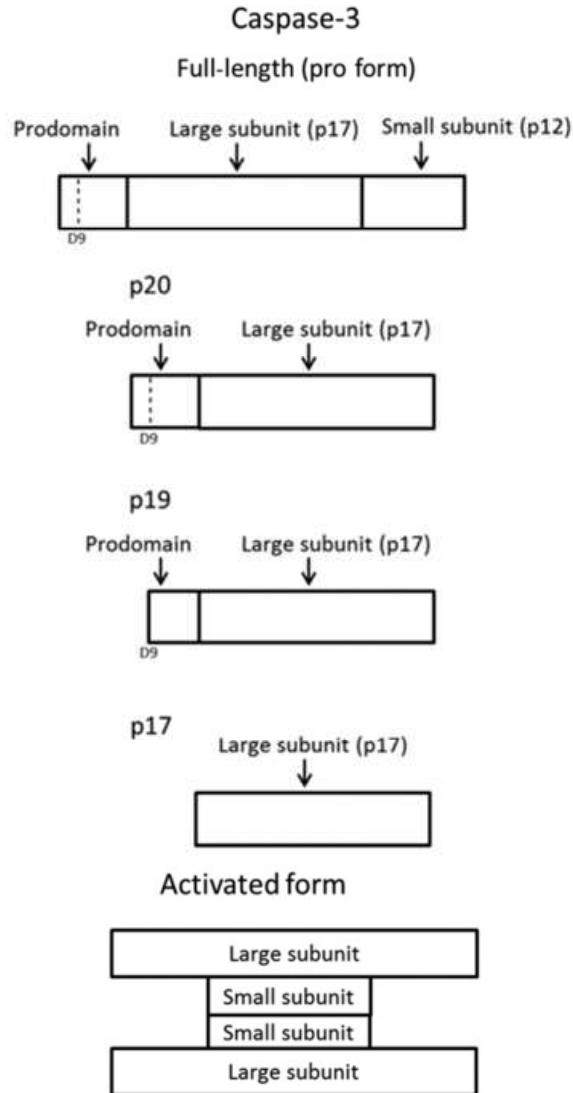


Figure 2.3 Procaspase-3 processing to active caspase-3. Caspase-3 zymogen form is composed of a pro-domain, a larger subunit (p17), and a smaller subunit (p12) connected by a cleavable linker. The caspase-3 gets activated upon cleavage by the effector caspases-6 or -7. After cleavage, larger and smaller subunits form a heterotetramer via hydrophobic interactions. Adapted and modified from reference (23).

2.5 Results and Discussion

2.5.1 Development of AbRGT using caspase-3 as a PoI

To demonstrate our method, we chose to monitor the specific activation of caspase-3 in the apoptosis signaling pathway using an ABFP, rhodamine-VAD-fluoromethyl ketone (Rh-VAD-FMK), in an MCF-7 cell line. The Rh-VAD-FMK probe comprises of rhodamine as a

fluorescent tag, VAD as a peptide recognition sequence for pan-caspases, and FMK as the reactive warhead for targeting cysteine proteases. Before performing cellular studies, active-site labeling of the caspase3 protease by the Rh-VAD-FMK probe was validated *in vitro* conditions.

2.5.1.1 *In vitro* labeling of recombinant caspase-3

2.5.1.1.1 Expression and purification of recombinant caspase-3

To begin with, recombinant human caspase-3 (rcaspase-3) was expressed and purified²⁴ using Ni-NTA column chromatography. The purified protein samples were characterized using 15% SDS-PAGE gel and yielded two bands at the expected size (17 kDa and 12 kDa) with high purity (Figure 2.4a). The samples were analyzed using MALDI TOF/TOF analyzer. Laser intensity was maintained at maximum, and mass was scanned between 10,000 Da and 40,000 Da. Caspase-3 expression was confirmed by peaks obtained at 12 kDa and 17 kDa in MALDI-ToF analysis (Figure 2.4b).

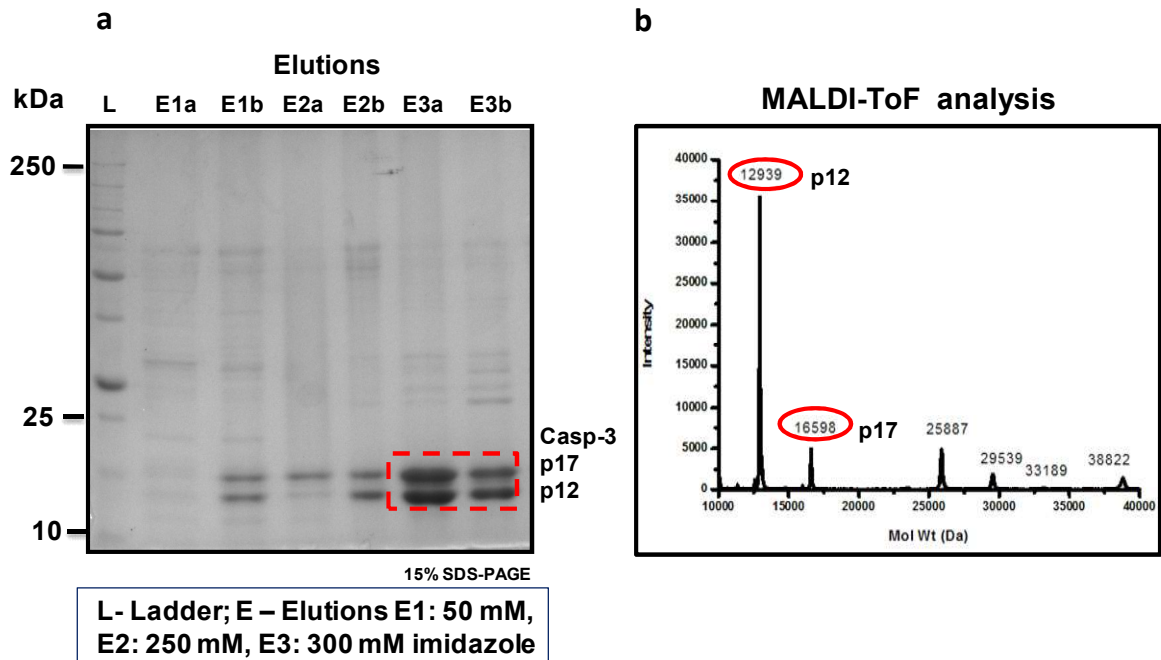


Figure 2.4 Characterization of recombinant caspase-3 (a) The SDS-PAGE analysis of the Ni-NTA affinity column purified caspase-3. Protein samples were run on 15% SDS-PAGE gel and stained with coomassie brilliant blue. Fractions were eluted with 50, 250, and 300 mM imidazole concentrations. (b) MALDI-ToF analysis of the purified caspase-3. The rcaspase-3 was mixed with matrix 0.1% trifluoroacetic acid (TFA) with 70:30 water/acetonitrile mixtures and laser fired. The identity of the purified enzyme was confirmed with the two peaks at 12939 and 16598 Da.

2.5.1.1.2 Michaelis-Menton kinetic assay and Lineweaver Burk plot

The Michaelis Menton kinetics assay was used to determine the activity of the rcaspase-3. The rate K_M/k_{cat} of the rcaspase-3 catalyzed chemical reaction was calculated by plotting velocity $[P]/t$ ($\mu\text{M}/\text{min}$) against different substrate concentration $[S]$ (Figure. 3a). The K_M and V_{max} values of rcaspase-3 were determined by reciprocating the values obtained by Michaelis Menton plot to obtain a linear graph, i.e., Lineweaver Burk plot. The intercept on the X-axis and Y-axis (Figure 2.5) signify the values of $-1/K_M$ ($-0.22 \mu\text{M}$) and $1/V_{max}$ ($1.1 \mu\text{M}/\text{min}$). The K_M and V_{max} values are calculated to be $4.5 \mu\text{M}$ and $0.9 \mu\text{M}/\text{min}$, respectively.

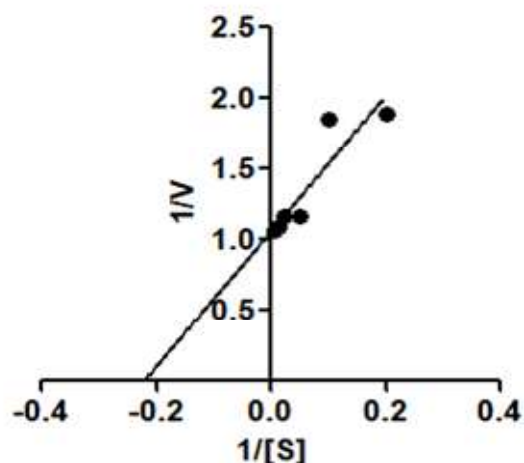


Figure 2.5 Lineweaver Burk plot for the determination of K_M and V_{max} of rcaspase-3. To obtain a linear graph, the values from the plot are reciprocated, and the K_M and k_{cat} values were calculated from the intercept at x and y-axis.

2.5.1.1.3 Determination of the k_{cat} of recombinant caspase-3

The k_{cat} of the enzyme was calculated using the equation $k_{cat} = V_{max}/[E_T]$. The $[E_T]$ is the total enzyme concentration, *i.e.*, 10 nM. The V_{max} is 1.2 $\mu\text{M}/\text{min}$ obtained from the Lineweaver Burk plot. The calculated k_{cat} value is 1.5/sec. The active enzyme concentration was determined by the graph plotted between hydrolysis rate versus inhibitor concentration (Figure 2.6), 200 nM. The obtained k_{cat} values indicate that rcaspase-3 is catalytically active and can be used to perform *in vitro* labeling by the Rh-VAD-FMK probe.

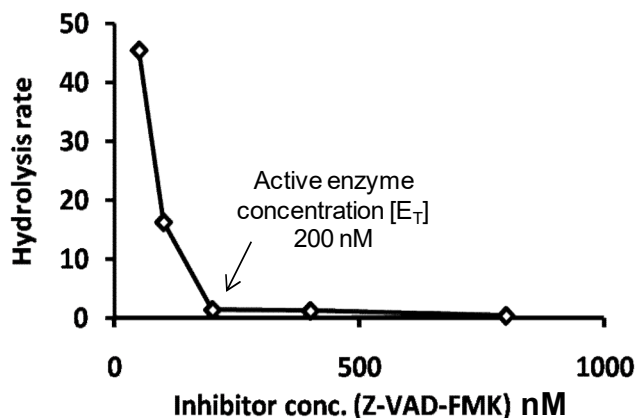


Figure 2.6 Active -site titration of rcaspase-3. Hydrolysis rate $[P]/t$ was plotted against the concentration of Z-VAD-FMK. The intercept on the X-axis reveals the concentration of the active rcaspase-3. The substrate DEVD-pNA was used at a final concentration of 50 μ M.

2.5.1.1.4 Labeling of recombinant caspase-3 by Rh-VAD-FMK probe

In order to demonstrate rcaspase-3 labeling by the Rh-VAD-FMK probe with good potency, rcaspase-3 was incubated with an increasing concentration (100, 500, and 2000 nM) of the Rh-VAD-FMK probe. The labeled protein samples were subjected to electrophoresis, and the resultant gel was imaged using an in-gel fluorescence scanner. The intense fluorescence signal of the rcaspase-3 p17 band was found even at the lowest probe concentration of 100 nM. The concentration-dependent increase in fluorescence intensity of the caspase-3 p17 band was observed (Figure 2.7a and b). The denaturation of the rcaspase-3 by heat before labeling by the Rh-VAD-FMK probe eliminates the fluorescence signal indicating that the reaction was driven through a specific mechanism between the rcaspase-3 active site and the FMK warhead of the probe (Figure 2.7c).

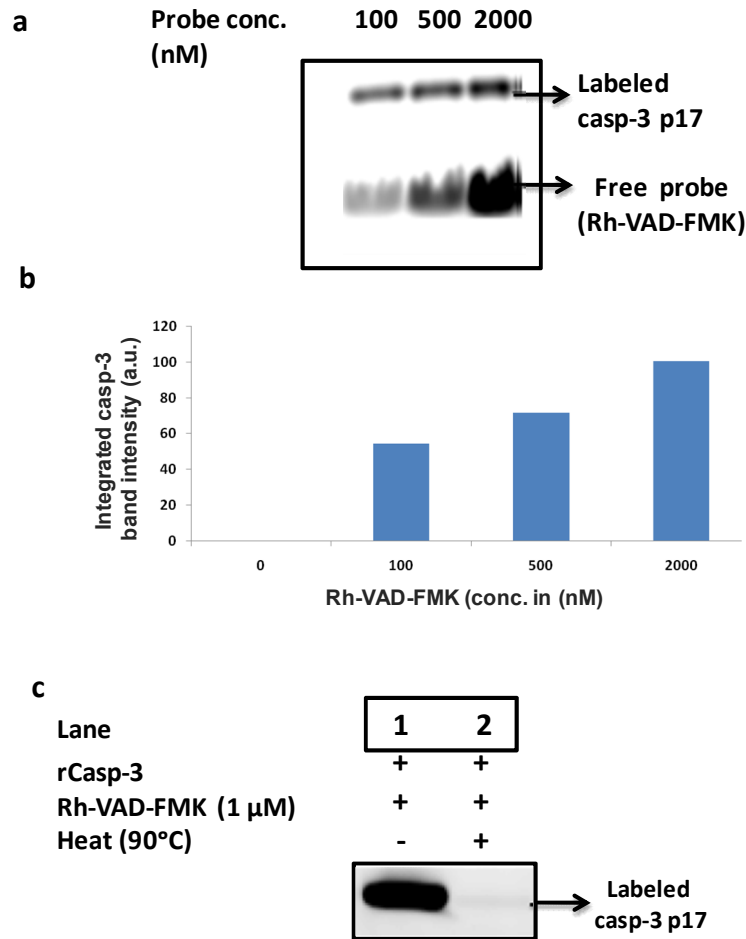


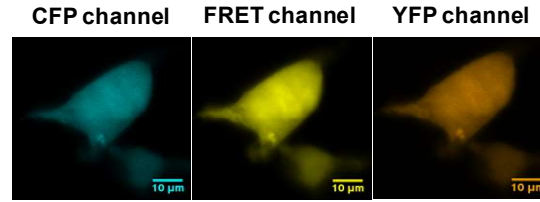
Figure 2.7 In vitro labeling of r-caspase-3 by Rh-VAD-FMK probe. (a) In-gel fluorescence image of purified r-caspase-3 (2 μ M) labeled by the Rh-VAD-FMK probe at different concentrations (100, 500, and 2000 nM). (b) Integrated band intensity values. (c) The specificity of the Rh-VAD-FMK probe (1 μ M) to label active enzyme (500 nM); (lane 1: active r-caspase-3 in the presence of Rh-VAD-FMK probe, lane 2: thermally denatured r-caspase-3 in the presence of Rh-VAD-FMK probe).

2.5.1.2 FRET standardization

Before applying AbRGT on determining the caspase-3 activation in the apoptosis pathway using the FRET approach, we first standardized FRET in the cellular system. To do that, we chose a standard FRET positive control plasmid construct. The standard FRET C5V plasmid encodes for a cyan fluorescent protein (CFP), (FRET donor) connected to a yellow fluorescent protein (YFP), (FRET acceptor), via a five amino acid linker (GGGGG). The two fluorescent proteins with overlapping spectral properties (emission spectrum of the donor

overlapping with the absorption spectrum), makes a good FRET pair. The C5V plasmid was over-expressed in the HEK-293 cell line, and the fluorescence signal was collected in CFP channel (CFP excitation and emission), FRET channel (CFP excitation and emission) and YFP channel (YFP excitation and emission). We observed the intense signal in all three channels (Figure 2.8). To confirm the presence of FRET, we performed the acceptor photobleaching method. The FRET efficiency was estimated by quantifying the donor, CFP fluorescence intensity before and after photobleaching from the fluorescence intensity graph (Figure 2.8). The FRET intensity is calculated to be $46\% \pm 2$, using the below equation. Thus, we confirmed and calculated the FRET efficiency by acceptor photobleaching method with C5V standard reference FRET plasmid construct taken as a positive control. Subsequently, we proceeded towards performing the FRET-based AbRGT approach for measuring caspase-3 activity in the apoptosis pathway.

$$FRET_{efficiency} = \frac{(D)_{post-bleac} - (D)_{pre-bleac}}{(D)_{post-bleach}}$$



FRET validation by using acceptor photo-bleaching method

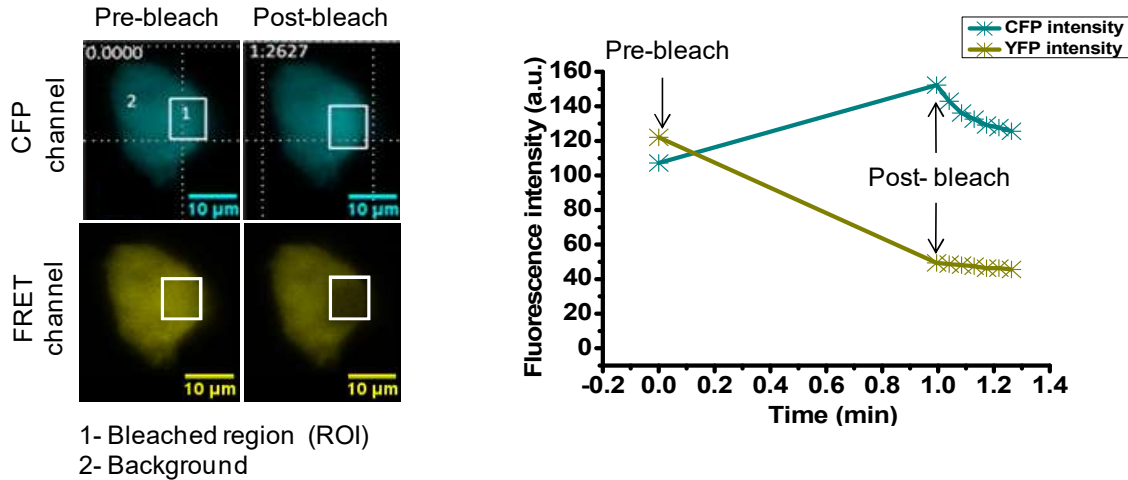


Figure 2.8 Acceptor photobleaching of the cells transfected with C5V standard FRET plasmid DNA construct. The region labeled with 1 show the bleached zone, region 2 shows the unbleached area *i.e.* background. (b) Quantitative measurement of the CFP and YFP intensities before and after bleaching over different time scales. CFP fluorescence increased 152.3 from 107.2 in a bleaching time of 0.9 minutes.

2.5.1.3 Imaging caspase-3 activation using AbRGT approach

Having demonstrated the labeling of rcaspase-3 by the Rh-VAD-FMK probe *in vitro* conditions, AbRGT is used to detect the specific activity of caspase-3 in the native cellular environment using the Rh-VAD-FMK probe. To do that, the MCF-7 cell line was chosen to perform cellular assays because it lacks endogenous caspase-3.²⁵ Cells were transfected with a pCMV3 plasmid vector encoding C-terminally tagged GFPspark (FRET donor) to caspase-3. For caspase-3 activity determination, it is necessary that GFPspark is tagged at the C-terminus of the caspase-3 and not at the N-terminus, as the N-terminal peptide of the zymogen caspase-3 is cleaved off of the protease during apoptosis as a part of the maturation process of the protease.²⁶

Transfected cells were treated with staurosporine (STS)^{27,28} (1 μ M), a pan-kinase inhibitor for 2, 4, 6, and 8 h or a TNF-related tumor-inducing ligand (TRAIL)^{29,30} (1 μ g/mL) for 5 h for apoptosis induction. Cells were then incubated with the Rh-VAD-FMK probe (1 μ M) (FRET acceptor) for an additional 2 h for probe labeling. Subsequently, cells were washed with phosphate buffer saline (PBS) to take out the unreacted Rh-VAD-FMK probe and imaged under a confocal fluorescence microscope.

The Rh-VAD-FMK probe was chosen because it has been previously shown that this probe labels caspase-3 with low selectivity³¹ and moderate affinity. Hence, it serves as a great probe to validate the technology, i.e., extensive probe engineering is not required in this case. Besides, the fluorophore (rhodamine derivative) attached to the Rh-VAD-FMK probe can act as an excellent FRET acceptor because its absorption spectrum overlaps well with the emission spectrum of GFPspark, which is one of the prerequisites for the efficient FRET process.

To monitor the specific caspase-3 activation, the fluorescence signal was collected in three different channels: the GFP channel (direct excitation and emission of GFP), the FRET channel (direct excitation of GFP and indirect emission from rhodamine), and the rhodamine (Rh) channel (direct excitation and emission of rhodamine). Diffused cytosolic distribution of the GFP signal was observed in STS or TRAIL untreated control cells [Figure 2.11 (i)] as procaspase-3 localization is known to be cytosolic.^{32,33} Caspase-3 GFPspark transfected cells showed a distinct punctate pattern³⁴ in GFP, FRET, and Rh channels in both STS [Figure 2.11 (ii)] and TRAIL [Figure 2.11 (iii)] treated cells after 4 and 5 h of treatment, respectively. The fluorescence signal in the FRET channel represents the presence of active caspase-3. The prominent difference between FRET and Rh channels was not visible in the images because of the restricted resolution of confocal microscopy due to its diffraction limit, i.e., 200 nm. To differentiate the fluorescence pattern in the two channels, super-resolution imaging experiments were performed [Figure 2.11 (ii)], using stimulated emission depletion (STED) microscopy³⁵ (Figure 2.9). STED microscopy aided in distinguishing the fluorescence pattern and labeling in the two channels, i.e., comparatively more precise labeling was found in the FRET channel than the Rh channel.

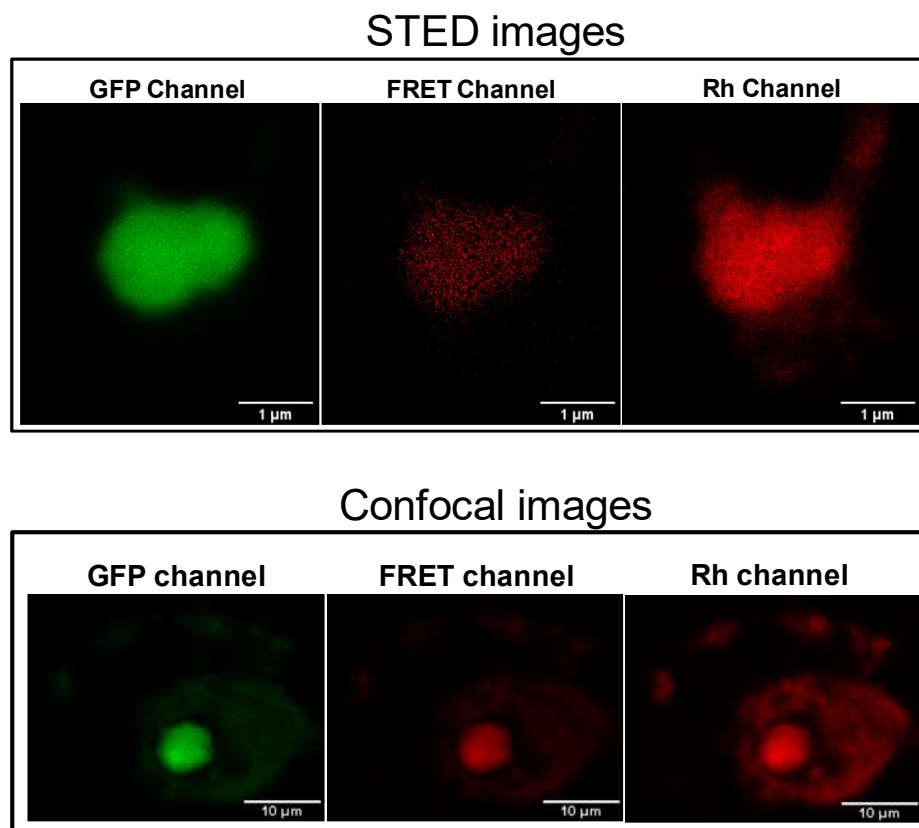


Figure 2.9 Specific detection of caspase-3 GFPspark in MCF-7 cells. Caspase-3 GFPspark (1 μg) transfected MCF-7 cells were treated with 1 μM of STS for 4 h and labeled by the Rh-VAD-FMK probe (1 μM). Cells were fixed, and the fluorescence signal was collected in GFP, FRET, and Rh channels. STED image (top) and confocal image (bottom).

The fluorescence signal obtained in the Rh channel in untransfected MCF-7 cells [Figure 2.11 b (iv)] depicts the presumable labeling of potential off-targets (cathepsin B, legumain, and other caspase proteases) by the Rh-VAD-FMK probe including the PoI caspase-3 GFP enzyme. To prove that the occurrence of the FRET effect [Figure 2.11 (ii)] is not because of random physical interaction between GFPspark and rhodamine dye, EGFP (1 μg) overexpressing MCF-7 cells were treated with or without STS (1 μM) for 4 h followed by labeling with the RhVAD-FMK probe. The diffused fluorescence signal throughout the cell was observed in the GFP channel in both STS treated or untreated cells since EGFP localization is known to be ubiquitous in the cell, including the nucleus.³⁶ The absence of the fluorescence signal in the FRET channel in both STS treated or untreated cells proves that there is no physical interaction between the Rh-VAD-FMK probe and EGFP.

Nonetheless, the fluorescence signal in the form of punctate labeling was obtained in the Rh channel in STS-treated but not in untreated cells representing the presumable activation of the other cysteine protease by STS treatment allowing its labeling by the Rh-VAD-FMK probe [Figure 2.11 (v) and (vi)]. However, EGFP transfected MCF-7 cells did not show any apoptotic cell body upon STS treatment that could be because of the lack of endogenous caspase-3 in this cell line. We replicated the EGFP control experiment in HEK-293 cells since it has endogenous caspase-3. EGFP transfected HEK-293 cells were induced to undergo apoptosis by the addition of STS (1 μ M) for 12 h. In the STS untreated cells, the diffused fluorescence signal was obtained throughout the cell in the GFP channel similar to MCF-7 cells, and the absence of the fluorescence signal was observed in FRET and Rh channels, as expected [Figure 2.11b (vii)]. However, STS treated HEK-293 cells were found to form apoptotic bodies, as evident by the fluorescence signal obtained in the GFP channel. The fluorescence signal in the FRET channel was absent, but prominent punctate labeling was observed in the Rh channel that further confirms the off target labeling by the Rh-VAD-FMK probe [Figure 2.11b (viii)]. The corrected total cell fluorescence (CTCF) of each image in GFP, FRET, and Rh channels in Figure 2.11b is calculated using ImageJ software (Figure 2.12).

2.5.1.4 Validation of the off-target labeling of other proteases by the Rh-VAD-FMK probe

Subsequently, an in-gel fluorescence assay was performed on Jurkat cells lysate to show the multiple off-target labelings of other proteases by the Rh-VAD-FMK probe that has also been elucidated in the previous reports.³¹ Jurkat cells were induced to undergo apoptosis by treatment with STS (1 μ M) for 4 h, followed by labeling with the Rh-VAD-FMK probe. The cell lysate (2 μ g/ μ L) showed multiple bands on SDS-PAGE gel upon rhodamine excitation at 561 nm laser, which proves the cross-labeling of other proteases by the Rh-VAD-FMK probe (Figure 2.10).

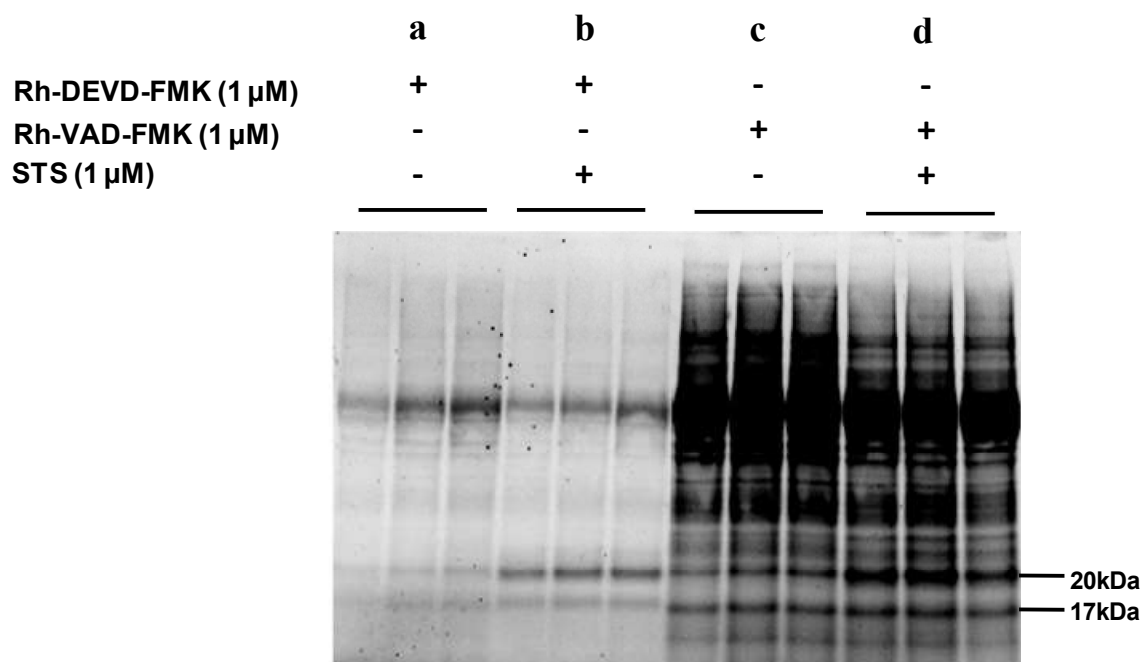
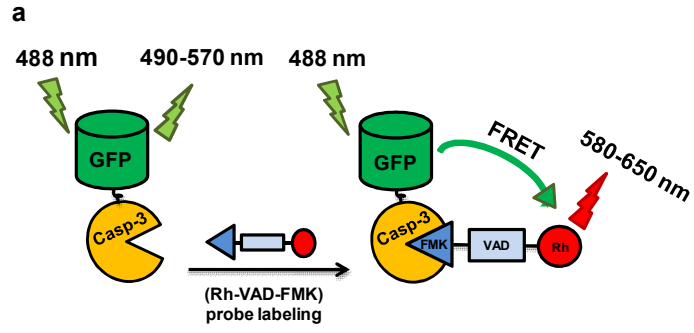


Figure 2.10 Cellular off-target labeling of Rh-VAD-FMK probe and Rh-DEVD-FMK probe shown in Jurkat cells. 2.5 million Jurkat cells were incubated with 1 μ M Rh-VAD-FMK probe or Rh-DEVD-FMK probe in the (b) presence or (c) the absence of STS (1 μ M) for 6 h. Cells are incubated (a) without and (d) with Rh-VAD-FMK probe or Rh-DEVD-FMK probe and STS. Cells were then lysed, and labeled proteins were analyzed by 12% SDS-PAGE followed by scanning for rhodamine fluorescence (Ex: 561 nm, Em: 605 nm) with a flat-bed laser scanner.

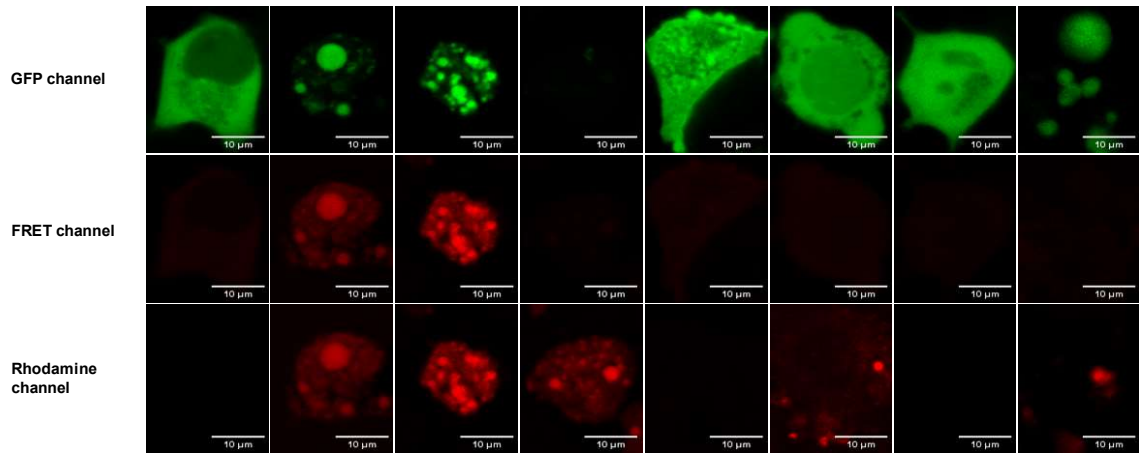
2.5.1.5 Acceptor photo-bleaching method to confirm the FRET occurrence

To prove that the fluorescence signal obtained in the FRET channel indeed manifests exclusive detection of caspase-3, acceptor photobleaching studies were carried out.^{37,38} Images in GFP and FRET channels were taken pre- and post-bleaching (Figure 2.11c). Rhodamine photobleaching in the region of interest (ROI), the area under the white square, was achieved by irradiating the cells with 100% intensity (561 nm), resulting in a rise in the GFP signal in ROI. Quantified GFP intensities in the rhodamine bleached region as compared to the unbleached region (Figure 2.11c), *i.e.*, 58 ± 3 and 6 ± 1 au, respectively ($*P \leq 0.00001$) confirming the in situ occurrence of FRET process with the FRET efficiency ($n = 15$ cells) of $35 \pm 1\%$.



b

	(i)	(ii)	(iii)	(iv)	(v)	(vi)	(vii)	(vii)
Cell line	MCF-7	MCF-7	MCF-7	MCF-7	MCF-7	MCF-7	HEK-293	HEK-293
Expression vector	Casp-3 GFP	Casp-3 GFP	Casp-3 GFP	Null	EGFP	EGFP	EGFP	EGFP
STS (1 μ M)	-	+	-	+	-	+	-	+
TRAIL (1 μ g/ml)	-	-	+	-	-	-	-	-



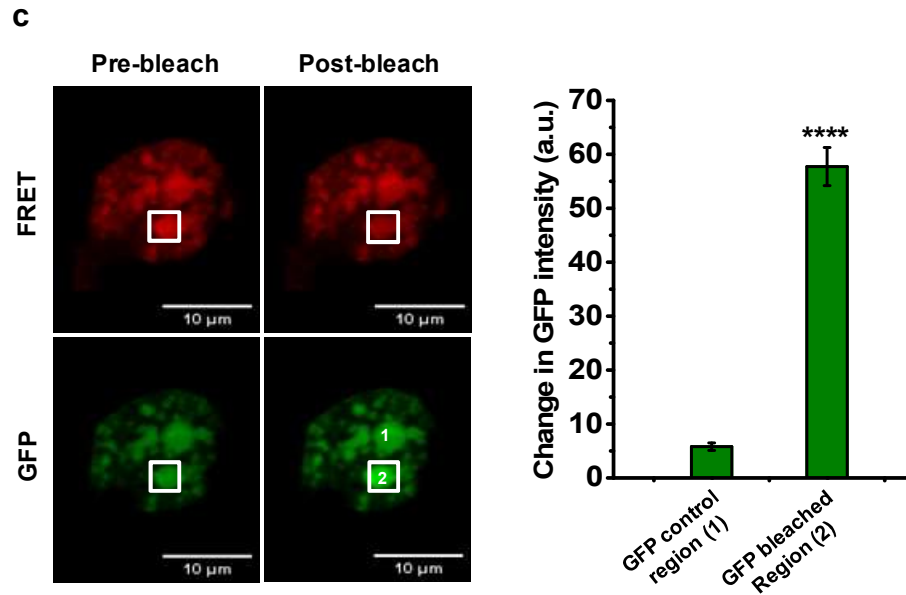


Figure 2.11 Development of AbRGT using caspase-3 as a target protease. (a) Schematic representation of AbRGT in determining the specific activation of the caspase-3 GFPspark fusion protein by the FRET effect utilizing the Rh-VAD-FMK probe. (b) The fluorescence signal was collected in GFP, FRET, and rhodamine channels. MCF-7 cells transfected with caspase-3 GFPspark (i) untreated or treated with (ii) STS (1 μ M) for 4 h or (iii) TRAIL (1 μ g/mL) for 5 h and then labeled by the Rh-VAD-FMK probe. (iv) Untransfected MCF-7 cells were treated with STS (1 μ M) for 4 h and then labeled by the Rh-VAD-FMK probe. MCF-7 cells transfected with enhanced green fluorescent protein (EGFP) plasmid treated with (v) STS (1 μ M) or without (vi) STS for 4 h and then labeled by the Rh-VAD-FMK probe. Scale bar, 10 μ m. HEK-293 cells transfected with enhanced green fluorescent protein (EGFP) plasmid treated without (vii) STS (1 μ M) or with (viii) STS for 4 h and then labeled by the Rh-VAD-FMK probe. (c) FRET validation between GFP and rhodamine fluorophores using the acceptor photobleaching method. Images for GFP and rhodamine fluorescence signals were collected in GFP and FRET channels pre- and postbleaching of rhodamine signals. (d) Quantification of the change in GFP fluorescence intensity after rhodamine photobleaching in both the GFP control region (1) and the GFP bleached region (2) (ROI), the area under the white square using the acceptor photobleaching method. Error bar represents the SEM for $n = 10$ cells ($*P < 0.00001$). Scale bar, 10 μ m, au, arbitrary units.

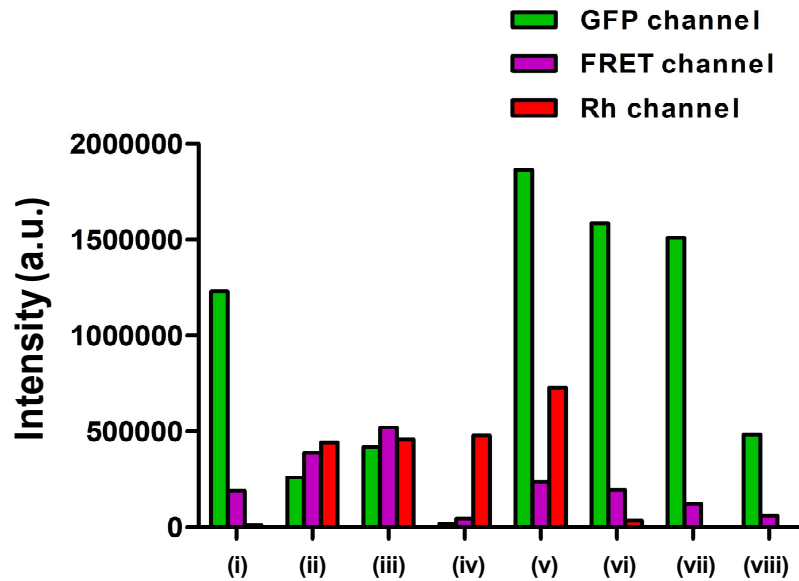


Figure 2.12 CTCF (corrected total cell fluorescence) is calculated in GFP, FRET, and Rh channels for each image in (Figure 2.11b) using Image J software. The procedure for quantification is described in the “Materials and Methods” section.

2.5.1.6 Imaging caspase-3 activation at different time points

Similar results were obtained for other time points as well, i.e., 2, 6, and 8 h of STS treatment (Figure 2.13a and b). Time-dependent imaging studies revealed enormous cell to cell variability on the onset of programmed cell death. This observation is similar to the results obtained by other researchers.³⁹

a

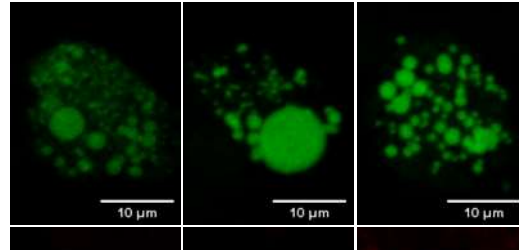
**STS treatment
Time (h)**

2 h

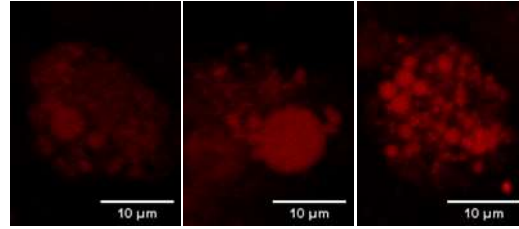
6 h

8 h

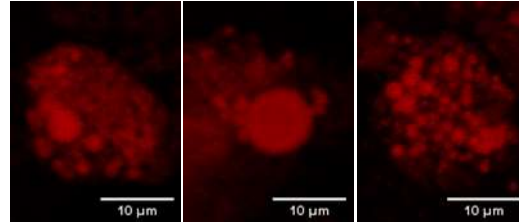
GFP channel



FRET channel

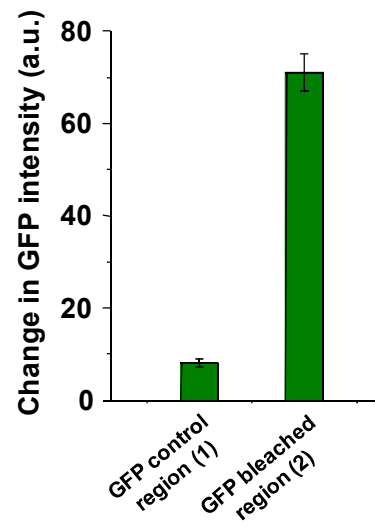
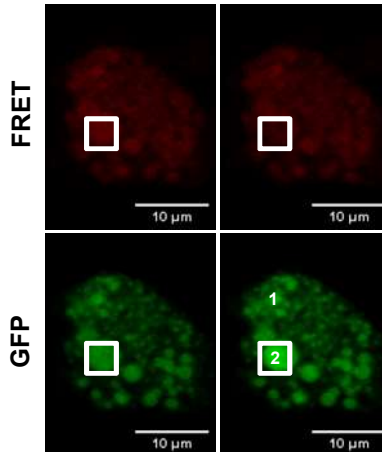


**Rhodamine
channel**



b

Pre-bleach Post-bleach



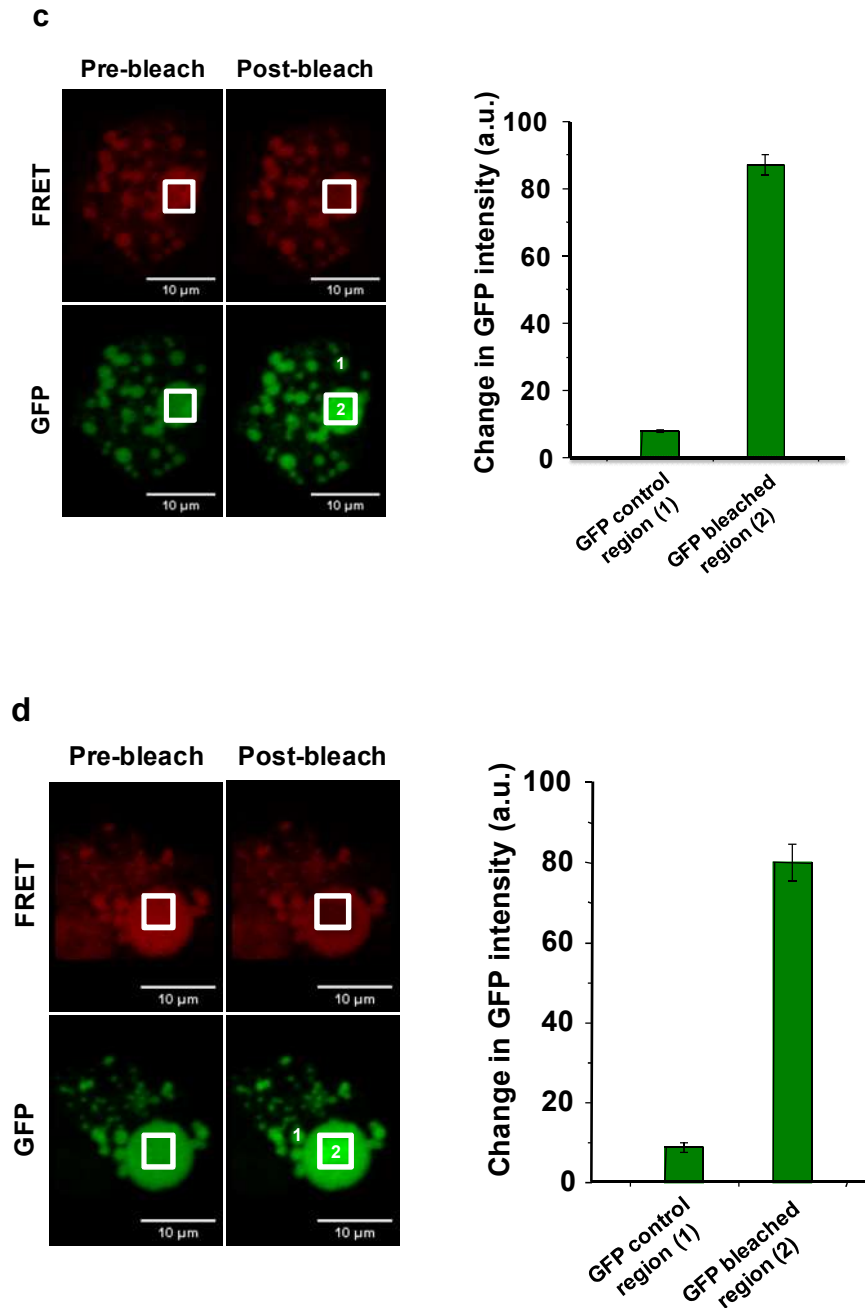
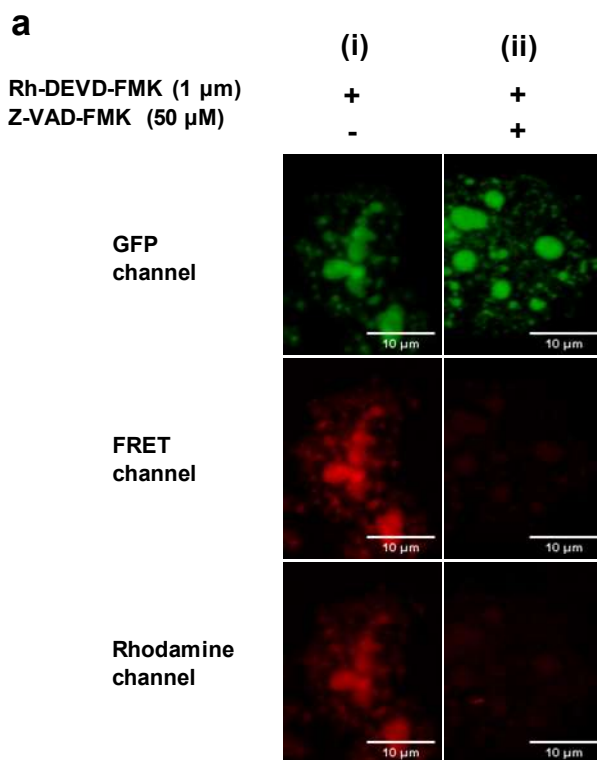


Figure 2.13 Time-dependent activation of caspase-3 GFPspark in MCF-7 cells upon STS (1 μ M) induction. MCF-7 cells transfected with 2 μ g of caspase-3 GFPspark plasmid and treated with 1 μ M of STS for 2, 6, and 8 h. Cells were then labeled with the Rh-VAD-FMK probe for an additional 2 h. (a) Images were collected in GFP, FRET, and Rh channels. (b) Images for GFP and rhodamine fluorescence signals were collected in GFP and FRET channels pre- and post-bleaching of rhodamine signals in ROI (region of interest), area under the white square, with 100% laser intensity (561 nm). FRET validation between GFP and rhodamine fluorophore using the acceptor photobleaching method for the MCF-7 cells with STS induction for 2, (c) 6, and (d) 8 h. I =

intensity (a.u.), arbitrary units. The calculated FRET efficiency for 2, 6, and 8 h are 38, 43, and 36%, respectively.

2.5.1.7 Imaging caspase-3 activation using Rh-DEVD-FMK probe

Caspase-3 activation is also monitored using another ABFP containing peptide sequence (DEVD) more selective for caspase-3, i.e., the Rh-DEVD-FMK probe. The Rh-DEVD-FMK probe also showed a similar pattern of the fluorescence signal in all three channels as that of the RhVAD-FMK probe with an estimated FRET efficiency of 35% (Figure 2.14a and b). These findings demonstrate that the exquisite specificity cannot be achieved only by simply changing the peptide recognition sequence to a more specific one.



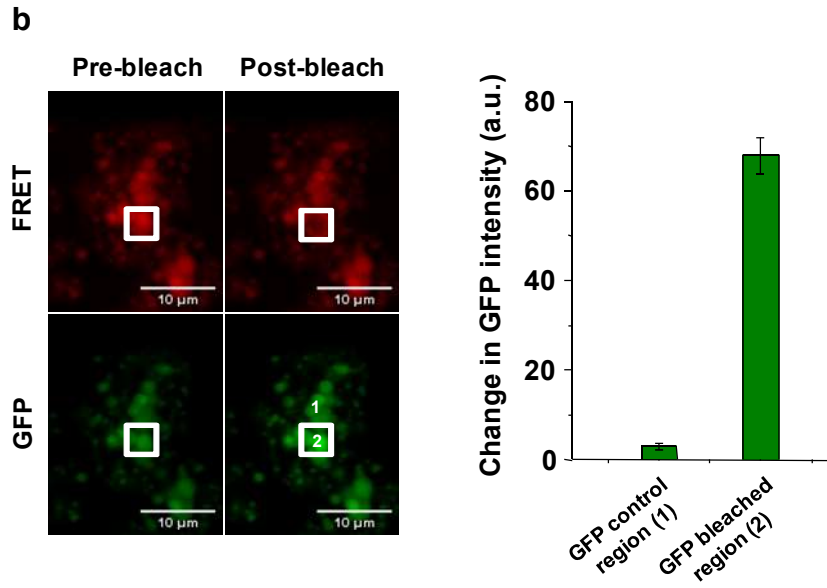


Figure 2.14 Applying AbRGT for specific detection of active caspase-3 GFPspark using the Rh-DEVD-FMK probe. Caspase-3 GFPspark (2 μg) transfected MCF-7 cells were treated with 1 μM of STS for 4 h and labeled with the Rh-DEVD-FMK probe (1 μM). (a) The fluorescence signal was collected in GFP, FRET, and Rh channels in the presence or absence of inhibitor Z-VAD-FMK (50 μM). (b) Acceptor photobleaching experiment was performed to confirm and calculate FRET efficiency—the rise in GFP intensity after rhodamine photobleaching in the background insignificant as compared to the ROI. The calculated FRET efficiency is 35%.

2.5.1.8 Imaging caspase-3 activation in HeLa and HEK-293 cells

Further, the versatility of the technology was demonstrated by detecting the activity of caspase-3 GFPspark in different cell lines, including HeLa and HEK-293. The same methodology was applied where HeLa and HEK-293 cells expressing caspase-3 GFPspark independently were induced to undergo apoptosis by STS (1 μM) treatment for 10 h and labeled by the Rh-VAD-FMK probe. In HeLa cells, a compounded (diffused and punctate) fluorescence pattern was observed in all three channels with a FRET efficiency of $32 \pm 2\%$ (Figure 2.15). On the contrary, HEK293 cells showed the diffused fluorescence pattern in all channels with a calculated FRET efficiency of $33 \pm 2\%$ (Figure 2.16).

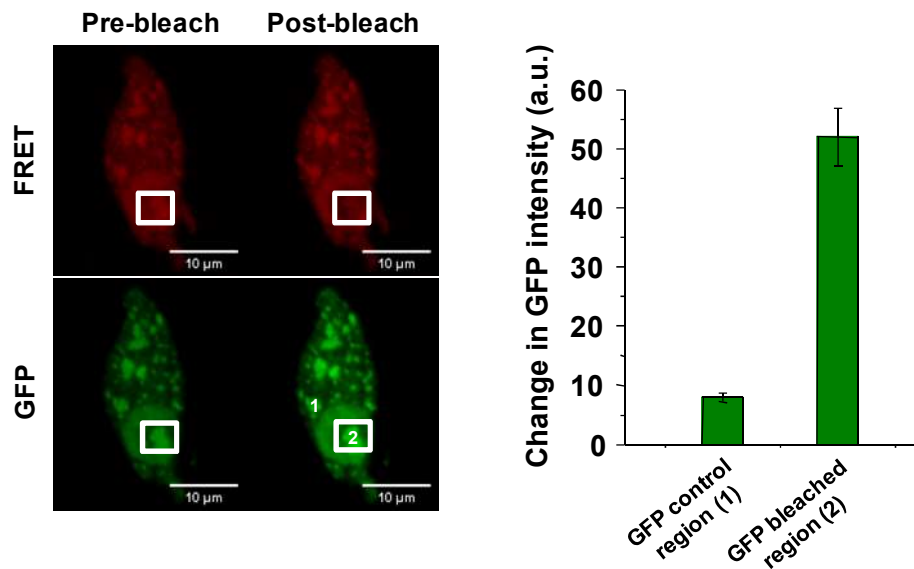


Figure 2.15 Specific detection of active caspase-3 in HeLa cells. Caspase-3 GFPspark (1 μ g) transfected HeLa cells were treated with STS (1 μ M) for 10 h. After 10 h of treatment, cells were labeled with the Rh-VAD-FMK probe (1 μ M) as described previously. Images were obtained in GFP and FRET channels. FRET validation between GFP and rhodamine fluorophore using the acceptor photobleaching method. Images were taken under GFP and FRET channels pre and post- rhodamine photobleaching in the ROI. The calculated FRET efficiency is $32 \pm 2\%$.

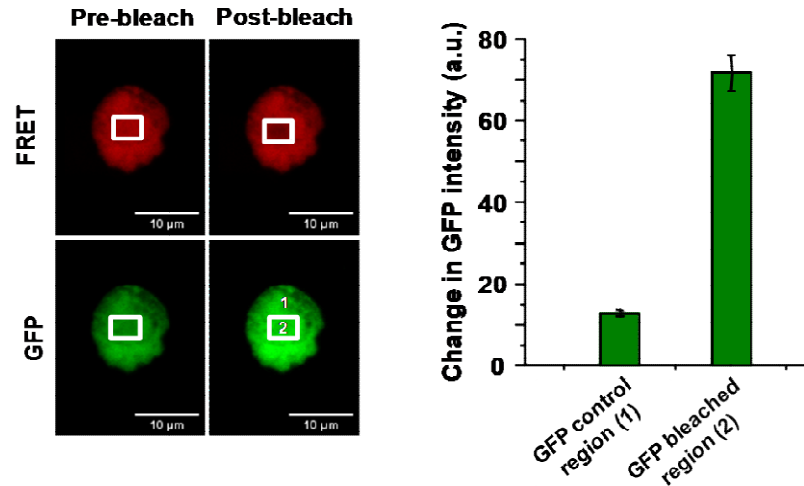


Figure 2.16 Specific detection of active caspase-3 GFPspark in HEK-293 cells. Caspase-3 GFPspark (1 μg) transfected in HEK-293 cells for 24 h and were treated with STS (1 μM) for 10 h. After 10 h of STS treatment, cells were labeled with the Rh-VAD-FMK probe (1 μM) as described previously. (a) Images were obtained in GFP and FRET channels. FRET validation between GFP and rhodamine fluorophore using the acceptor photobleaching method. Images were taken under GFP and FRET channels pre and post- rhodamine photobleaching in the ROI. (b) The rise in GFP intensity in the ROI is 72, and the background is 13. The calculated FRET efficiency is $33 \pm 2\%$.

2.5.1.9 Optimization of the time window of caspase-3 or -7 activation in HeLa cells

The time point of 10 h for STS treatment in HeLa cells was chosen based on the substrate-based reporter assay. The cleavage of the FRET pair substrate, for executioner caspases, i.e., cyan fluorescent protein (CFP)-DEVDR-yellow fluorescent protein (YFP), was monitored during the time course of 12 h in the CFP-DEVDR-YFP plasmid transfected HeLa cells. Disruption of the FRET signal was observed at 10 h time-point in the live-cell imaging indicative of the activation of executioner caspases (Figure 2.17).

2.5.1.10 Confirmation of cleaved caspase-3 by western blotting

The presence of cleaved caspase-3 p17 fragment in the immunoblotting assay was also observed at 18 and 24 h time points of STS (1 μM) treatment in HeLa cells lysate, ensuring the presence of active caspase-3 (Figure 2.18).

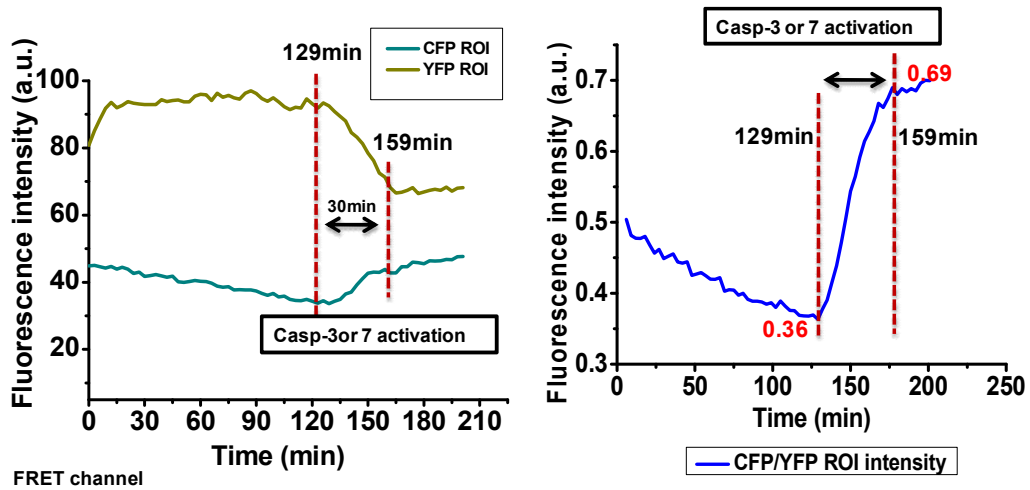


Figure 2.17 Time courses of cleavage for CFP-DEVDR-YFP plasmid in the HeLa cell line. Time is relative to the first frame taken after 8 h of STS treatment. (a) Fluorescence intensity of cyan fluorescent protein (CFP) and yellow fluorescent protein (YFP) in the CFP channel was plotted against time. (b) CFP to YFP intensity ratio was plotted against time. The percentage rise in the CFP/YFP intensity ratio was 47%. Rise in CFP/YFP intensity ratio is an indirect measure of caspase-3/7 activation.

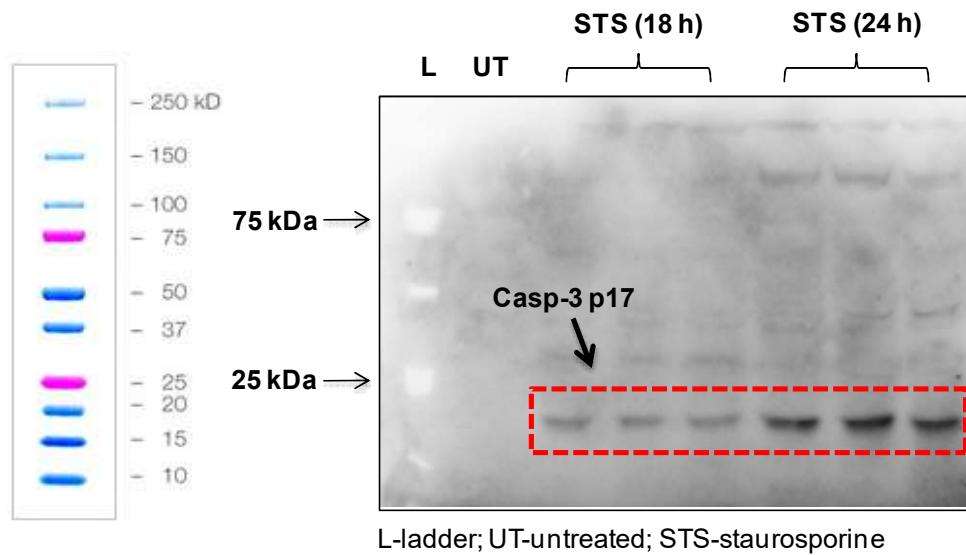


Figure 2.18 Western blot analysis shows the expression of cleaved caspase-3 p17 fragment after 18 and 24 h of STS (1 μ M) treatment in HeLa cells. Lysate loading was done in triplicates. The double-headed arrow is representing three lanes with the same sample.

2.6 Conclusion

Here, we disclose a simple but powerful method called “Activity-based Reporter Gene Technology (AbRGT)” for imaging of “active enzyme” in the live cell with an unprecedented specificity. The exquisite imaging of the target protease is achieved by taking advantage of both reporter gene technology and the synthetic chemistry (ABFP) method. By fusing a reporter tag (GFP fluorescent protein) to PoI followed by covalent labeling of PoI by an ABFP (acceptor) led to the in situ formation of the FRET pair. The non-specific labeling of the ABFP creates a highly specific FRET pair that reports only the activity of the target protease but not the other proteases in the cell. We have demonstrated that the AbRGT is a method that provides an opportunity to specifically image the function of any “active enzyme” in an intact fixed or live cell. We have validated our approach by demonstrating its applicability by specifically imaging the function of caspase-3 in the apoptosis signaling pathway, independently in three different cell lines (HeLa, HEK-293, and MCF-7).

2.7 Materials and methods

2.7.1 Reagents

Staurosporine drug (S5921) was purchased from Sigma. The Rh-VAD-FMK probe (ab65616) and the Rh-DEVD-FMK probe (ab65617) were procured from Abcam. TRAIL recombinant protein (RPA139Hu01) was obtained from Cloud Clone Corporation.

2.7.2 Expression and purification of recombinant human caspase-3

Transformation: Human recombinant caspase-3 (rcaspase-3) His-tag cloned gene in pET 23b vector (pET23b Casp-3 His-tag); (Addgene plasmid # 11821) was transformed in BL21 (DE3) strain of E.coli cells. For transformation, 1 μ L (100 ng) of plasmid was added in 25 μ L of competent BL21 (DE3) cells and kept in ice for 30 mins. After incubating it on ice for 30 mins, heat shock was given for 90 secs at 42 °C in a water bath. 950 μ L of *Luria-Bertani* (LB) medium was added and incubated at 37 °C for 1 h at the thermomixer, 400 rpm. The transformed cells were centrifuged at 4500 rpm for 5 mins. The pellet obtained after centrifugation was resuspended in 100 μ L LB and added on the LB agar plate containing ampicillin antibiotic. The LB agar plate with transformed cells was then kept at 37 °C, incubated for 12 h. After 12 h, a single colony was picked and added to a 5 ml culture for overexpression. **Overexpression of rcaspase-3:** The protein was overexpressed in BL21 (DE3) strain of E.coli cells (2 L culture) at 37 °C to an O.D of 0.6 before induction with 0.2 mM IPTG for 3 h at 30 °C. The cells were pelleted down at 6000 rpm for 10 mins at 4 °C and resuspended in lysis buffer containing 100 mM Tris-HCl, pH-8; 100 mM NaCl and 20 mM imidazole and lysed using a sonicator. After sonication, the sample was centrifuged for 30 mins at 20,000 rpm. **Purification of caspase-3 His-tag by affinity column chromatography using Ni-NTA column:** After removal of cellular debris, the supernatant was incubated with Ni-NTA column pre-equilibrated with buffer A (100 mM Tris-HCl; 100 mM NaCl and 20 mM imidazole). The column was washed with an 8-bed volume of buffer A twice. After incubating the column with buffer A, protein lysate was loaded in the Ni-NTA column. The column was incubated with protein lysate was then washed with 10 column volumes of buffer B (10 mM Tris-HCl; 500 mM NaCl 4, and 20 mM imidazole) twice. Protein was then eluted in 1 ml fractions with 6 ml of elution buffer, buffer C (50

mM Tris-HCl, pH-8; and 150 mM NaCl and 250 mM imidazole. Fractions were checked on SDS-PAGE for purity, followed by dialysis against buffer A. The protein was concentrated and stored at -80 °C.

2.7.3 MALDI- ToF analysis

The molecular mass of purified enzyme caspase-3 samples was analyzed in Linear High Mass mode in AB Sciex 4800 plus MALDI-ToF/ToF analyzer using 4000 Series Explorer software. The scanning range was between 10,000 Da and 40,000 Da. MALDI Matrix Preparation: 4 mg of dihydroxyacetone phosphate (DHAP) was dissolved in 150 μ L of ethanol (solution A). 4.5 mg of 1, 2 - diamino cyclohexane (DAHC) was dissolved in 200 μ L of milli-Q (solution B). Both the solutions were sonicated using a bath sonicator for 1 min and vortexed for another min. 50 μ L of solution B was mixed with solution A to yield solution C. Solution C was vortexed for one more minute to yield matrix mixture. MALDI Sample Preparation: Purified enzyme samples (100 μ M), 2% trifluoroacetic acid (TFA), and MALDI matrix (solution C) were mixed in a 1:1:1 ratio. The enzyme sample was then kept undisturbed. Samples were spotted on the MALDI plate upon crystallization and air-dried for 15 mins. The plate was then loaded and fired to get accurate molecular weight in the +1 state.

2.7.4 Michaelis-Menton kinetics assay

K_M and V_{max} of the rcaspase-3 were calculated using Michaelis Menton Kinetic Assay. The protease activity was determined in a colorimetric assay. The reaction mixture containing standard caspase assay buffer (20 mM PIPES, pH-7.5, 100 mM NaCl, 1 mM EDTA, 10 mM DTT, 0.1 (w/v) CHAPS, 10% sucrose, Caspase-3 (10 nM) with caspase substrate incorporating amino acid sequence DEVD conjugated to para-nitroaniline (DEVD-*p*NA) in increasing concentrations, 5 μ M, 10 μ M, 20 μ M, 40 μ M, 80 μ M, 160 μ M. The reaction mixture was incubated for 10 minutes at 37°C. Caspase activity was correlated with the cleavage after the second aspartate of the substrate DEVD-*p*NA and the amount of *p*NA released from DEVD-*p*NA. *p*NA release was monitored by absorbance at 405 nm. Substrate concentration was plotted against velocity, v , ($[C]/t$), and Michaelis Menton equation (given below) was used for the determination of K_M and V_{max} .

$$1/V = [K_M/V_{\max} [S] + 1/ V_{\max}]$$

Where V is the initial velocity, K_M (Michaelis constant) is the substrate concentration at $0.5 V_{\max}$, V_{\max} is the maximum velocity of the enzyme catalyzing the substrate, $[S]$ is the substrate concentration.

2.7.5 Determination of k_{cat} of caspase-3

k_{cat} of the enzyme can be calculated by determining the active enzyme concentration in the preparation of purified protein. For this purpose, Z-VAD-FMK, one of the widely known covalent inhibitors of pan-caspase, was used. For this assay, the caspase enzyme (10 nM) was incubated with varying concentrations of the inhibitor Z-VAD-FMK (50, 100, 200, 400, 800 nM) in standard caspase buffer for 30 min at 37 °C and then diluted into the caspase substrate DEVD-pNA (50 μ M). The release of pNA was monitored at 405 nm. The rate of hydrolysis (Y-axis) was plotted against inhibitor Z-VAD-FMK (X-axis) concentration. The total concentration of active enzyme was determined from the intercept of the X-axis. k_{cat} of the enzyme was calculated by using the following equation

$$k_{\text{cat}} = V_{\max} / [E]_T$$

k_{cat} is the turnover number, the amount of substrate catalyzed by the enzyme per second, V_{\max} is the maximum velocity, $[E]_T$ is the amount of active enzyme concentration.

2.7.6 Recombinant caspase-3 labeling by Rh-VAD-FMK probe

2 μ M of the purified recombinant caspase-3 was incubated with various concentrations of the (100, 500, and 2000 nM) for 30 mins at 37 °C. The samples were analyzed by SDS-PAGE, and active site labeling was visualized by scanning gels on a GE Typhoon flat-bed scanner (excitation/emission 561/605). For labeling of denatured caspase-3, purified caspase-3 was subjected to heating at 90°C for 30 mins followed by incubation with the Rh-VAD-FMK probe.

2.7.7 In-gel fluorescence assay

2.5 million Jurkat cells were seeded in 25 cm² flask, and the flask was kept in the cell incubator overnight. STS (1 μM) or vehicle dimethyl sulfoxide (DMSO) was added, followed by the addition of the Rh-VAD-FMK probe (1 μM). After 6 h, the cells were trypsinized, and the cell pellet was stored at -80 °C until further processing of cells. The cell pellet was thawed to room temperature, and 100 μL of 1X phosphate buffer saline (PBS) buffer was added to make cell suspension. Probe sonicator was used to lyse the cells (20 cycles ~ 20 secs). After the cell lysis procedure, the standards for protein assay were prepared from a stock solution of bovine serum albumin (BSA) of 0.25, 0.5, 0.75, 1.0, 1.50, and 2.0 mg. 25 μL of reagent A, 5 μL of the proteome, or standard solution, 200 μL of reagent B was mixed and incubated for 10 mins. The absorbance of the sample was measured at 650 nm. From the standard solution, the concentration of the unknown proteome was calculated. All the samples were adjusted to the protein concentration of 1 mg/ml. To 100 μL of proteome solution, 100 μl of sample buffer was added. The samples were loaded on to 18-well 12% Tris Gel. The gel was scanned with excitation and emission wavelength of 561 and 605 nm for the Rh-VAD-FMK probe. Image J software was used to integrate the band intensity.

2.7.8 Cell culture methods

MCF-7 cells borrowed from Dr. Mayurika Lahri's. HeLa and HEK-293 cells are borrowed from Dr. Siddhesh Kamat's laboratory, IISER Pune. MCF-7, HEK-293, and HeLa cells were cultured in Dulbecco's modified Eagle's medium (DMEM) (Gibco) supplemented with 10% fetal bovine serum (FBS) (Gibco), 100 mg/mL penicillin, and 100 mg/mL streptomycin (Gibco). Cells were maintained at a density of 1×10^6 cells in the T25 plate in a humidified atmosphere of 5% CO₂ at 37 °C.

2.7.9 Plasmids and transient transfection

The caspase-3 GFPspark plasmid (Cat: HG10050-ACG) was procured from Sino Biological. For transfection, cells were seeded in a 6-well plate at a density of 0.4 million cells/well. At 60–70% confluency, cells were transiently transfected for 24 h at 37 °C with

1 μg of the GFP tagged plasmid DNA construct and 5 μL of Lipofectamine 2000 (Invitrogen) according to the manufacturer's instructions. 24 h posttransfection, cells were visualized under a GFP filter for GFPspark expression under a fluorescence microscope at 10 \times magnification.

2.7.10 Labeling of active caspases in apoptotic cells by Rh-VAD-FMK probe

After 24 h of transfection, cells were treated with STS (1 μM) drug or TRAIL (1 $\mu\text{g}/\text{mL}$) for apoptotic induction and incubated for 2, 4, 6, and 8 h at 37 $^{\circ}\text{C}$ in a humidified atmosphere of 5% CO_2 . Cells were gently scraped off from the surface at the end of apoptotic induction and centrifuged at 3000 rpm for 5 min. The cell pellet was resuspended in 300 μL of fresh DMEM containing 1 μM of the RhVAD-FMK probe or the Rh-DEVD-FMK probe and incubated for an additional 2 h at 37 $^{\circ}\text{C}$ in a humidified atmosphere of 5% CO_2 . Cells were again centrifuged at 3000 rpm for 5 min, and the supernatant was decanted. Cells were washed with 1 \times PBS, thrice, and finally resuspended in 20 μL of 1 \times PBS. The cell suspension was put on a slide, and a coverslip was placed over it. It was left for air drying. Slides were then imaged for GFP, FRET, and rhodamine fluorescence signals under confocal microscopy.

2.7.11 Fluorescence imaging studies and FRET procedure

Images were collected on a Zeiss LSM710 confocal microscope with a 25 mW argon laser using Zen10 software. The laser was tuned to lines at 488 nm (excitation laser for GFP) and 561 nm (excitation laser for rhodamine). Cells were examined with a 40 \times 1.3 NA Zeiss oil immersion objective and 2.4 \times zoom. Images were collected in the three channels; the GFP channel, argon laser tuned at 488 nm with 2% intensity and fluorescence emission was collected in emission range of 490–550 nm; the Rh channel, argon laser tuned to 561 nm laser with 2% intensity and fluorescence emission was collected in the range 550–650 nm; and the FRET channel with excitation laser of the GFP channel and emission range of the rhodamine channel. Images were captured and processed using ImageJ software.

2.7.12 Acceptor photobleaching method

We used the acceptor photobleaching method to confirm FRET occurrence and also to calculate FRET efficiency. In this method, donor intensity (GFP) rises after acceptor (rhodamine) photobleaching manifests FRET occurrence. Cells were bleached for rhodamine fluorescence signals in the FRET channel at the region of interest (ROI), the area under the white box, with 100% intensity (561 nm) for 200 iterations. Fluorescence intensities pre- and postbleaching of rhodamine were determined, and change in GFP intensity after pre- and post-bleach was calculated. FRET efficiency was calculated using the equation mentioned below.⁴⁰ (D) is the donor intensity.

$$FRET\ efficiency = \frac{(D)_{post-bleach} - (D)_{pre-bleach}}{(D)_{post-bleach}}$$

2.7.13 Live-cell microscopy and image analysis

Cells were transferred to phenol red-free CO₂ independent medium (Invitrogen) with 10% FBS and 1% penicillin and streptomycin. Time-lapse imaging with Zeiss LSM710 confocal microscope at 60X magnification (frames every 3 mins) was captured over an 8-12 h time point. CFP and YFP intensity changes were observed.

2.7.14 Quantitative analysis

Corrected total cell fluorescence (CTCF) for each image in the GFP, FRET, and Rh channels were measured in the region of interest (ROI) using Image J software. The polygon selection was chosen to create the ROI, and the region next to the cell, which has no fluorescence, was chosen as a background. ROI was kept constant across all the channels for measurements. The image parameters like area, mean grey value, and integrated density within the ROI and the background were measured using Image J only. The CTCF of each image was calculated using equation (1). A graph was plotted to compare and contrast the fluorescence intensities across the three channels using GraphPad Prism software. CTCF = Integrated density – (Area of the selected cell X Mean fluorescence of background readings) [Equation-1].

2.7.15 STED imaging

Stimulated emission depletion (STED) microscopy can obtain super-resolution images with a theoretical resolution of approximately 20 nm that also surpasses the diffraction limit of confocal microscopy. Images were acquired on Leica TCS –STED-3X nanoscope with a 100x, NA 1.4 oil objective using Leica Application Suite X (LAS X) software in the STED mode. Caspase-3 GFPspark transfected MCF-7 fixed cells labeled by the Rh-VAD-FMK probe were excited with the excitation wavelength of 488 nm and 561 nm of a pulsed white light laser (WLL) with a laser intensity of 10 %. HyD gated detectors were used to collect the emission wavelength with the appropriate bandwidth for the respective channels. The STED acquisition was made using the following sequence, and the images were captured between frames; In a first sequence, GFP channel, GFP was excited with 488 nm, depleted with STED depletion laser of 775 nm (laser intensity-85%), and the final emission was collected in the range 490- 550 nm; In a second sequence, rhodamine channel, rhodamine was excited with 561 nm, depleted with STED laser 775 nm (laser intensity- 70%) and the final emission was collected in the range 570- 670 nm; In the third sequence, FRET channel, GFP was excited with 488 nm, and the final emission was collected in the range of rhodamine channel. Images were processed using Image J (Fiji) software.

2.7.16 Immunoblotting

HeLa cells were seeded in 6 wells plate at a density of 0.6 million. At 70% confluence, cells were treated with 1 μ M STS and incubated in a humidified atmosphere of 5% CO₂/95% air. Cells were then lysed in hypotonic lysis buffer [50 mM piperazine-N,N'-bis(2-ethanesulfonic acid) PIPES, pH 7.4; 10 mM KCl; 5 mM MgCl₂; 2 mM ethylenediaminetetraacetic acid (EDTA); 4 mM dithiothreitol (DTT)] after 18 h and 24 h of STS treatment. Total protein lysate was extracted and subjected to 12% SDS-PAGE. Proteins were then transferred to polyvinylidene difluoride (PVDF) membrane and subsequently probed with anti-caspase-3 Asp175 antibody (Abcam). Immunoreactive bands were then visualized by enhanced chemiluminescence of horseradish peroxidase (HRP) substrate according to the manufacturer's instructions.

2.7.17 Plasmid information

S.No.	Plasmid Name	Plasmid Backbone	Source	Addgene Vector db No	Insert source/name	Gene bank acc No
1.	pCMV3-CASP-3-GFPspark	pCMV3-C-GFPspark	SinoBiological	Not applicable	<i>H. sapiens</i> (human)	NM_004346.3
2.	pET23b-Casp3-His	pET23b	Addgene	Plasmid #11821	<i>H. sapiens</i> (human)	Not mentioned
3.	C5V	pEGFP C1	Addgene	Plasmid #26394	Not mentioned	Not mentioned
4.	pECFP-DEVDR-Venus	pECFP-C1	Addgene	Plasmid #24537	Synthetic	Not mentioned

Table 1: Table representing the plasmids information.

2.8 References

- 1 Matrisian, L. M. & Hogan, B. L. Growth factor-regulated proteases and extra cellular matrix remodeling during mamlian development. *Curr. Top. Dev. Biol.* **24**, 219-259 (1990).
- 2 Riewald, M. & Ruf, W. Mechanistic coupling of protease signaling and initiation of coagulation by tissue factor. *Proc. Natl. Acad. Sci. U.S.A.* **98**, 7742-7747 (2001).
- 3 Alnemri, E. S. Mammalian cell death proteases: a family of highly conserved aspartate specific cysteine proteases. *J. Cell. Biochem.* **64**, 33-42 (1997).
- 4 van Kempen, L. C., de Visser, K. E. & Coussens, L. M. Inflammation, proteases and cancer. *Eur. J. Cancer* **42**, 728-734 (2006).
- 5 Abdel-Rahman, H. M. *et al.* Design of inhibitors against HIV, HTLV-I, and Plasmodium falciparum aspartic proteases. *Biol. Chem.* **385**, 1035-1039 (2004).
- 6 Pandey, A. & Mann, M. Proteomics to study genes and genomes. *Nature* **405**, 837-846 (2000).
- 7 Liu, Y., Patricelli, M. P. & Cravatt, B. F. Activity-based protein profiling: the serine hydrolases. *Proc. Natl. Acad. Sci. U.S.A.* **96**, 14694-14699 (1999).
- 8 Weissleder, R. & Ntziachristos, V. Shedding light onto live molecular targets. *Nat. Med.* **9**, 123-128 (2003).
- 9 Blum, G. *et al.* Dynamic imaging of protease activity with fluorescently quenched activity-based probes. *Nat. Chem. Biol.* **1**, 203-209 (2005).
- 10 Jessani, N. *et al.* Carcinoma and stromal enzyme activity profiles associated with breast tumor growth in vivo. *Proc. Natl. Acad. Sci. U.S.A.* **101**, 13756-13761 (2004).
- 11 Berger, A. B., Vitorino, P. M. & Bogyo, M. Activity-based protein profiling. *Am J Pharmacogenomics* **4**, 371-381 (2004).
- 12 Mitra, R. D., Silva, C. M. & Youvan, D. C. Fluorescence resonance energy transfer between blue-emitting and red-shifted excitation derivatives of the green fluorescent protein. *Gene* **173**, 13-17 (1996).
- 13 Bullok, K. & Piwnica-Worms, D. Synthesis and characterization of a small, membrane-permeant, caspase-activatable far-red fluorescent peptide for imaging apoptosis. *J. Med. Chem.* **48**, 5404-5407 (2005).
- 14 Sexton, K. B., Witte, M. D., Blum, G. & Bogyo, M. Design of cell-permeable, fluorescent activity-based probes for the lysosomal cysteine protease asparaginyl endopeptidase (AEP)/legumain. *Bioorganic Med. Chem. Lett.* **17**, 649-653 (2007).
- 15 Edgington, L. E. *et al.* Noninvasive optical imaging of apoptosis by caspase-targeted activity-based probes. *Nat. Med.* **15**, 967 (2009).
- 16 Bullok, K. E. *et al.* Biochemical and in vivo characterization of a small, membrane-permeant, caspase-activatable far-red fluorescent peptide for imaging apoptosis. *Biochemistry* **46**, 4055-4065 (2007).

- 17 Hoffmann, C. *et al.* A FLAsH-based FRET approach to determine G protein–coupled
receptor activation in living cells. *Nat. Methods* **2**, 171-176 (2005).
- 18 Wang, X. The expanding role of mitochondria in apoptosis. *Genes Dev.* **15**, 2922-
2933 (2001).
- 19 Schulze-Osthoff, K., Ferrari, D., Los, M., Wesselborg, S. & Peter, M. E. Apoptosis
signaling by death receptors. *Eur. J. Biochem.* **254**, 439-459 (1998).
- 20 Fulda, S. & Debatin, K.-M. Extrinsic versus intrinsic apoptosis pathways in
anticancer chemotherapy. *Oncogene* **25**, 4798-4811 (2006).
- 21 Loreto, C. *et al.* The role of intrinsic pathway in apoptosis activation and
progression in Peyronie’s disease. *BioMed Res. Int.* **2014** (2014).
- 22 Rotonda, J. *et al.* The three-dimensional structure of apopain/CPP32, a key mediator
of apoptosis. *Nat. Struct. Biol.* **3**, 619-625 (1996).
- 23 Suita, H., Shinomiya, T. & Nagahara, Y. Caspase-6 induces 7A6 antigen
localization to mitochondria during FAS-induced apoptosis of jurkat cells.
Anticancer Res. **37**, 1697-1704 (2017).
- 24 Stennicke, H. R. & Salvesen, G. S. Caspases: preparation and characterization.
Methods **17**, 313-319 (1999).
- 25 Jänicke, R. U., Sprengart, M. L., Wati, M. R. & Porter, A. G. Caspase-3 is required
for DNA fragmentation and morphological changes associated with apoptosis. *J.*
Biol. Chem. **273**, 9357-9360 (1998).
- 26 Salvesen, G. S. & Dixit, V. M. Caspase activation: the induced-proximity model.
Proc. Natl. Acad. Sci. U.S.A. **96**, 10964-10967 (1999).
- 27 Bertrand, R., Solary, E., O'Connor, P., Kohn, K. W. & Pommier, Y. Induction of a
common pathway of apoptosis by staurosporine. *Exp. Cell Res.* **211**, 314-321
(1994).
- 28 Jacobsen, M., Weil, M. & Raff, M. C. Role of Ced-3/ICE-family proteases in
staurosporine-induced programmed cell death. *J. Cell Biol.* **133**, 1041-1051 (1996).
- 29 Walczak, H. *et al.* Tumorcidal activity of tumor necrosis factor–related apoptosis–
inducing ligand in vivo. *Nat. Med.* **5**, 157-163 (1999).
- 30 Jo, M. *et al.* Apoptosis induced in normal human hepatocytes by tumor necrosis
factor-related apoptosis-inducing ligand. *Nat. Med.* **6**, 564-567 (2000).
- 31 Berger, A. B., Sexton, K. B. & Bogyo, M. Commonly used caspase inhibitors
designed based on substrate specificity profiles lack selectivity. *Cell Res.* **16**, 961-
963 (2006).
- 32 Samali, A., Zhivotovsky, B., Jones, D. P. & Orrenius, S. Detection of pro-caspase-3
in cytosol and mitochondria of various tissues. *FEBS Lett.* **431**, 167-169 (1998).
- 33 Mancini, M. *et al.* The caspase-3 precursor has a cytosolic and mitochondrial
distribution: implications for apoptotic signaling. *J. Cell Biol.* **140**, 1485-1495
(1998).

- 34 Böing, A. *et al.* Active caspase-3 is removed from cells by release of caspase-3-enriched vesicles. *Biochim Biophys Acta Mol Cell Res* **1833**, 1844-1852 (2013).
- 35 Hein, B., Willig, K. I. & Hell, S. W. Stimulated emission depletion (STED) nanoscopy of a fluorescent protein-labeled organelle inside a living cell. *Proc. Natl. Acad. Sci. U.S.A.* **105**, 14271-14276 (2008).
- 36 Böhm, C. *et al.* SorLA signaling by regulated intramembrane proteolysis. *J. Biol. Chem.* **281**, 14547-14553 (2006).
- 37 Szaba Jr, G., Pine, P. S., Weaver, J. L., Kasari, M. & Aszalos, A. Epitope mapping by photobleaching fluorescence resonance energy transfer measurements using a laser scanning microscope system. *Biophys. J.* **61**, 661-670 (1992).
- 38 Bastiaens, P. & Jovin, T. M. Microspectroscopic imaging tracks the intracellular processing of a signal transduction protein: fluorescent-labeled protein kinase C beta I. *Proc. Natl. Acad. Sci. U.S.A.* **93**, 8407-8412 (1996).
- 39 Albeck, J. G. *et al.* Quantitative analysis of pathways controlling extrinsic apoptosis in single cells. *Mol. Cell* **30**, 11-25 (2008).
- 40 Gordon, G. W., Berry, G., Liang, X. H., Levine, B. & Herman, B. Quantitative fluorescence resonance energy transfer measurements using fluorescence microscopy. *Biophys. J.* **74**, 2702-2713 (1998).

Chapter 3

Applications of Activity-based Reporter Gene Technology (AbRGT)

3.1 Introduction

The inhibitors that are capable of blocking protease activity can be potential drug candidates and hence beneficial for testing drug targets.^{1,2} Substrate-based probes have shown applications for imaging of protease activity in cells.^{1,2} Similarly activity-based fluorescent probes (ABFP) is also been utilized for the imaging of protease. Poreba, Marcin, *et al.* have utilized ABFP for imaging cathepsin L in breast cancer cells.³ It is also utilized for the screening of protease inhibitors.

Methods that can image protease activity has shown severa

Herein, we demonstrate the different applications of AbRGT. It can be used as a tool to screen inhibitors of protease. The method can be applied to study the activation of any protease-of-interest (PoI). It can also be utilized to image the “active-state” of a protease, in an unknown signaling pathway, in the native cellular environment.

3.2 Results

3.2.1 Utilization of AbRGT for inhibitors screening

Herein, we demonstrate the application of AbRGT in screening drug targets for a protease. To show that the method can be employed for screening purposes, we have carried out a proof-of-concept inhibitor screening experiment. We chose to screen inhibitors for caspase-3 as over-activation of caspase-3 leads to several diseases such as acute neurological diseases,³ Huntington disease,⁴ Parkinson’s disease,⁵ Alzheimer’s disease,⁶ etc., and hence serves as a great target. For our studies, we chose Z-VAD-FMK^{7,8} and Q-VD-OPh⁹ (pan-caspase inhibitors) because both of these inhibitors have been shown to covalently modify the active site of caspase-3 and other cysteine proteases. Also, the substrate scope of these two inhibitors is markedly different because of their sequence (VAD vs. VD) and the warhead functionalities (FMK vs. OPh), therefore serving as excellent inhibitors to validate the technology. Fluorescence imaging studies of the STS (1 μ M) treated caspase-3 GFPspark overexpressing MCF-7 cells were carried out in the presence and absence [Figure 3.1 (i) and (iii)] of the Z-VAD-FMK inhibitor (50 μ M) and also in the absence of the Rh-

VAD-FMK probe [Figure 3.1 (ii)]. The fluorescence signal in the FRET channel was effectively suppressed in the presence of the Z-VAD-FMK inhibitor (50 μ M) because both the probe and inhibitor contain the identical warhead (FMK) and recognition sequence (VAD) and hence would compete for covalent labeling of the same target. The inhibitor was added 50-fold excess (50 μ M) compared to the Rh-VAD-FMK probe (1 μ M), all active cysteine proteases, including caspase-3 GFPspark protease, were labeled by the inhibitor, thus abolishing the formation of the in situ FRET pair. However, in the presence of the Q-VD-Oph inhibitor (50 μ M), the FRET signal was found to be diminished, but definite punctate labeling was still detected in the Rh channel, indicating the cross-labeling of proteases other than caspase3 GFPspark by the Rh-VAD-FMK probe [Figure 3.1 (iv)]. Also, the fluorescence signal in the GFP channel did not overlap with the Rh channel. Unlike the Z-VAD-FMK inhibitor, the Q-VD-Oph inhibitor did not abolish the signal in the Rh channel. These results suggest that the substrate preference of the Q-VD-Oph inhibitor is different compared to the Z-VAD-FMK inhibitor. However, both the compounds efficiently inhibited the activity of caspase-3 GFPspark as apparent from total signal loss in the FRET channel. The CTCF of each image in GFP, FRET, and Rh channels in Figure 3.1 is calculated using ImageJ software (Figure 3.2).

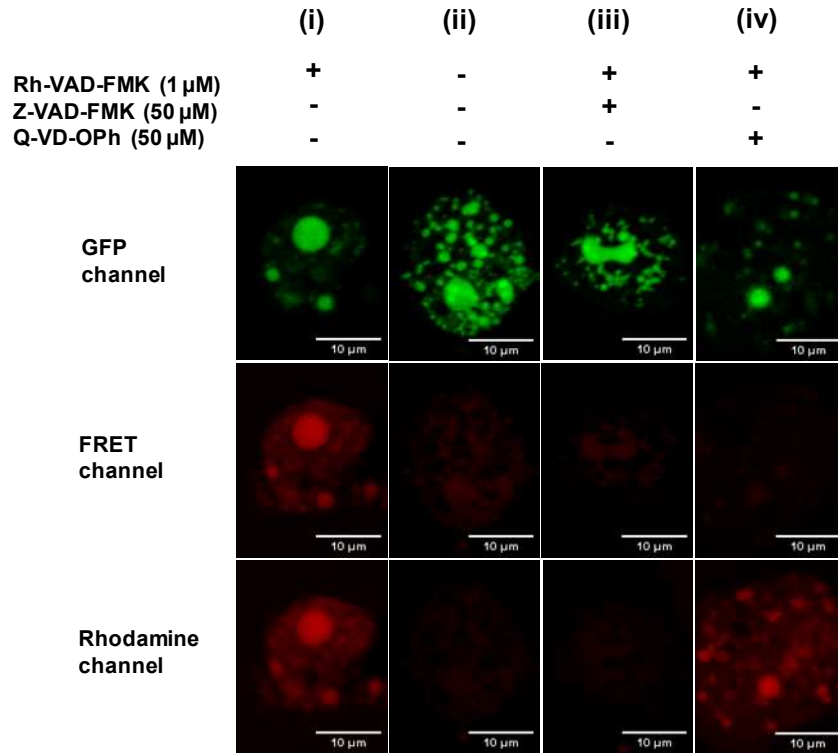


Figure 3.1 Confocal microscopy images of MCF-7 cells in GFP, FRET, and rhodamine channels. Caspase-3 GFPspark transfected MCF-7 cells were treated with STS for 4 h and labeled (i) with or (ii) without the Rh-VAD-FMK probe. Cells were pre-treated with (iii) the Z-VAD-FMK inhibitor (50 μ M) and (iv) Q-VD-OPh (50 μ M) pan-caspase inhibitors 1 h before the Rh-VAD-FMK probe labeling. Scale bar, 10 μ m.

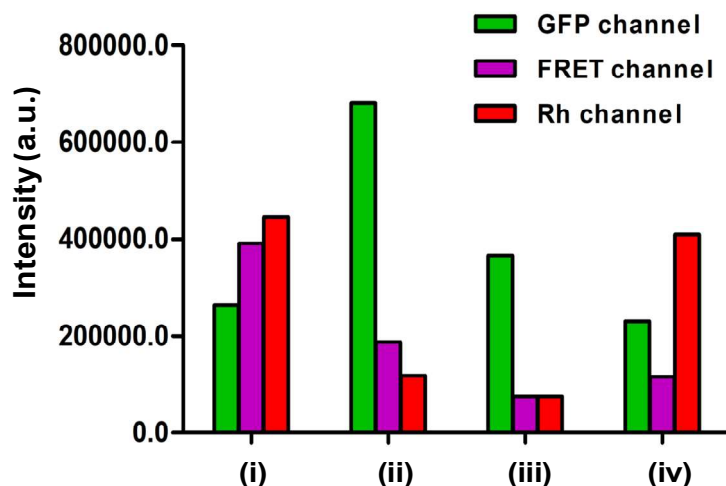


Figure 3.2 CTCF is calculated in GFP, FRET, and Rh channels for each image in (Figure 3.1) using ImageJ software.

3.2.2 Specific imaging of other caspases by AbRGT

Previously, AbRGT was demonstrated by using caspase-3 GFPspark as a target PoI. To further show the AbRGT can be applied to any PoI, we chose to image the specific activation of other proteases, caspase-7 (executioner caspase) and caspase-8, and -9 (initiator caspases), in the apoptosis signaling pathway.

3.2.2.1 Specific imaging of caspase-7 activation in the apoptosis pathway

Procaspase-7 is an executioner caspase in the apoptosis pathway, synthesized as a 35 kDa zymogen, primarily localized to cytoplasm.¹⁰ The procaspase-7 constitutes of a propeptide followed by a large subunit p20 (blue), linker sequence, and the small subunit p10 (green). The processing of procaspase-7 involves the cleavage after Asp₂₃ by initiator caspases resulting in the removal of the propeptide. The second cleavage after Asp₁₉₈ and Asp₂₀₆ leads to the subsequent removal of the linker sequence. The p20 and p10 subunit assemble to form a dimer that creates an active site on each site of the mature caspase-7 (Figure 3.3).^{11,12}

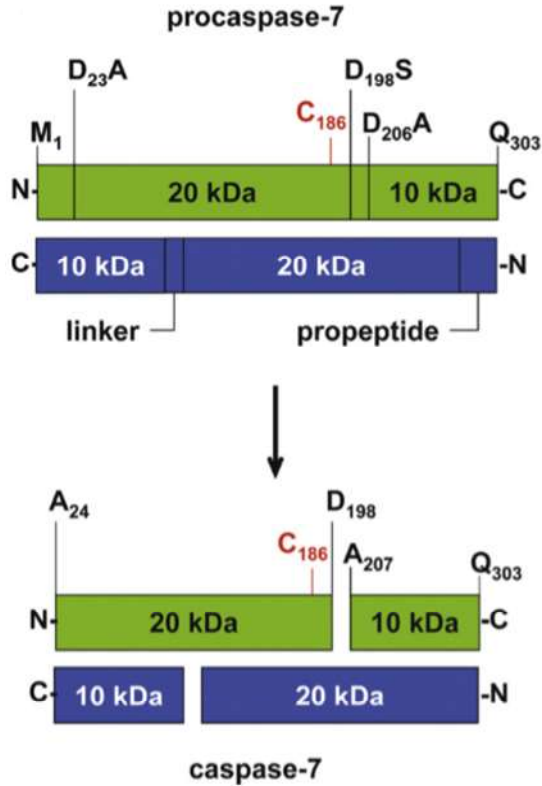


Figure 3.3 Schematic representation of procaspase-7 processing to active caspase-7. Schematic representation of the procaspase-7 and active caspase-7 homodimer (shown in green and blue, respectively). The procaspase-7 constitutes of 303 amino acids. (M_1) and (Q_{303}) indicates the identity and position of the first and last amino acid, respectively, in the amino acid sequence of procaspase-7. The active site cysteine residue Cys186 is indicated in red. The procaspase-7 is proteolytically cleaved by initiator caspases after Asp₂₃, localized between the propeptide and the large p20 subunit. Subsequent cleavage after Asp₁₉₈ and Asp₂₀₆ results in the removal of the linker region between the p20 and p10 subunits. Removal of the propeptide and linker sequences by proteolytic cleavage leads to the generation of p20 and p10 subunits that assemble to form the active caspase-7 homodimer. Adapted with permission from reference (11). Copyright © 2009 Elsevier.

To visualize the “active-state” of caspase-7, standard AbRGT methodology was applied. Exogenously expressed caspase-7 GFPspark in MCF-7 cells (MCF-7/casp-7 GFPspark) was triggered to undergo apoptosis and labeled by the Rh-VAD-FMK probe. The GFP channel manifests punctate morphology [Figure 3.4a (i)] similar to caspase-9 GFPspark [Figure 3.4b (i)]. The fluorescence signal in the FRET channel represented the presence of active caspase-7 GFPspark and was confirmed using the acceptor photobleaching experiment with calculated FRET efficiency of $32 \pm 2\%$ [Figure 3.6 (a and b)].

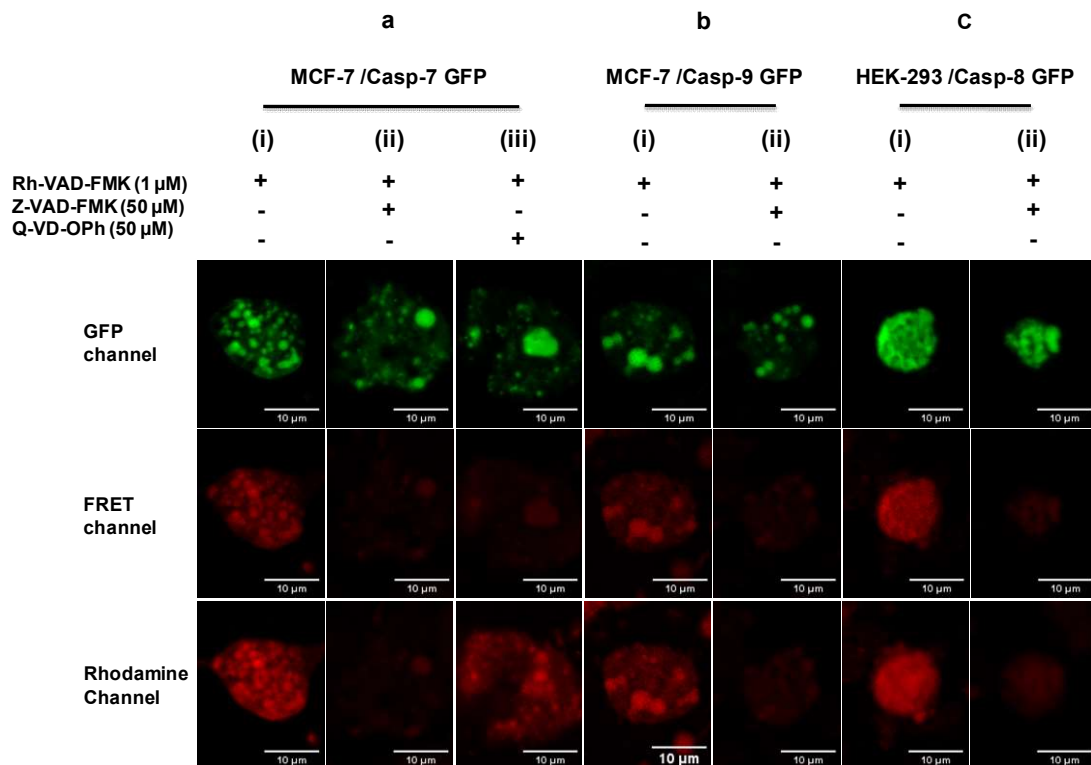


Figure 3.4 Confocal images of MCF-7 cells in GFP, FRET, and Rh channels. Caspase-7 GFPspark transfected MCF-7 cells were treated with STS (1 μ M) for 6 h and labeled (a) (i) by the Rh-VAD-FMK probe (1 μ M). Cells were pre-treated (a) (ii) with the Z-VAD-FMK inhibitor (50 μ M) or (a) (iii) Q-VD-OPh (50 μ M) pan-caspase inhibitors 1 h before the Rh-VAD-FMK probe labeling. Caspase-9 GFPspark transfected MCF-7 cells were treated with STS (1 μ M) for 4 h and labeled (b) (i) by the Rh-VAD-FMK probe (1 μ M). Cells were pre-treated (b) (ii) with the Z-VAD-FMK inhibitor (50 μ M) 1 h before the Rh-VAD-FMK probe labeling. Caspase-8 GFPspark transfected HEK-293 cells were treated with TRAIL (1 μ g/mL) for 5 h and labeled (c) (i) by the Rh-VAD-FMK probe. Cells were pre-treated (c) (ii) with the Z-VAD-FMK inhibitor (50 μ M) 1 h before the Rh-VAD-FMK probe labeling. Scale bar, 10 μ m.

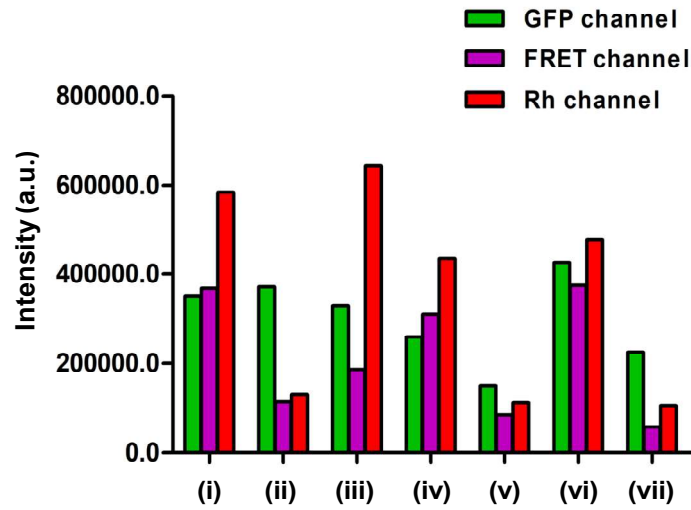


Figure 3.5 CTCF is calculated in GFP, FRET, and Rh channels for each image in (Figure 3.4) using Image J software.

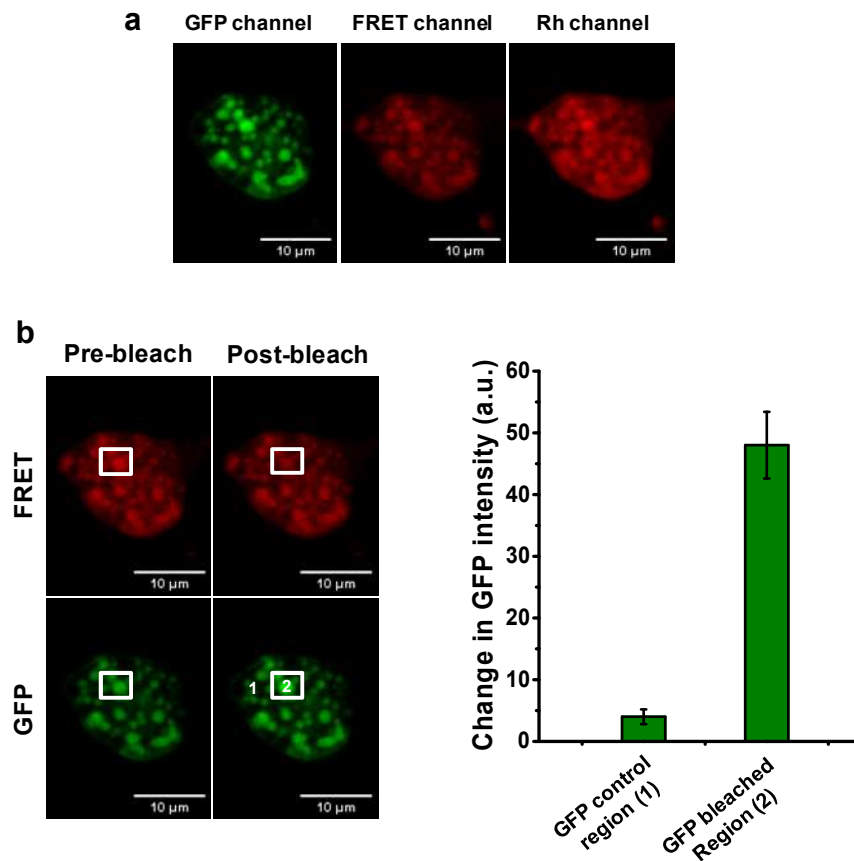
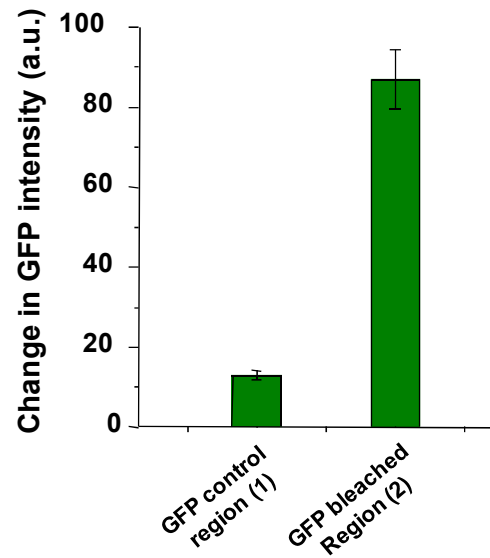
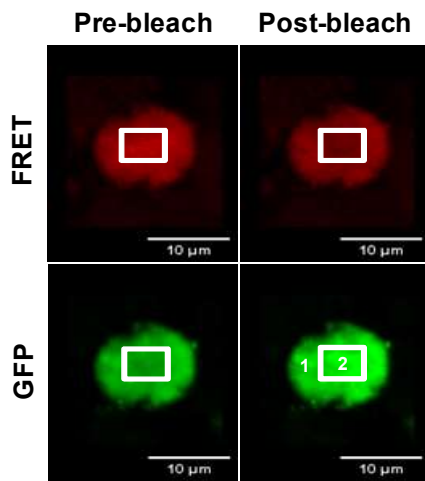
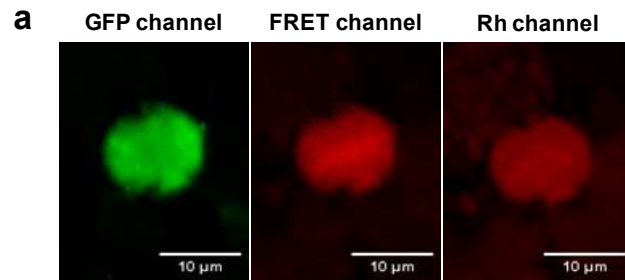


Figure 3.6 Specific detection of caspase-7 GFPspark in MCF-7 cells. Caspase-7 GFPspark (1 μ g) transfected MCF-7 cells were treated with 1 μ M of STS for 5 h and labeled with the Rh-VAD-FMK probe (1 μ M). Cells were fixed, and the fluorescence signal was collected in (a) GFP, FRET, and Rh channels. (b) Acceptor photobleaching was done to confirm the FRET signal, as described previously. Bar graph representing a rise in GFP intensity in ROI after rhodamine photobleaching. FRET efficiency was calculated to be $32 \pm 2\%$.

The fluorescence signal in the Rh channel depicts the cross-labeling of other cysteine proteases, including endogenous caspase-7 by the Rh-VAD-FMK probe. Pretreatment of the cells with the Z-VAD-FMK inhibitor (50 μ M) abolished the fluorescence signal in the FRET and Rh channels [Figure 3.4a (ii)]. However, pretreatment of the cells with the Q-VD-OPh inhibitor (50 μ M) indeed abolished the fluorescence signal in the FRET channel but not in the Rh channel. Significant punctate labeling was seen in the Rh channel [Figure 3.4a (iii)], indicating the evidence of cross-labeling by the Rh-VAD-FMK probe. Similar results were obtained for HEK-293 cells as well [Figure 3.7 (a and b)].



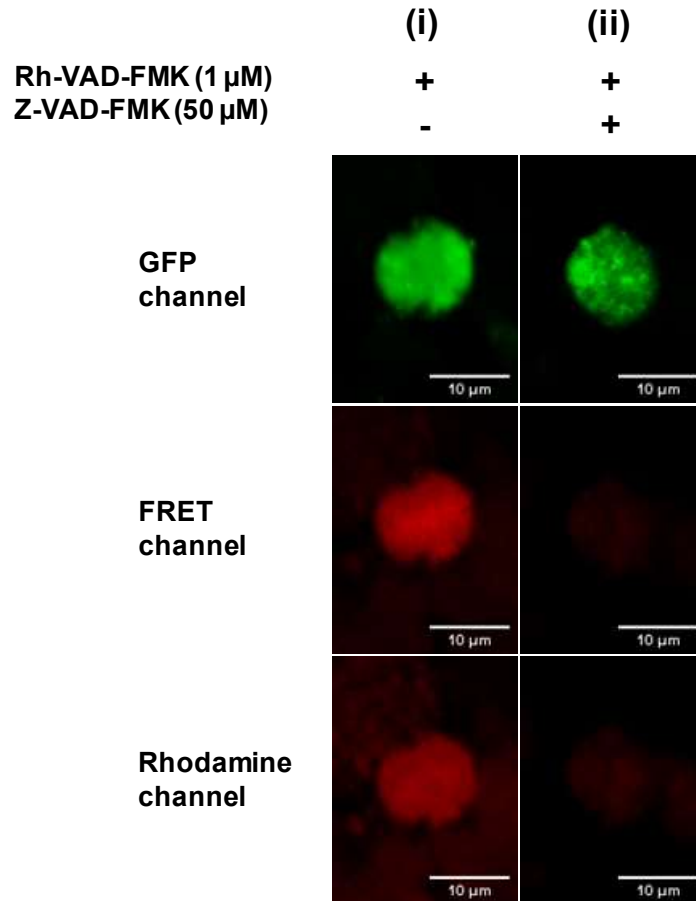


Figure 3.7 Specific detection of caspase-7 GFPspark in HEK-293 cells. Caspase-7 GFPspark (1 μ g) transfected HEK-293 cells were treated with STS (1 μ M) for 10 h and labeled with the Rh-VAD-FMK probe (1 μ M) for 2 h. Cells were washed, fixed, and the fluorescence signal was collected in (a) GFP, FRET, and Rh channels. (b) Acceptor photobleaching was done to confirm the FRET signal, as described previously. Bar graph representing the rise in GFP intensity in ROI after rhodamine photobleaching. FRET efficiency was calculated to be $33 \pm 2\%$. (b) The fluorescence signal was collected in GFP, FRET, and Rh channels in the (i) absence or (ii) presence of inhibitor Z-VAD-FMK (50 μ M).

3.2.2.2 Specific imaging of caspase-9 activation in the apoptosis pathway

Similarly, the AbRGT approach was also applied to monitor the specific activation of initiator caspases -9. Procaspace-9 is synthesized as a 46 kDa zymogen and is known to be localized in the mitochondria¹³ and nucleus.¹⁴ It is constituted of three domains, the N-terminal prodomain followed by a large p20 (~20 kD) and a small subunit p10 (~20 kD).¹⁵ The large and small subunit forms the catalytic domain known as the large subunit catalytic

domain (LSCD) and the small subunit catalytic domain (SSCD). The prodomain contains the caspase activation and recruitment domains (CARD) domain, also known as the adaptor domain. Proteolytic processing is not required for the activation of procaspase-9 as it is activated upon interaction with the endogenous cytosolic complex, apoptotic protease activating factor 1 (Apaf1)/cyto-*c*.¹⁶

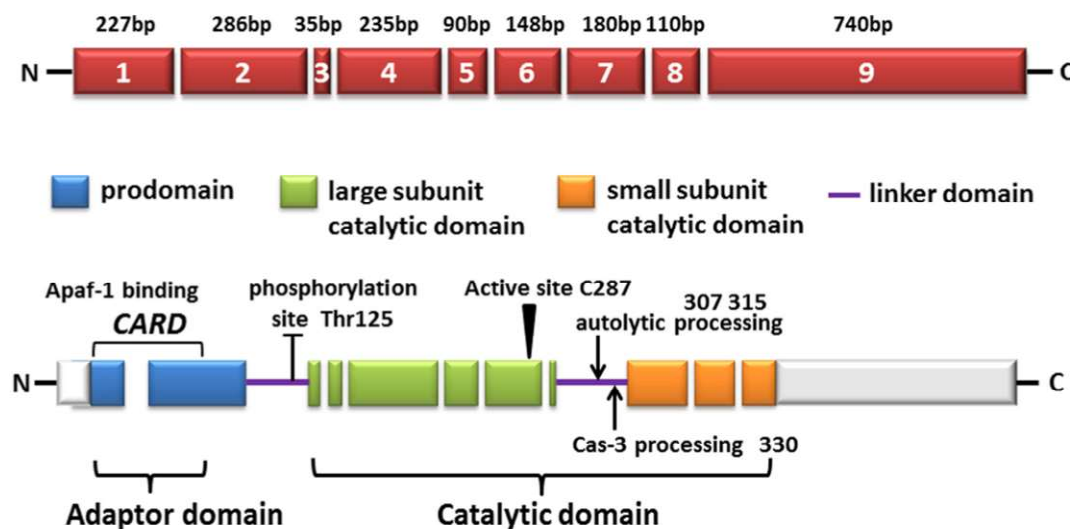


Figure 3.8 Schematic representation of human caspase-9. Exons are numbered from 1 to 9 inside the red boxes, and their respective lengths are indicated on the top. The predicted amino acid structure is represented with the translated regions shown in different colors. The transcribed but untranslated exon regions are shown as white boxes. The pro-domain containing the caspase activation and recruitment domains (CARD) domain, also called the adaptor domain, is shown as blue boxes. The large subunit catalytic domain (LSCD) and the small subunit catalytic domain (SSCD) are shown as green and oranges boxes, respectively. Both LSCD and SSCD form the catalytic domain. The linker domain (LD) is shown as a purple line. The amino acid residues location involved in the proteolytic processing of the procaspase-9 molecule and the post-translation modification sites are also indicated. Adapted with permission from reference (17). Copyright © 2017 Li *et al.*

Apoptosis was induced in MCF-7 and HEK-293 cells overexpressing caspase-9 GFPspark independently and labeled by the Rh-VAD-FMK probe. The signal in the FRET channel implies the specific activation of caspase-9 GFPspark [Figure 3.4b (i)]. The calculated FRET efficiencies in MCF-7 and HEK-293 cells are $30 \pm 1\%$ and $35 \pm 2\%$, respectively [Figures 3.9 and 3.10 (a and b)]. As expected, pretreatment cells with the Z-VAD-FMK inhibitor ($50 \mu\text{M}$) suppressed the fluorescence signal in FRET and Rh channels [Figure 3.4b (ii)].

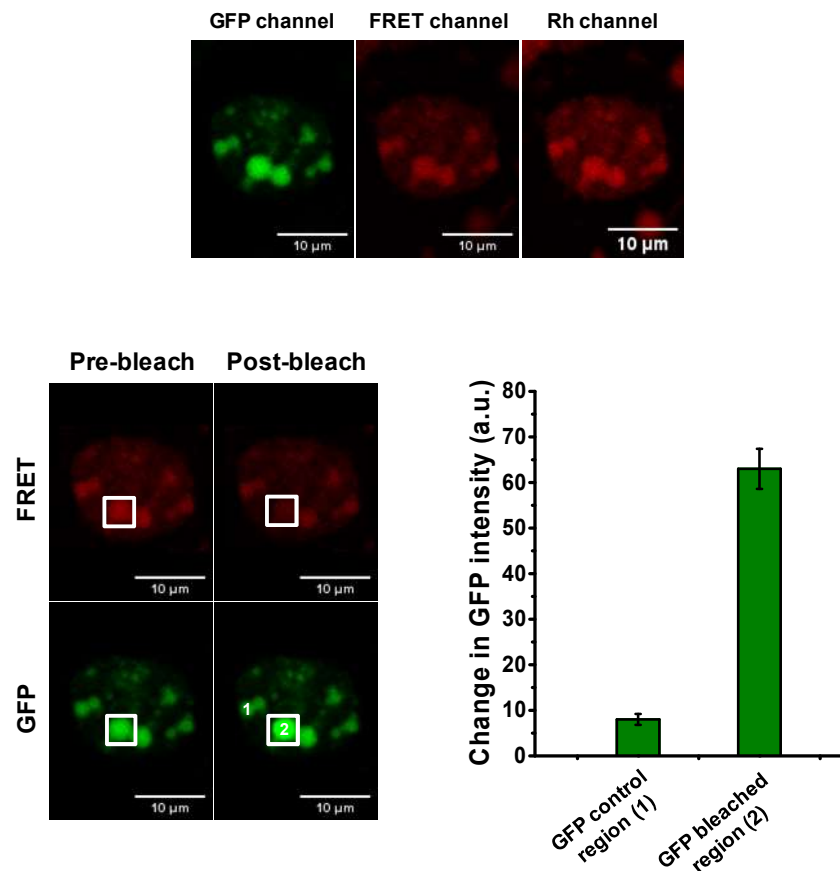
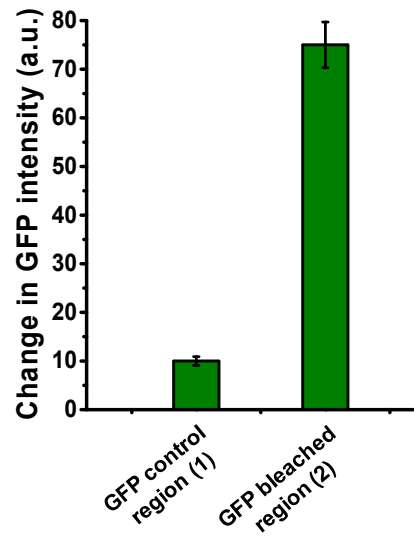
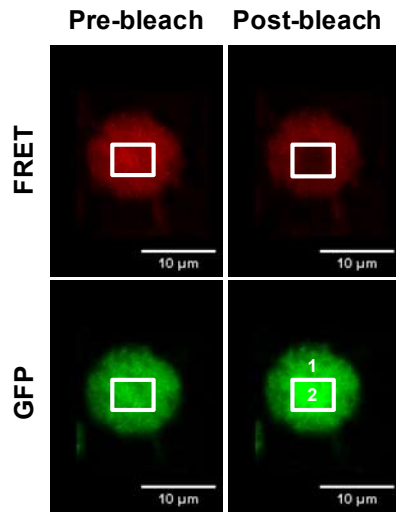
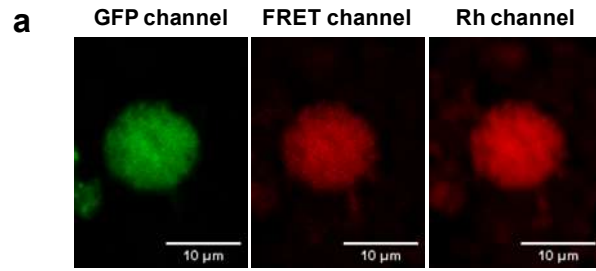


Figure 3.9 Specific detection of Caspase-9 GFPspark in MCF-7 cells. Caspase-9 GFPspark (1 μg) transfected MCF-7 cells were treated with STS (1 μM) for 4 h and labeled with the Rh-VAD-FMK probe (1 μM). Cells were fixed, and the fluorescence signal was collected in GFP, FRET, and Rh channels. Acceptor photobleaching was done to confirm the FRET signal, as described previously. Bar graph representing a rise in GFP intensity in ROI after rhodamine photobleaching. FRET efficiency was calculated to be $30 \pm 1\%$.



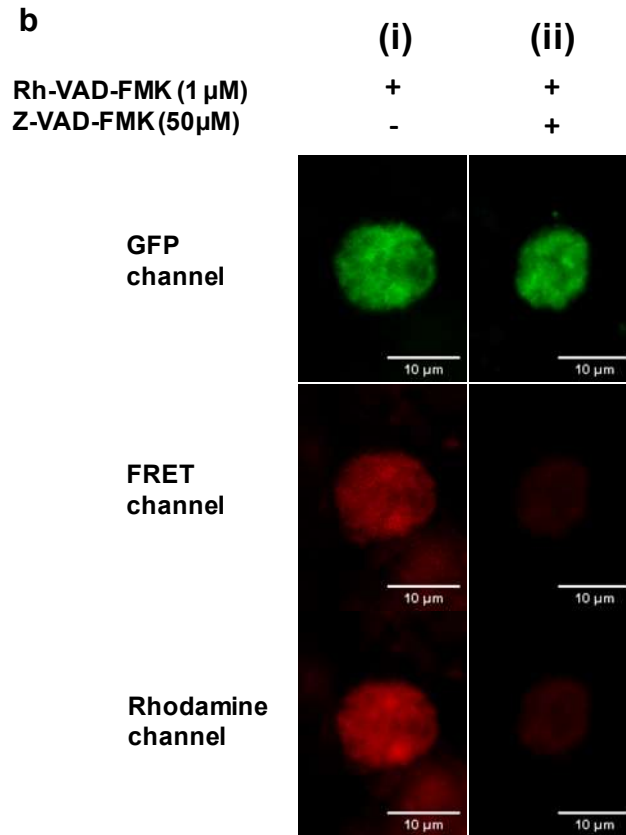


Figure 3.10 Specific detection of caspase-9 GFPspark in HEK-293 cells. Caspase-9 GFPspark (1 μ g) transfected HEK-293 cells were treated with STS (1 μ M) for 4 h and labeled by the Rh-VAD-FMK probe (1 μ M) for 2 h. Cells were washed, fixed, and the fluorescence signal was collected in (a) GFP, FRET, and Rh channels. Acceptor photobleaching was done to confirm the FRET signal, as described previously. Bar graph representing a rise in GFP intensity in ROI after rhodamine photobleaching. FRET efficiency was calculated to be $35 \pm 2\%$. (b) The fluorescence signal was collected in GFP, FRET, and Rh channels in the (i) absence or (ii) presence of inhibitor Z-VAD-FMK (50 μ M).

3.2.2.3 Specific activation of caspase-8 activation in the apoptosis pathway

Likewise, we then measured the specific caspase-8 activation using the AbRGT approach. Procaspase-8 is an initiator caspase, primarily localized to the mitochondria as an inactive 55 kDa zymogen and released into the cytoplasm upon apoptosis stimulus.¹⁸ Procaspase-8 is composed of two domains, a prodomain followed by a catalytic domain. Prodomain is constituted of two tandem death effector domains (DEDs), whereas, catalytic domain comprises of a large p18 and a small p12 subunit. Procaspase-8 processing occurs in two steps. Step 1 involves the proteolytic cleavage between p18 and p12 subunits. Whereas step 2 involves the proteolytic cleavage at D216, and D384, generating two active subunits p18

and p10, and also prodomain. The p18 and p12 subunits assemble to form a heterotetramer (p18₂-p10₂), active caspase-8 (Figure 3.11).¹⁹

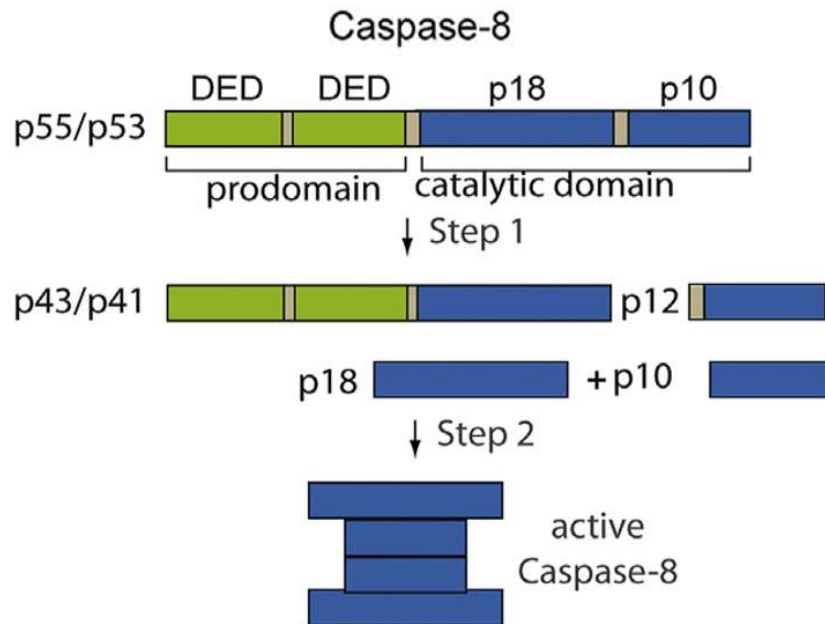


Figure 3.11 Schematic representation of procaspase-8 processing to active caspase-8. The initiator caspase, procaspase-8 p55/p53, comprises of a prodomain followed by a catalytic subunit. The prodomain consists of two tandem death effector domains (DEDs), and the catalytic subunit consists of a large p18 and a small p10 subunit. The processing of procaspase-8 involves the autocatalytic cleavage of procaspase-8 and is a sequential two-step-process. In step 1, the first cleavage occurs at residue D374 generating two subunits, p43/p41 and p12. Step 2 involves cleavage of D216, and D384, resulting in two active subunits, p18 and p10, and the prodomain p26/p24. The processed caspase-8 forms a heterotetramer (p18₂-p10₂), active caspase-8. Adapted with permission from reference (20). Copyright © 2013 Federation of European Biochemical Societies.

Further, the same method is used for specific detection of active caspase-8 in HEK-293 cells, which were subjected to apoptosis through the extrinsic mechanism. Caspase-8 GFPspark transfected HEK-293 cells were treated with TRAIL (1 µg/mL) for 6 h and labeled by the Rh-VAD-FMK probe. TRAIL is a well-known agent proven to induce apoptosis through the extrinsic mechanism. The diffused fluorescence signal was found in all three channels [Figure 3.4c (i)], and the presence of active caspase-8 GFPspark is shown by the fluorescence signal in the FRET channel. The calculated FRET efficiency in the FRET channel is 31 ± 1% (Figure 3.12). The signal in the FRET and Rh channels was lost upon pretreatment with the Z-VAD-FMK inhibitor [Figure 3.4c (ii)]. The CTCF of each

image in GFP, FRET, and Rh channels in Figure 3.4 is calculated using ImageJ software (Figure 3.5).

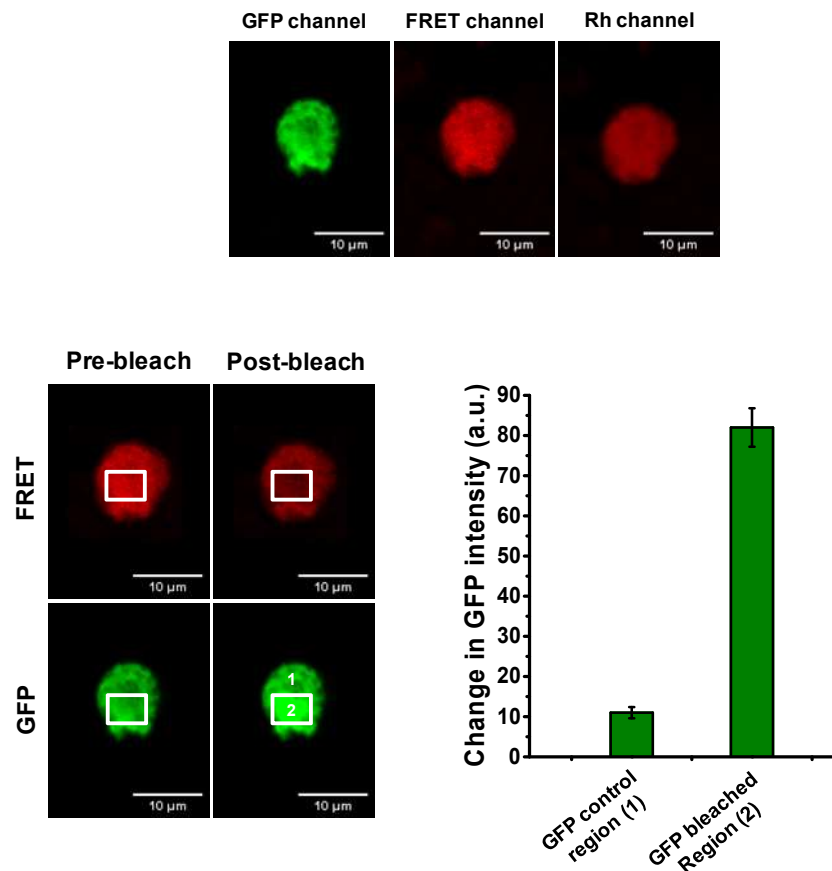


Figure 3.12 Specific detection of caspase-8 GFPspark in HEK-293 cells. Caspase-8 GFPspark (1 μ g) transfected HEK-293 cells were treated with TRAIL (1 mg/ml) for 6 h and labeled with the Rh-VAD-FMK probe (1 μ M) for 2 h. Cells were washed, fixed, and the fluorescence signal was collected in GFP, FRET, and Rh channels. Acceptor photobleaching was done to confirm the FRET signal, as described previously. Bar graph representing a rise in GFP intensity in ROI after rhodamine photobleaching. FRET efficiency was calculated to be $31 \pm 1\%$.

3.2.3 Direct imaging of cathepsin-B activation in the apoptosis pathway using AbRGT

Another application of AbRGT is its capability of imaging the “active-state” of a protease in a signaling pathway in a native cellular environment. To demonstrate that, we validated the active-state of cathepsin-B proteases in the apoptosis signaling pathway. Cathepsin-B is

a lysosomal cysteine peptidase that cleaves off the internal peptide bonds. Human cathepsin-B is synthesized as 37 kDa inactive zymogen, preprocathepsin-B at the rough endoplasmic reticulum (RER). Preprocathepsin-B undergoes proteolytic cleavage, removing signal peptide (SP, residue 1-17) to generate procathepsin. The resultant procathepsin-B is subsequently translocated to the lysosomes via the Golgi apparatus. The procathepsin-B is further auto-processed to remove propeptide (Pro, residue 18-79), resulting in the formation of 27 kDa active mature cathepsin B (residue 80-333). Cathepsin-B is subsequently cleaved internally to generate a light and heavy chain linked by a disulfide bond (Figure 3.13).²¹

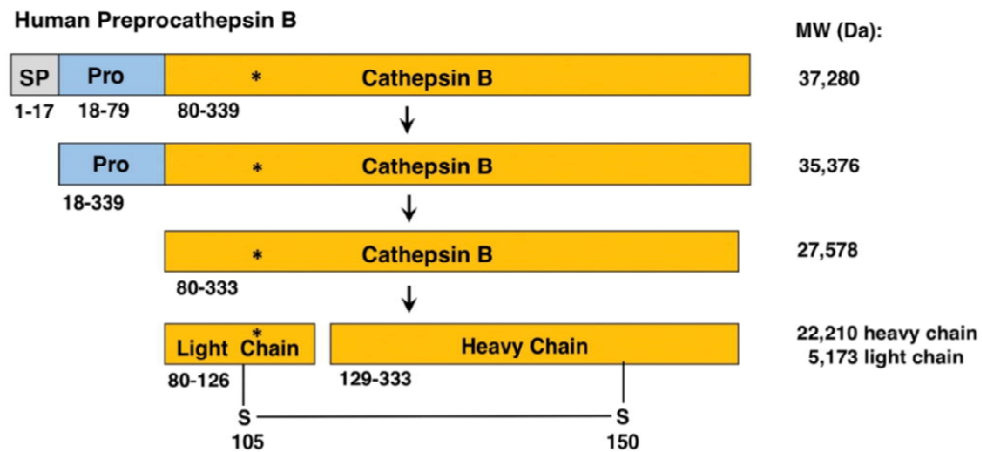


Figure 3.13 Preprocathepsin B zymogen processing to active cathepsin B. Preprocathepsin B, a 37 kDa protease, is synthesized at the rough endoplasmic reticulum (RER). The N-terminal signal sequence (SP, 17 residues) is cleaved off at the RER by signal peptidase to generate 35 kDa procathepsin-B (residues 18-333). The resultant procathepsin-B is subsequently translocated through the Golgi apparatus to lysosomes. The procathepsin B undergoes autoprocessing to cleave off the propeptide (Pro), resulting in the formation of the 27 kDa active, mature cathepsin-B (residues 80-333). Cathepsin B is further processed to form light and heavy chains linked by a disulfide bond. The asterisk (*) represents the active site Cys108. The sequences source of these forms of cathepsin-B were NCBI (196) and UniProt (197) protein sequence databases. Note: The residue 80 of preprocathepsin B may be referred to as residue 1 of the N-terminal of mature cathepsin-B with an active site Cys29. Adapted with permission from reference²¹. Copyright © 2020 Elsevier.

Evidence from the literature suggests that cathepsin-B plays a significant role in the caspase-dependent apoptosis pathway.²² Muir and co-workers have used activity-based probe profiling to show the release of cathepsin B from lysosomes to the cytosol, thus

showing the participation in the caspase-dependent cell death pathway (Figure 3.14). The role of cathepsin-B in the apoptotic pathway has been studied using invasive techniques such as in-gel fluorescence and immunoblotting;²³ however, these methods do not provide an opportunity to study the spatiotemporal activation of cathepsin-B in real-time in the apoptotic pathway.

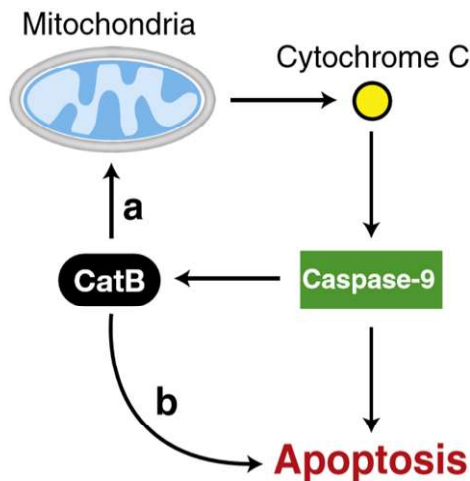


Figure 3.14 Schematic representation of the intrinsic apoptotic pathway involving cathepsin-B as a positive regulator. Two non-mutually exclusive mechanisms, represented as a and b, of the cathepsin B involvement in the apoptosis pathway, are proposed. The active caspase-9 results in the release of cathepsin-B from the lysosome to the cytosol. In pathway a, cytosolic cathepsin-B causes the release of more cytochrome c from the mitochondria that further activates additional caspase-9 by a positive feedback loop. The cathepsin-B can also be directly involved in apoptosis (pathway b) by proteolyzing proteins containing canonical caspase cleavage sites. Adapted with permission from reference (23). Copyright © 1998, Cell Press.

3.2.3.1 Validation of cathepsin B localization in the lysosome

Using our method, we attempted to image the direct activation of cathepsin-B. To do that, cathepsin-B GFPspark transfected HEK-293 cells were stained with acidotropic lysosomal marker LysoTracker (50 nM) to validate its localization in the lysosome.²⁴ The apoptosis was induced via an intrinsic mechanism using STS. Untreated control cells were found to be co-localized with LysoTracker while no co-localization was observed in STS-treated cells, and instead, a diffused fluorescence pattern was seen (Figure 3.15). This is because apoptosis induction leads to the translocation of cathepsin B from lysosomes to the cytoplasm, followed by cleavage of protein targets by cathepsin-B.^{25,26}

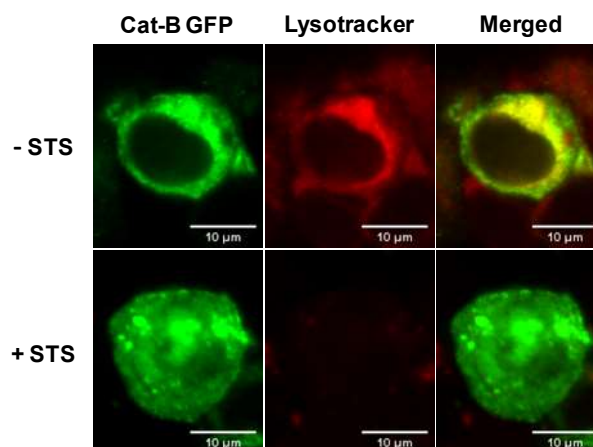


Figure 3.15 Co-localization of cathepsin-B GFP and LysoTracker. Cathepsin-B GFPspark (1 µg) plasmid transfected in HEK-293 cells and then labeled with LysoTracker (50 nM) for 1 h and treated with STS (1 µM) for 1 h. The cells were fixed with 4% PFA, washed, and images under GFP and red channels. GFP signal was found to be co-localized with the red fluorescence signal in the absence of STS, and no co-localization was seen in the presence of STS.

3.2.3.2 Cathepsin B activation in the apoptosis pathway

To directly image the cathepsin B activation in the apoptosis pathway, cathepsin B GFP expressing HEK-293 cells were treated with STS (1 µM) for 4 h and then labeled by the Rh-VAD-FMK probe (1 µM) for 2 h. The bright diffused fluorescence signal was obtained in the FRET channel manifests the presence of active cathepsin B [Figure 3.16a (i)]. The fluorescence signal was entirely abolished in the FRET channel when cells were pre-treated with the Z-VAD-FMK or E-64 inhibitor, an epoxide-based cysteine peptidase inhibitor^{27,28} (50 µM), independently [Figure 3.16a (ii)]. The less intense fluorescence signal was retained in the Rh channel in the case of the Z-VAD-FMK inhibitor. However, in E-64 inhibitor pre-treated cells, sharp, intense punctate labeling was observed in the Rh channel [Figure 3.16a (iii)], indicating the cross-labeling of other active cysteine proteases by the Rh-VAD-FMK probe. The fluorescence signal was absent in the cells that were neither pre-

treated with an inhibitor nor labeled by the Rh-VAD-FMK probe [Figure 3.16a (iv)]. These results manifest that the substrate scope of the E64 inhibitor is different compared to the Z-VAD-FMK inhibitor because the E-64 inhibitor is more selective as compared to the Z-VAD-FMK inhibitor. The calculated FRET efficiency of the fluorescence signal obtained in the FRET channel is $37 \pm 1\%$ for (n = 10) cells (Figure 3.16b). The CTCF of each image in GFP, FRET, and Rh channels in Figure 3.16a is calculated using ImageJ software (Figure 3.17).

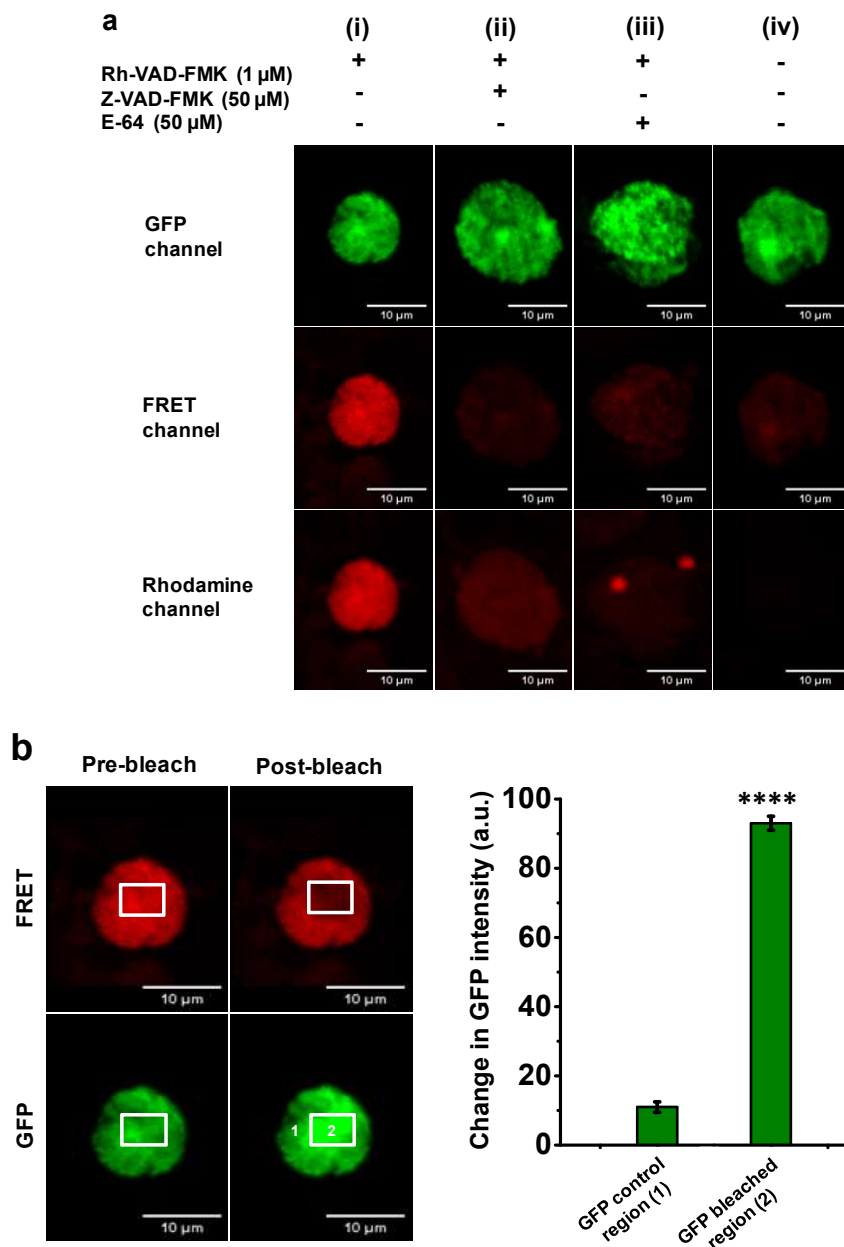


Figure 3.16 Confocal microscopy images of HEK-293 cells in GFP, FRET, and Rh channels. Cathepsin B GFPspark transfected HEK-293 cells were treated with STS (1 μ M) for 4 h and labeled (a) (i) with or (a) (iv) without the Rh-VAD-FMK probe. Cells were pre-treated with (a) (ii) the Z-VAD-FMK inhibitor (50 μ M) or (a) (iii) the E-64 inhibitor (50 μ M) 1 h before the Rh-VAD-FMK probe labeling. (b) Quantification of the change in GFP fluorescence intensity after rhodamine photobleaching in both the GFP control region (1) and the GFP bleached region (2) (ROI), the area

under the white square using the acceptor photobleaching method. Error bar represents the SEM for $n = 10$ cells ($*P < 0.00001$). Scale bar, $10 \mu\text{m}$, au, arbitrary units.

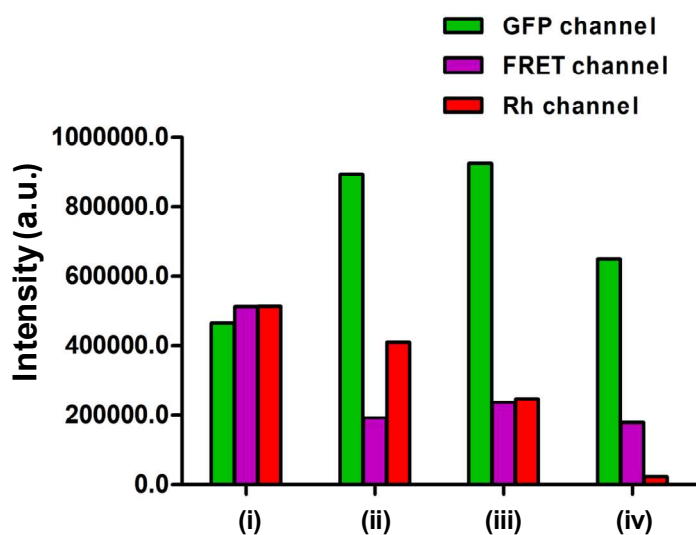


Figure 3.17 CTCF is calculated in GFP, FRET, and Rh channels for each image in (Figure 3.16a) using Image J software.

We showed applications of AbRGT in (i) inhibitors screening of proteases, (ii) imaging the function of any PoI, (iii) validating the activation of a protease in a signaling pathway. The method offers several advantages over the existing methods. For instance, ABFP method provides an opportunity to backtrack the signal produced by the target enzyme, however, this is achieved by postprocessing of cell or tissue lysate after the imaging experiment.^{50,51} This invasive technique has several disadvantages such as (i) the spatial and temporal information (fluorescence signal) is lost when the cells are subjected to an invasive procedure such as homogenization of cells, (ii) in-gel fluorescence studies impose significant limits on the amount of sample needed, (iii) backtracking of the signal produced by low protein abundance may not be possible, (iv) this method is highly laborious and cannot be translated to high-throughput studies, (v) extensive probe engineering is required which results in complicated chemical synthesis, and (vi) requirement of very expensive mass-spectrometry facilities. In contrast, our method has the following favorable features: it (i) is simple and straightforward, (ii) provides unprecedented specificity, (iii) does not involve postprocessing of cell or tissue lysates, (iv) enables direct visualization of localized protease activity at the subcellular scale, (v) provides single-cell resolution, and (vi) can be used for inhibitor profiling. However, our method does have some limitations like any other methods; unlike substratebased reporter assay and ABFP methods, our technology cannot be applied to image the function of endogenous proteases without tagging it to a reporter protein. Also, overexpression of certain proteases is lethal in certain cell lines. For new protease targets, cloning of target gene tagged to a reporter protein is required. It also lacks signal amplification.

3.3 Conclusion

In conclusion, we have demonstrated different applications of AbRGT. The method is utilized in screening inhibitors for caspase-3 protease. We validated our approach by using known pan-caspase inhibitors Z-VAD-FMK^{7,8} and Q-VD-Oph⁹. The loss in the FRET signal was observed in the cells pre-treated with inhibitors showing the method is successful in inhibitor screening assays.

To show that the tool can be applied to image the function of any protease, we visualized the “active-state” of other caspases (caspase-7, -8, and -9) in the apoptosis signaling

pathway in MCF-7, HeLa, HEK-293 cells. We have also demonstrated that this technique can be used to image the function of the protease in various signaling pathways. We have studied the function of cathepsin-B in the apoptosis signaling pathway that has previously been done using invasive techniques such as in-gel fluorescence and immunoblotting.²³

Looking forward, this method has enormous potential in a variety of applications; considering protease upregulation and downregulation are implicated in various diseases, one could envisage using this technique to image the function of the uncharacterized protease in various signaling pathways.

3.4 Material and Methods

3.4.1 Reagents

The Q-VD-OPh inhibitor (SML0063), the E-64 inhibitor (E3132), and were purchased from Sigma. The Z-VAD-FMK inhibitor (G7231) was obtained from Promega.

3.4.2 Inhibitor Assay

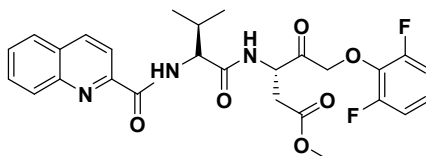
Cells were pre-treated with 50 μ M of Z-VAD-FMK or Q-VD-OPh or E-64 inhibitors 1 h before the Rh-VAD-FMK probe or the Rh-DEVD-FMK probe labeling and incubated for 1 h at 37 °C in a humidified atmosphere of 5% CO₂. Cells were gently scraped off from the surface at the end of inhibitor treatment and centrifuged at 3000 rpm for 5 min. Cells were then labeled with the Rh-VAD-FMK probe or the Rh-DEVD-FMK probe, as described in the previous section.

3.4.3 Plasmid information

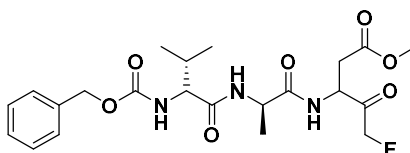
S.No.	Plasmid name	Plasmid backbone	Source	Addgene vector db No	Insert source/name	Gene bank acc No
1.	pCMV3-CASP-7-GFPspark	pCMV3-C-GFPspark	SinoBiological	Not applicable	<i>H. sapiens</i> (human)	NM_001227.3
2.	pCMV3-CASP-9-GFPspark	pCMV3-C-GFPspark	SinoBiological	Not applicable	<i>H. sapiens</i> (human)	NM_001229.2
3.	pCMV3-CASP-8-GFPspark	pCMV3-C-GFPspark	SinoBiological	Not applicable	<i>H. sapiens</i> (human)	NM_033355.3
4.	pCMV3-CTSB-GFPspark	pCMV3-C-GFPspark	SinoBiological	Not applicable	<i>H. sapiens</i> (human)	NM_001908.3

3.4.4 Caspase inhibitors structures

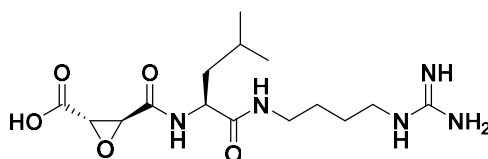
Inhibitor 1: Q-VD-OPh



Inhibitor 2: Z-VAD-FMK



Inhibitor 3: E-64



3.5 References

- 1 Bullok, K. E. *et al.* Biochemical and in vivo characterization of a small, membrane-permeant, caspase-activatable far-red fluorescent peptide for imaging apoptosis. *Biochemistry*, **46**, 4055-4065 (2007).
- 2 To, T. L. *et al.* Rationally designed fluorogenic protease reporter visualizes spatiotemporal dynamics of apoptosis in vivo. *Proc. Natl. Acad. Sci. U.S.A.*, **112**, 3338-3343 (2015).
- 3 Poreba, M.,. Selective imaging of cathepsin L in breast cancer by fluorescent activity-based probes. *Chemical science*, *9*(8), 2113-2129 (2018).
- 1 Himi, T., Ishizaki, Y. & Murota, S. i. A caspase inhibitor blocks ischaemia-induced delayed neuronal death in the gerbil. *Eur. J. Neurosci.* **10**, 777-781 (1998).
- 2 Li, H. *et al.* Caspase inhibitors reduce neuronal injury after focal but not global cerebral ischemia in rats. *Stroke* **31**, 176-180 (2000).
- 3 Deshmukh, M. Caspases in ischaemic brain injury and neurodegenerative disease. *Apoptosis* **3**, 387-394 (1998).
- 4 Toulmond, S. *et al.* Neuroprotective effects of M826, a reversible caspase-3 inhibitor, in the rat malonate model of Huntington's disease. *Br. J. Pharmacol.* **141**, 689-697 (2004).
- 5 Hartmann, A. *et al.* Caspase-3: a vulnerability factor and final effector in apoptotic death of dopaminergic neurons in Parkinson's disease. *Proc. Natl. Acad. Sci. U.S.A.* **97**, 2875-2880 (2000).
- 6 Louneva, N. *et al.* Caspase-3 is enriched in postsynaptic densities and increased in Alzheimer's disease. *Am. J. Pathol.* **173**, 1488-1495 (2008).
- 7 Zhu, H., Fearnhead, H. O. & Cohen, G. M. An ICE-like protease is a common mediator of apoptosis induced by diverse stimuli in human monocytic THP. 1 cells. *FEBS Lett.* **374**, 303-308 (1995).
- 8 Slee, E. A. *et al.* Benzyloxycarbonyl-Val-Ala-Asp (OMe) fluoromethylketone (Z-VAD. FMK) inhibits apoptosis by blocking the processing of CPP32. *Biochem. J.* **315**, 21-24 (1996).
- 9 Caserta, T. M., Smith, A., Gultice, A. D., Reedy, M. & Brown, T. L. Q-VD-OPh, a broad spectrum caspase inhibitor with potent antiapoptotic properties. *Apoptosis* **8**, 345-352 (2003).
- 10 Zhivotovsky, B., Samali, A., Gahm, A. & Orrenius, S. Caspases: their intracellular localization and translocation during apoptosis. *Cell Death Differ.* **6**, 644-651 (1999).
- 11 Lamkanfi, M. & Kanneganti, T.-D. Caspase-7: a protease involved in apoptosis and inflammation. *Int. J. Biochem. Cell Biol.* **42**, 21-24 (2010).
- 12 Chai, J. *et al.* Crystal structure of a procaspase-7 zymogen: mechanisms of activation and substrate binding. *Cell* **107**, 399-407 (2001).

- 13 Krajewski, S. *et al.* Release of caspase-9 from mitochondria during neuronal apoptosis and cerebral ischemia. *Proc. Natl. Acad. Sci. U.S.A.* **96**, 5752-5757 (1999).
- 14 Ritter, P. M. *et al.* Nuclear localization of procaspase-9 and processing by a caspase-3-like activity in mammary epithelial cells. *Eur. J. Cell Biol.* **79**, 358-364 (2000).
- 15 Kuida, K. Caspase-9. *Int. J. Biochem. Cell Biol.* **32**, 121-124 (2000).
- 16 Stennicke, H. R. *et al.* Caspase-9 can be activated without proteolytic processing. *J. Biol. Chem.* **274**, 8359-8362 (1999).
- 17 Li, P. *et al.* Caspase-9: structure, mechanisms and clinical application. *Oncotarget* **8**, 23996 (2017).
- 18 Qin, Z.-H. *et al.* Pro-caspase-8 is predominantly localized in mitochondria and released into cytoplasm upon apoptotic stimulation. *J. Biol. Chem.* **276**, 8079-8086 (2001).
- 19 Blanchard, H. *et al.* The three-dimensional structure of caspase-8: an initiator enzyme in apoptosis. *Structure* **7**, 1125-1133 (1999).
- 20 Matthes, Y., Raab, M., Knecht, R., Becker, S. & Strebhardt, K. Sequential Cdk1 and Plk1 phosphorylation of caspase-8 triggers apoptotic cell death during mitosis. *Mol Oncol* **8**, 596-608 (2014).
- 21 Hook, V. *et al.* Cathepsin B in neurodegeneration of Alzheimer's disease, traumatic brain injury, and related brain disorders. *Biochim Biophys Acta Proteins Proteom*, 140428 (2020).
- 22 Turk, B. *et al.* Apoptotic pathways: involvement of lysosomal proteases. *Biol. Chem.* **383**, 1035-1044 (2002).
- 23 Pratt, M. R., Sekedat, M. D., Chiang, K. P. & Muir, T. W. Direct measurement of cathepsin B activity in the cytosol of apoptotic cells by an activity-based probe. *Chem. Biol.* **16**, 1001-1012 (2009).
- 24 Willemer, S., Bialek, R. & Adler, G. Localization of lysosomal and digestive enzymes in cytoplasmic vacuoles in caerulein-pancreatitis. *Histochemistry* **94**, 161-170 (1990).
- 25 Kirkegaard, T. & Jäättelä, M. Lysosomal involvement in cell death and cancer. *Biochim Biophys Acta Mol Cell Res* **1793**, 746-754 (2009).
- 26 Guicciardi, M. E. *et al.* Cathepsin B contributes to TNF- α -mediated hepatocyte apoptosis by promoting mitochondrial release of cytochrome c. *J. Clin. Investig.* **106**, 1127-1137 (2000).
- 27 Hanada, K. *et al.* Isolation and characterization of E-64, a new thiol protease inhibitor. *Agric. Biol. Chem.* **42**, 523-528 (1978).
- 28 Barrett, A. J. *et al.* L-trans-Epoxy succinyl-leucylamido (4-guanidino) butane (E-64) and its analogues as inhibitors of cysteine proteinases including cathepsins B, H and L. *Biochem. J.* **201**, 189-198 (1982).

29. Fonović, M. and Bogyo, M. Activity-based probes as a tool for functional proteomic analysis of proteases. *Expert Rev. Proteomics* **5**, 721– 730 (2008).
30. Fonovic, M. and Bogyo, M. Activity based probes for proteases: applications to biomarker discovery, molecular imaging and drug screening. *Curr. Pharm. Des.* **13**, 253– 261 (2007).

Chapter 4

Development of BRET-approach of Activity-based Reporter Gene Technology (AbRGT)

4.1 Introduction

Methods to detect protease activity broadly falls under two categories; substrate-based reporter assays and activity-based fluorescent probes.¹ These methods target a family of protease and therefore lack specificity towards a particular protease. Moellering and co-workers have reported a method called activity-dependent proximity ligation (ADPL) platform that can image a specific protease-of-interest (PoI) with high spatial resolution.² However, the method requires a specific antibody against the PoI. It is also challenging to translate the method to *in vivo* studies.

Parallely, we have also reported the development of a fluorescence resonance energy transfer (FRET) based method called “Activity-based reporter gene technology (AbRGT)” for the exquisite imaging of protease activity.³ The readout of AbRGT is based on the FRET effect. The FRET approach of AbRGT allows the microscopic level visualization of active protease in a cellular system with high spatial resolution. The major limitation of the FRET process is that it requires an external laser for the excitation of the donor that can sometimes cause an unwanted excitation of acceptor due to the overlapping excitation spectra of the donor and acceptor, resulting in autofluorescence. The background caused by autofluorescence can be easily subtracted in single-cell imaging experiments. However, in the cell population-based experiments, it contributes to the high background that reduces the sensitivity of the assay; therefore, the FRET-based AbRGT approach can not be translated to high-throughput studies.^{4,5} BRET method also has an added advantage over FRET method in capturing intermolecular interactions in living subject as such studies are difficult to perform using FRET method due to autofluorescence and signal attenuation⁶⁻⁸ Sam Gambhir and co-workers have demonstrated the utility of BRET reporters for imaging the rapamycin induced FKBP12 and FRB proteins interaction in living subjects.⁹

To expand the AbRGT for the high-throughput studies, we have developed the bioluminescence resonance energy transfer (BRET)-approach of AbRGT. BRET is a non-radiative form of energy transfer between a luciferase enzyme and a fluorophore molecule. The conversion of luciferin to oxyluciferin by luciferase releases photons, which is

transferred to the acceptor molecule, resulting in the excitation of the acceptor molecule. The acceptor molecule further emits the energy at a longer wavelength resulting in the BRET effect.^{10,11} BRET method has shown applications in detecting protein-protein interaction in a high throughput assay format.^{12,13} Recently, the BRET method is utilized to identify the binding characteristics of a drug with a cellular target in intact cells in target engagement assays.¹⁴⁻¹⁷ Here, we demonstrate that BRET-approach of AbRGT is capable of detecting specific protease activity and can be used for screening protease inhibitors in a high-throughput assay format.

4.2 Results

4.2.1 The concept of BRET-approach of AbRGT

The BRET-approach of AbRGT is schematically depicted in (Figure 4.1). Here, the protease-of interest (PoI) is cloned into a plasmid vector encoding for the luciferase gene generating a luciferase-tagged PoI recombinant plasmid (Figure 4.1a). Luciferase-tagged PoI plasmid is expressed in a suitable cell line (Figure 1b.). An appropriate stimulus is applied to the cells for the activation of PoI (Figure 4.1c). Cells were then incubated with an activity-based fluorescent probe (ABFP) for the labeling of PoI (Figure 4.1d). The choice of ABFP should be such that it allows a significant spectral overlapping between its excitation and the emission of luciferase. Subsequently, luciferase substrate luciferin is added to the cells. The luciferin will be converted to oxyluciferin by luciferase leading to the generation of photons. The photons will be transferred to the ABFP, causing the excitation of ABFP, resulting in the BRET effect (Figure 4.1e).

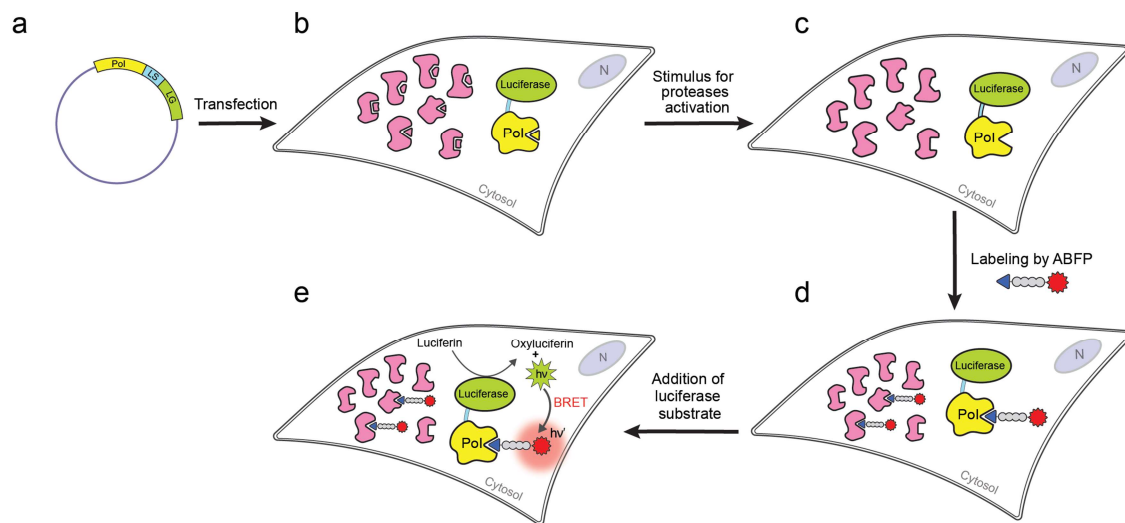


Figure 4.1 Schematic representation of the BRET approach of AbRGT. (a) Generation of a plasmid vector encoding for the luciferase tagged to the protease-of-interest (PoI); LS: linker sequence and LG: luciferase gene. Vector encoding the PoI tagged luciferase is expressed in a suitable cell line. (b) Cells expressing PoI tagged to luciferase enzyme along with the endogenous protease (pink) of the same or different families. Cells are subjected to an appropriate stimulus for the activation of PoI tagged to luciferase. (c) Cells expressing the active PoI tagged luciferase and other endogenous proteases. Cells are incubated with an activity-based fluorescent probe (ABFP) with appropriate warhead and fluorophore. (d) Labeling of the PoI tagged luciferase enzyme along with other endogenous proteases of the same family by an ABFP. (e) Labeling of PoI by an ABFP creates an instantaneous BRET pair that reports the activity of the PoI.

4.2.2 Choice of the BRET donor and acceptor

To develop the BRET approach of AbRGT, RLuc 8.6, and rhodamine was chosen as a BRET donor and acceptor, respectively. RLuc 8.6 is a 36 kDa enzyme that uses coelenterazine h as a substrate and emits at 535 nm wavelength.¹² The rhodamine dye is excited at a wavelength of 561 nm, and the emission occurs at 590 nm.

To determine the compatibility of RLuc 8.6 and rhodamine as a suitable BRET donor and acceptor, respectively, the spectral overlap between the two was analyzed. To obtain the RLuc 8.6 spectra, MCF-7 cells were transiently transfected with RLuc 8.6 plasmid. After 24 h of transfection, RLuc 8.6 substrate coelenterazine h was added to the cells. Immediately after substrate addition, the emission from RLuc is recorded from 500-700 nm.

The emission maxima for the RLuc 8.6 was observed at a bandpass filter 520-540 nm, consistent with the previous reports where the maxima are obtained at 535 nm.¹² Afterwards, the excitation and emission spectra of rhodamine were acquired. To do that, we diluted the Rh-VAD-FMK probe in 1X PBS (Rh-VAD-FMK probe: 1X PBS, 1: 500 uL) and excited from 500-700 nm. The excitation maxima are observed at 561 nm, similar to the reported values. The values of RLuc 8.6 and rhodamine spectrum were normalized and merged to evaluate the spectral overlapping between the RLuc 8.6 emission and the rhodamine excitation (Figure 4.2). The significant spectral overlapping (540-600 nm) between the RLuc 8.6 emission (green spectrum) and rhodamine excitation (blue spectrum) was observed that establishes RLuc 8.6 and rhodamine as suitable BRET pair. However, we could also observe the spectral overlapping (560-680 nm) between the RLuc 8.6 emission (green spectrum) and the rhodamine emission (red spectrum) that amounts to spectral bleed through. The bleed-through values are subtracted in BRET calculations to obtain a corrected BRET value.

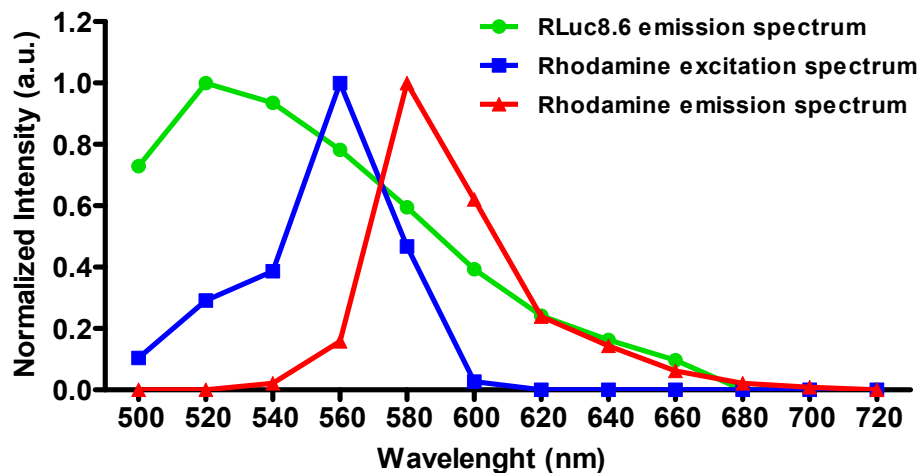


Figure 4.2 Schematic illustration of the spectral overlap between the normalized RLuc 8.6 emission spectra and the normalized excitation and emission spectra of the rhodamine dye. The RLuc 8.6 is excited by the addition of substrate, coelenterazine h, and the bioluminescence emission spectrum is recorded (green line). The rhodamine is excited with a 561 nm laser (blue line), and the emission spectra are recorded (red line). RLuc and rhodamine spectra are obtained separately using suitable filter combinations and merged to evaluate the spectral overlapping between the RLuc emission and rhodamine excitation and emission.

4.2.3 Development of BRET-approach of AbRGT

4.2.3.1 Cloning of caspase-3 into RLuc 8.6 vector

To develop the BRET-approach of AbRGT, we chose caspase-3 as our PoI, as we have already demonstrated the caspase-3 activation via the FRET-approach of AbRGT. The human caspase-3 gene was amplified by polymerase chain reaction (PCR) from pCMV3-C-OFPspark using suitable primers. The amplified caspase-3 gene was digested with restriction enzymes Hind III and Bgl II. The digested caspase-3 gene was cloned into the pCMV-GGS-RLuc 8.6 vector between the Hind III and Bgl II restriction sites using PCR dependent restriction enzyme based cloning method. The resultant caspase-3 RLuc 8.6 clone was confirmed by restriction digestion and DNA sequencing (Figure 4.3).

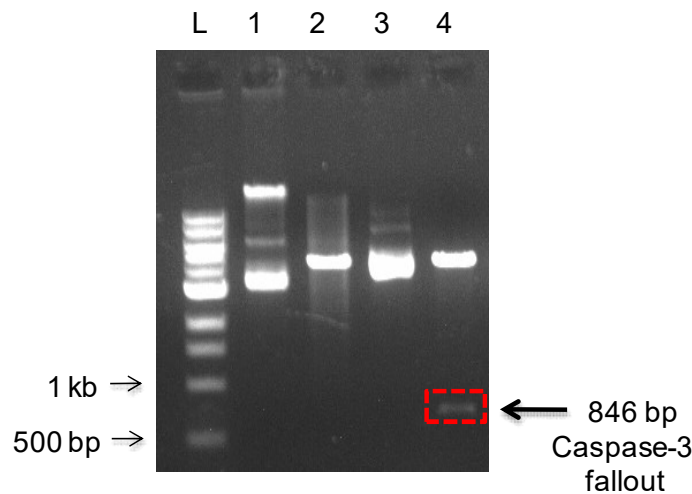


Figure 4.3 Recombinant pCMV-GGS-RLuc 8.6-caspase-3 plasmid was confirmed by restriction digestion analysis using Hind III and Bgl II Lane L, 1 kb DNA ladder; Lane 1, undigested pCMV-GGS-RLuc 8.6 plasmid; Lane 2, pCMV-GGS-RLuc 8.6 plasmid digested with Hind III and Bgl II; Lane 3, undigested recombinant plasmid pCMV-GGS-RLuc 8.6-caspase-3; Lane 4, recombinant pCMV-GGS-RLuc 8.6-caspase-3 plasmid digested with Hind III and Bgl II.

4.2.3.2 Expression of caspase-3 RLuc 8.6 vector in MCF-7 cells

The expression of the recombinant caspase-3 RLuc 8.6 plasmid vector was determined by examining the RLuc8.6 activity. For this, MCF-7 cells were transiently transfected with caspase-3 RLuc 8.6 or RLuc 8.6 plasmid. 24 h post-transfection, RLuc 8.6 substrate,

coelenterazine h was added to the caspase-3 RLuc 8.6, RLuc 8.6 transfected MCF-7 cells and the untransfected MCF-7 cells. Immediately after coelenterazine h addition, average radiance was recorded for each sample. The average radiance values is an indicative of RLuc 8.6 activity in the cells. The average radiance values for RLuc 8.6 transfected MCF-7 cells (3.8×10^6 photons/sec/cm²/sr) is higher as compared to the caspase-3 RLuc transfected cells (5.9×10^5 photons/sec/cm²/sr) as RLuc 8.6 activity is compromised in caspase-3 RLuc 8.6 fusion construct. However, the average radiance value of caspase-3 RLuc 8.6 transfected MCF-7 cells is significantly higher as compared to the untransfected cells (2.6×10^3 photons/sec/cm²/sr), confirming that the recombinant caspase-RLuc 8.6 plasmid is appropriately expressing in MCF-7 cells (Figure 4.4).

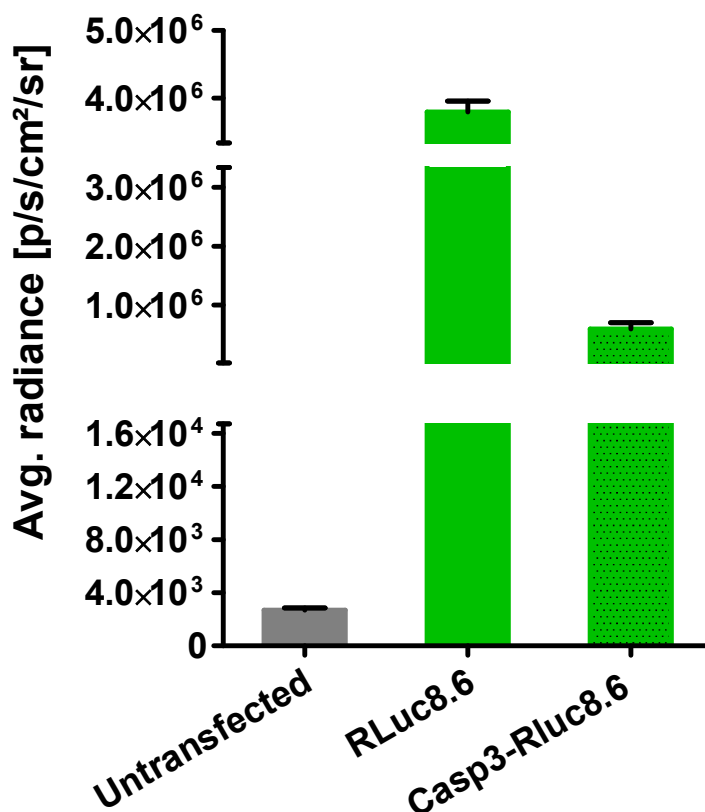


Figure 4.4 The expression of recombinant pCMV-GGS-RLuc 8.6-caspase-3 (Casp-3 RLuc 8.6) and pCMV-GGS-RLuc8.6 (RLuc8.6) was determined by examining the average radiance values. The bar graph representing the average radiance values [p/s/cm²/sr] for untransfected MCF-7 cells, RLuc 8.6 and the caspase-3 RLuc 8.6 transfected MCF-7 cells.

4.2.3.3 Quantification of caspase-3 activation using BRET-approach of AbRGT

To determine the specific caspase-3 activation, caspase-3 RLuc 8.6 plasmid was overexpressed in the MCF-7 cell line since it is caspase-3 null. The cells were subjected to treatment with STS (1 μ M) for 4 h for the induction of apoptosis. The STS triggers apoptosis via the intrinsic pathway and leads to the activation of caspases. Subsequently, cells were incubated with ABFP, Rh-VAD-FMK probe (BRET acceptor) for the labeling of PoI and other proteases of the same family. The RLuc 8.6 substrate coelenterazine h was added to the cells, and the average radiance was recorded in the donor emission channel, RLuc 8.6 (520-540 nm), and the acceptor emission channel, rhodamine (580-600 nm) channel. The BRET measurements were done by calculating the mBRET values for the STS treated versus untreated samples using the following equation.⁷ Here, acceptor and donor are represented by (A) and (D), respectively. The mBRET values represent the quantification of specific caspase-3 activation in MCF-7 cells.

$$\begin{aligned} \text{A/D channel emission ratio} &= \frac{\text{Acceptor channel emission}}{\text{Donor channel emission}} \\ \text{BRET ratio} &= \frac{\text{Acceptor channel emission (D + A)}}{\text{Donor channel emission (D + A)}} \\ &\quad - \frac{\text{Acceptor channel emission (D only)}}{\text{Donor channel emission (D only)}} \\ \text{mBRET unit} &= \text{BRET ratio} * 1000 \end{aligned}$$

The calculated mBRET value for the STS treated sample is 60 ± 0.4 , which is significantly higher as compared to the UT control, 11 ± 9.2 (Figure 4.5). The rise in mBRET values in the STS treated samples is an indicative of the specific caspase-3 activation in MCF-7 cells.

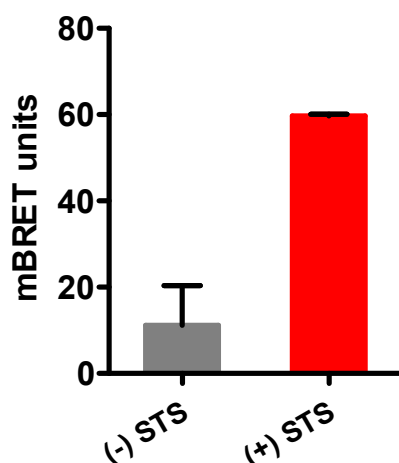


Figure 4.5 Caspase-3 RLuc 8.6 transfected MCF-7 cells were treated with or without STS (1 μ M) for 4 h. Subsequently, cells were incubated with the Rh-VAD-FMK probe for 1 h, followed by coelenterazine h addition. Immediately after coelenterazine h addition, average radiance was recorded, and the mBRET values for both the STS treated and untreated cells were calculated.

4.2.3.4 Screening protease inhibitors in a high-throughput assay using BRET-approach of AbRGT

Here, we show that the BRET approach of AbRGT can be used for the high-throughput screening of protease inhibitors. For our experiment, we chose four different inhibitors; Z-VAD-FMK,^{18,19} Q-VD-OPh,²⁰ E-64,^{21,22} and cpm-VAD-CHO. Here, Z-VAD-FMK, E-64, and Q-VD-OPh are irreversible inhibitors, while cpm-VAD-CHO is a reversible inhibitor. Here, cpm is the cell-permeable peptide with a peptide sequence (-Ala-Ala-Val-Ala-Leu-Leu-Pro-Ala-Val-Leu-Leu-Ala-Leu-Leu-Ala-Pro-). We chose Z-VAD-FMK, Q-VD-OPh, E-64 and cpm-VAD-CHO for our assay because these inhibitors target different range of substrate. The mechanism of action of these inhibitor is very different because of their warhead functionalities *i.e* FMK, OPh, epoxide and CHO and peptide recognition sequence VAD, VD, L and VAD. However, Z-VAD-FMK and cpm-VAD-CHO share the same peptide recognition sequence. Also, the Z-VAD-FMK, E-64, and Q-VD-OPh covalently modifies the active-site of caspase-3 and are irreversible inhibitors whereas, cpm-VAD-CHO is a reversible inhibitor. Therefore, these inhibitors serves as the interesting candidates to screen caspase-3 inhibitors in high-throughput assay using the BRET - approach of AbRGT.

To validate the applicability of the BRET approach of AbRGT in screening caspase-3 inhibitors in a high-throughput format, caspase-3 RLuc transfected MCF-7 cells in 96 well plates were treated with STS (1 μ M) for 4 h. Subsequently, after STS treatment, cells were incubated with Z-VAD-FMK or Q-VD-OPh E-64 or cpm-VAD-CHO at two different concentrations (25 or 50 μ M) for 1 h. Cells were then labeled with the Rh-VAD-FMK probe for 1 h, followed by the addition of coelenterazine h. Immediately after coelenterazine h addition, average radiance was recorded in the donor emission and the acceptor emission channel. The BRET measurements were done by calculating the mBRET values of each sample. The calculated mBRET value of the sample, in the absence of inhibitor, is 60 ± 0.4 . The mBRET values dropped in the presence of the inhibitor in the sample. The drop in the mBRET values is an indicative of the loss of caspase-3 activity as it gets effectively inhibited in the presence of inhibitor. The highest drop was observed for Q-VD-OPh inhibitor, followed by Z-VAD-FMK, caspase-inhibitor-II, and E-64 (Q-VD-OPh > Z-VAD-FMK > cpm-VAD-CHO > E-64) (Figure 4.6). This signifies that Q-VD-OPh and E-64 is the most and least potent inhibitor for caspase-3 respectively.

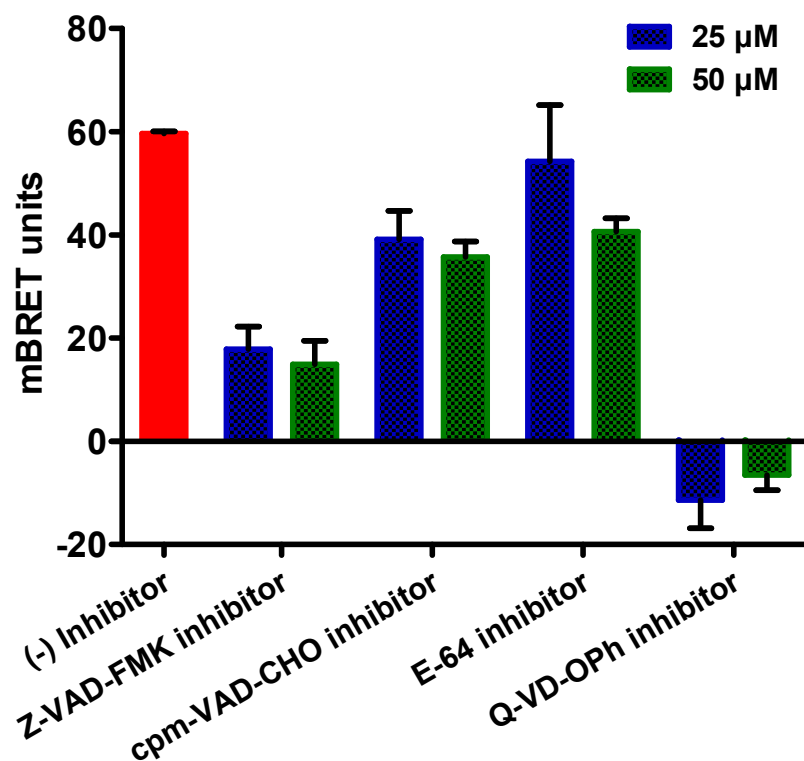


Figure 4.6 BRET approach of AbRGT for screening inhibitors in a 96 well plate. Caspase-3 RLuc 8.6 transfected MCF-7 cells treated with STS (1 μ M) for 4 h. Cells were subsequently treated with different inhibitors, Z-VAD-FMK, cpm-VAD-CHO, E-64, Q-VD-OPh at concentrations 25 or 50 μ M for 1 h. After inhibitor treatment, cells were incubated with the Rh-VAD-FMK probe for 1 h, followed by the substrate coelenterazine h addition. The average radiance was recorded in the acceptor and the donor channel, the mBRET values are calculated and represented as a bar graph.

However, we observed high error bars in the mBRET values for the samples which could be because of variable caspase-3 RLuc (donor) concentration in the cells due to transient transfection. In order to enhance the dynamic range of the system, we developed the stable clones of MCF-7 cells expressing caspase-3 RLuc protein.

4.2.3.5. Quantification of caspase-3 activation in Caspase-3 RLuc expressing stable MCF-7 clones

Luciferase activity in the MCF7 Caspase3-GGS-RLuc8.6 clone no. 2, 3, 4 was measured by the addition of luciferase substrate, coelentrazine. Immediately after substrate addition, average radiance value was recorded and plotted as a bar graph (Figure 4.7). The MCF7

Caspase3-GGS-RLuc8.6 clone no. 2 cells shows the highest luciferase activity ($\sim 1 \times 10^6$ photons/sec/cm²/sr) and is selected for further experiments.

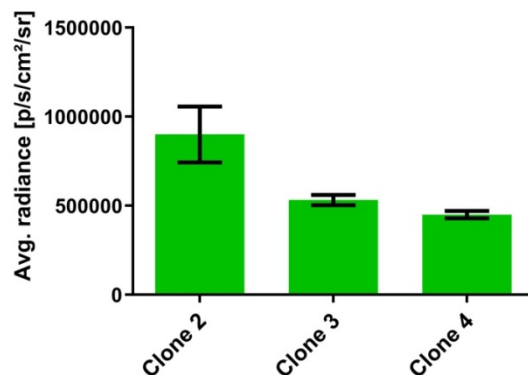


Figure 4.7 The average radiance for caspase-3 RLuc 8.6 stably transfected clone no. 2, 3, and 4 of MCF-7 cells was recorded in the donor channel and represented as a bar graph.

We further quantified the caspase-3 activity in the clone 2 cells by the BRET-approach of AbRGT. MCF-7 Caspase3-GGS-RLuc8.6 clone no. 2 cells were treated with increasing concentration (0, 50, 100, and 200 nM) of STS for 4 h. Subsequently, cells were incubated with Rh-VAD-FMK probe for 1 h followed by the addition of coelenterazine. Immediately after substrate addition, average radiance was recorded and the mBRET values were calculated and plotted as a bar graph (Figure 4.8).

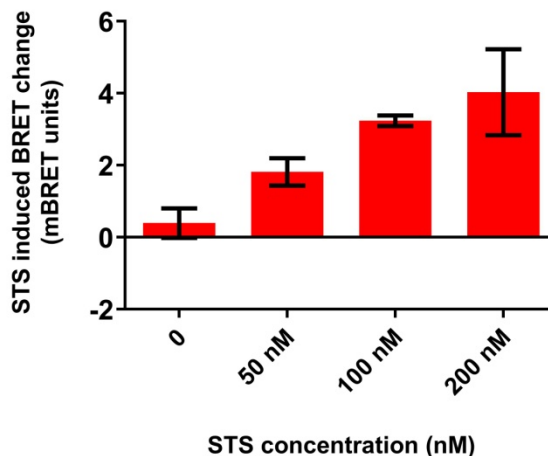


Figure 4.8 MCF7 Caspase3-GGS-RLuc8.6 clone no. 2 cells were treated with increasing concentrations of STS (0, 50, 100, and 200 nM) for 4 h. Subsequently, cells were incubated with the Rh-VAD-FMK probe for 1 h, followed by coelenterazine h addition. Immediately after coelenterazine h addition, average radiance was recorded, and the mBRET values were calculated and represented as a bar graph.

We found a linear dose-dependent increase in mBRET values upon STS treatment indicative of the concentration dependent activation of caspase-3. A ~4-fold increase in mBRET was found at 200 nM of STS concentration as compared to the untreated cells. Also, precise error bar in the mBRET values were obtained indicates that stably expressing caspase-3 MCF-7 cells is better than the transiently transfected caspase-3 MCF-7 cells to determine the specific caspase-3 activation via the BRET-approach of AbRGT. Further, these results show the potential of the BRET-approach of AbRGT for the quantification of protease activation and for the high-throughput screening of protease inhibitors in cells.

4.3 Conclusion

In conclusion we have shown the development of BRET approach of AbRGT by determining the specific caspase-3 activation in a population-based cell assay. The method utilizes a PoI tagged luciferase protein and an ABFP targeting PoI and other proteases. The BRET between the luciferase protein and fluorophore of ABFP gives an indirect readout of the caspase-3 activation. The BRET effect is expressed in the mBRET values which indicates the quantification of specific caspase-3 activation in the cells. We have shown the applicability of the method in screening caspase-3 inhibitors. For this purpose, we had

chosen, Z-VAD-FMK, Q-VD-OPh, E-64 and cpm-VAD-CHO as known caspase-3 inhibitors. We found that Z-VAD-FMK and E-64 are the most and least potent inhibitors of caspase-3 respectively. We also show that the stably expressing caspase-3 RLuc 8.6 MCF-7 is better than the transiently transfected caspase-3 RLuc 8.6 MCF-7 cells to perform to quantify the caspase-3 activation by the BRET-approach of AbRGT. Further, these results conclude the capability of the method to screen protease inhibitors in a high throughput assay.

4.4 Materials and methods

4.4.1 Reagents

Lipofectamine 2000 (11668-027), E-64 protease inhibitor (E3132), Q-VD-OPh hydrate (SML0063), cpm-VAD-CHO (218830), staurosporine (S5921) are procured from Sigma. Rh-VAD-FMK probe (ab65616) with Z- VAD-FMK inhibitor was obtained from Abcam.

4.4.2 Cloning

For caspase-3 RLuc 8.6 recombinant vector preparation, 846 bp of the human caspase-3 gene was PCR amplified from pCMV3-C-OFPspark plasmid using suitable primers. The amplified 846 bp caspase-3 PCR product was digested with Hind III and Bgl II restriction enzymes and cloned into pCMV-GGS-RLuc 8.6 vector between the restriction sites Hind III and Bgl II using a PCR based method for restriction cloning. The clones are confirmed by DNA sequencing.

4.4.3 Transient transfections

MCF-7 cells were seeded in a 35 mm dish and were transiently transfected with caspase-3 RLuc 8.6 recombinant plasmid at 70-80% cell confluency. 24 h post-transfection, the cells were trypsinized and distributed in a 96 well black plate with a clear bottom (20,000 cells/well). Cells were allowed to attach overnight by overnight incubation in a humidified atmosphere of 5% CO₂ at 37 °C before the start of experiments.

4.4.4 Luciferase assay

After 24 h of transfection, RLuc 8.6 substrate, coelenterazine h (50 μ L of the 1 mg/mL stock, dissolved in 1X PBS) was added to each well. Immediately after substrate addition, cells were analyzed for luciferase activity using IVIS spectrum with an open filter and an integration time of 60 secs, and the average radiance for each well was recorded.

4.4.4 Caspase-3 activity measurement

For the caspase-3 activity measurements, caspase-3 RLuc 8.6 transfected MCF-7 cells in a 96 well clear bottom plate were treated with STS (1 μ M) for 4 h. Cells were then incubated with the Rh-VAD-FMK probe for an additional 1 h. Subsequently, RLuc 8.6 substrate, coelenterazine h, was added to the cells, and the average radiance value for each well was taken immediately using an IVIS spectrum.

4.4.5 Inhibitors screening in a high-throughput format

For inhibitors screening, caspase-3 RLuc 8.6 transfected MCF-7 cells in 96 well plates with clear bottom were pretreated with different inhibitors. The treatment of the inhibitors was given for 1 h and 1 h before Rh-VAD-FMK probe incubation. Different concentrations of inhibitors (25 and 50 μ M) were tested. Subsequently, the caspase-3 labeling was performed by incubation of the cells with the Rh-VAD-FMK probe for 1 h. For BRET studies, coelenterazine h was added to the cells, and immediately after substrate addition, the average radiance was recorded.

4.4.6 Stable clone

The MCF7 cells were seeded in a 35 mm plate at 60-70% confluency and subsequently transfected with pCMV-Caspase3-GGS-RLuc8.6 plasmid by using Lipofectamine 2000 (Thermo Fisher) as per manufacturer's instructions. The transfected cells were incubated for 48 hrs for the expression of the transfected plasmid. Transfected cells were then grown in

RPMI under Zeocin (300 µg/ml), an antibiotic selection marker, to allow colony formation from single cells in a 10 cm plate. The plate was incubated till colonies were formed. Colonies formed from single cells were picked up and grown in 96-well plate. After cells attain confluency in a 96-well plate, they were transferred to a 24-well plate, and then clones were grown in bulk to check the expression of Caspase3-RLuc8.6 protein with respect to luciferase activity RLuc8.6. The clones with high luciferase activity were selected for further experiments.

4.4.7 BRET measurements

To perform the BRET measurements for each sample, ROIs were drawn for each well, and the values of average radiance (photons/sec/cm²/sr) were obtained. The average radiance values were acquired for the donor channel (donor emission channel, 520-540 nm, RLuc8.6), and the acceptor channel (acceptor emission channel, 580-600 nm, rhodamine). The acceptor/donor channel emission (A/D) ratio was calculated for the donor (D) only, and the donor + acceptor (D+A) sample. A/D channel emission ratio of the D only sample was subtracted from the D+A sample to obtain the BRET ratio.⁷ Subsequently, mBRET values were calculated by multiplying the values of the BRET ratio to 1000. The analysis was performed using Living Image software version 4.5 for the IVIS spectrum, and the calculations were done using MS excel; data is statistically analyzed and represented using Graph Prism software version 6.5.

$$\text{A/D channel emission ratio} = \frac{\text{Acceptor channel emission}}{\text{Donor channel emission}}$$

$$\text{BRET ratio} = \frac{\text{Acceptor channel emission (D + A)}}{\text{Donor channel emission (D + A)}} - \frac{\text{Acceptor channel emission (D only)}}{\text{Donor channel emission (D only)}}$$

$$\text{mBRET unit} = \text{BRET ratio} * 1000$$

4.4.8 Plasmids and primers information

S.No.	Plasmid name	Plasmid backbone	Source	Addgene vector db no.	Insert source/name	Gene bank acc No
1.	pCMV3-CASP-3-OFPspark	pCMV3-C-OFPspark	SinoBiological	Not applicable	<i>H. sapiens</i> (human)	<u>NM_004346.3</u>
2.	CL.17 pCMV-GGS-RLuc 8.6	pCMV-GGS-RLuc 8.6	Dr. Abhijit De's lab, ACTREC	Not applicable	-	-

S.No.	Primer name	DNA sequence
1.	Forward primer (FP) Casp-3 HindIII	5' gccAAGCTTgccaccATGGAGAACAACACTGAAAAC TC 3'
2.	Reverse primer (RP) Casp-3 BglII	5' gccAGATCTGTGATAAAAATAGAGTTCTTTGTG 3'

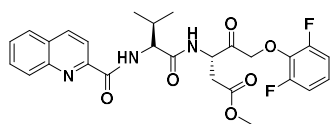
HindIII restriction site- A|AGCTT

BglII restriction site- A|GATCT

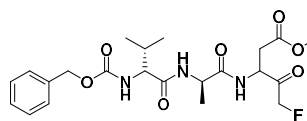
Kozak sequence- gccacc

4.4.9 Inhibitors structure

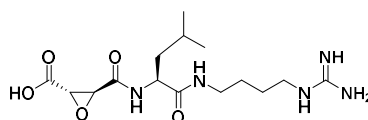
Q-VD-OPh



Z-VAD-FMK



E-64



4.5 References

1. Baruch, A., Jeffery, D. A. & Bogyo, M. Enzyme activity—it's all about image. *Trends Cell Biol.*, **14**, 29-35 (2004).
2. Li, G. *et al.* An activity-dependent proximity ligation platform for spatially resolved quantification of active enzymes in single cells. *Nat. Commun.*, **8**, 1-12 (2017).
3. Bathla, P. and Sandanaraj, B. S. Development of Activity-Based Reporter Gene Technology for Imaging of Protease Activity with an Exquisite Specificity in a Single Live Cell. *ACS Chem. Biol.*, **14**, 2276-2285 (2019).
4. Boute, N., Jockers, R. & Issad, T. The use of resonance energy transfer in high-throughput screening: BRET versus FRET. *Trends Pharmacol. Sci.*, **23**, 351-354 (2002).
5. Deriziotis, P., Graham, S. A., Estruch, S. B., & Fisher, S. E. Investigating protein-protein interactions in live cells using bioluminescence resonance energy transfer. *J. Vis. Exp.* **87**, (2014)
6. De, Abhijit, and Gambhir, S. S., Noninvasive imaging of protein-protein interactions from live cells and living subjects using bioluminescence resonance energy transfer. *FASEB J.* **19**, 2017-2019 (2005).
7. Dragulescu-Andrasi, A. *et al.* Bioluminescence resonance energy transfer (BRET) imaging of protein–protein interactions within deep tissues of living subjects. *Proc. Natl. Acad. Sci. U.S.A.* **108**, 12060-12065 (2011).
8. Xia, Z., and Rao, J., Biosensing and imaging based on bioluminescence resonance energy transfer. *Curr. Opin. Biotechnol.* **20**, 37-44 (2009).
9. De, A., Loening, A. M., and Gambhir, S. S., An improved bioluminescence resonance energy transfer strategy for imaging intracellular events in single cells and living subjects. *Cancer Res.* **67**, 7175-7183 (2007).
10. Xu, Y., Piston, D. W. & Johnson, C. H. A bioluminescence resonance energy transfer (BRET) system: application to interacting circadian clock proteins. *Proc. Natl. Acad. Sci. U.S.A.*, **96**, 151-156 (1999).
11. Pflieger, K. D. & Eidne, K. A. Illuminating insights into protein-protein interactions using bioluminescence resonance energy transfer (BRET). *Nature methods* **3**, 165-174 (2006).
12. De, A., Ray, P., Loening, A. M. & Gambhir, S. S. BRET3: a red-shifted bioluminescence resonance energy transfer (BRET)-based integrated platform for imaging protein-protein interactions from single live cells and living animals. *The FASEB J.*, **23**, 2702-2709 (2009).
13. Machleidt, T. *et al.* NanoBRET: A Novel BRET Platform for the Analysis of Protein–Protein Interactions. *ACS chem. biol.*, **10**, 1797-1804 (2015).
14. Robers, M., Dart, M., Woodroffe, C. *et al.* Target engagement and drug residence time can be observed in living cells with BRET. *Nat Commun* **6**, 1-10 (2015).

15. Schürmann M, Janning P, Ziegler S, Waldmann H. Small-Molecule Target Engagement in Cells. *Cell Chem. Biol.* **23**, 435-441 (2016).
16. Ong, L. L., *et al.* A high-throughput BRET cellular target engagement assay links biochemical to cellular activity for bruton's tyrosine kinase. *SLAS Discov.* **25** 176-185 (2020).
17. Robers M.B., *et al.* Quantitative, real-time measurements of intracellular target engagement using energy transfer. *Methods Mol. Biol.*, **1888** 45-71 (2019).
18. Zhu, H., Fearnhead, H. O. & Cohen, G. M. An ICE-like protease is a common mediator of apoptosis induced by diverse stimuli in human monocytic THP. 1 cells. *FEBS Lett.* **374**, 303-308 (1995).
19. Slee, E. A. *et al.* Benzyloxycarbonyl-Val-Ala-Asp (OMe) fluoromethylketone (Z-VAD. FMK) inhibits apoptosis by blocking the processing of CPP32. *Biochem. J.* **315**, 21-24 (1996).
20. Caserta, T. M., Smith, A., Gultice, A. D., Reedy, M. & Brown, T. L. Q-VD-OPh, a broad spectrum caspase inhibitor with potent antiapoptotic properties. *Apoptosis* **8**, 345-352 (2003).
21. Hanada, K. *et al.* Isolation and characterization of E-64, a new thiol protease inhibitor. *Agric. Biol. Chem.* **42**, 523-528 (1978).
22. Barrett, A. J. *et al.* L-trans-Epoxy succinyl-leucylamido (4-guanidino) butane (E-64) and its analogues as inhibitors of cysteine proteinases including cathepsins B, H and L. *Biochem. J.* **201**, 189-198 (1982).

Chapter 5

Conclusions and future directions

5.1 Summary of the thesis

To address the need for new imaging methods for studying protease function, several methods have been developed with mixed success. Fluorescence microscopy coupled with substrate-based reporter assays (both genetic and synthetic substrate) is being routinely used to monitor the function of “active proteases” in the (patho) physiological processes. However, most of the substrate-based reporters lack target specificity and the ABFP methods shows cross-reactivity towards other proteases. Achieving absolute specificity is a major challenge associate with these methods. To overcome some of the limitations associated with existing methods, we disclose the design and development of a new technology called “Activity-based Reporter Gene Technology” (AbRGT).

As discussed in chapter-2, we showed that AbRGT is a simple and powerful method for imaging of “active protease” in the live cell with an unprecedented specificity. The exquisite imaging of the target protease is achieved by taking advantage of both reporter gene technology and synthetic chemistry (ABFP) knowledge. By fusing a reporter tag (GFP, green fluorescent protein) to the protease of interest (PoI) followed by covalent labeling of PoI by an ABFP (acceptor) led to the in situ formation of FRET pair. The nonspecific labeling of the probe creates a highly specific FRET pair that reports only the activity of the target protease but not the other proteases in the cell.

As a proof-of-concept, we have applied this method to study the function of caspase-3 protease in both intrinsic and extrinsic apoptosis signaling pathways. To study the specific activation of caspase-3 in the apoptosis signaling pathway, caspase-3 is labeled by 1) GFPspark and 2) Rhodamine-linked small molecule that labels the active site of the cysteine protease (Rh-VAD-FMK probe). The FRET between the GFPspark and rhodamine dye of the Rh-VAD-FMK probe was measured as an indirect readout of the caspase-3 activation. By detecting specific caspase-3 activation in the apoptosis pathway, we demonstrated that AbRGT is a method that provides an opportunity to study the function of a protease of interest (PoI) with absolute specificity. We showed that the absolute specificity can not be achieved by simply changing the peptide recognition sequence to a more specific one. We also demonstrated that there is an enormous cell to cell variability on

the onset of programmed cell death, and this observation is consistent with the previous reports.¹

Furthermore, in chapter 3, we demonstrated different applications of AbRGT. As a potential application, we have shown that this method can be used as a tool to screen inhibitors of protease. We validated our approach by screening the known inhibitors of caspases (Z-VAD-FMK and Q-VD-OPh) and cathepsin B (E-64). We also demonstrated the applicability of the method in specifically imaging the function of any protease of interest (PoI). For our studies, we imaged the specific activation of five different target proteases (caspase-3, -7, -8, and -9 and cathepsin-B), independently in three different cell lines (HeLa, HEK-293, and MCF-7). In addition, we also show that the method can be applied to detect the protease activation in a signaling pathway. Using our approach, we imaged the direct cathepsin B activation in the apoptosis pathway as the function of cathepsin B has not been previously detected in the apoptosis pathway in a noninvasive way.

FRET-approach of AbRGT has certain limitations as the FRET process requires an external laser for the excitation of the donor molecule that can result in photobleaching. It also sometimes causes an unwanted excitation of the acceptor molecule due to the overlapping excitation spectra of the donor and acceptor molecules, causing autofluorescence. To overcome these limitations, we have developed a bioluminescence resonance energy transfer (BRET)-approach of AbRGT, which is discussed in Chapter 4. The BRET approach of AbRGT utilizes the tagging of luciferase to the protease of interest (PoI) followed by labeling of the cells with ABFP. The energy generated during the conversion of luciferin (luciferase substrate) to oxyluciferin will be transferred to the fluorophore of ABFP, resulting in the BRET effect. The BRET signal is an indirect readout of the protease activation. To develop the BRET approach, caspase-3 is tagged to Rluc 8.6 and expressed in MCF-7 cells. The cells were induced to undergo apoptosis for caspase-3 activation, followed by the labeling of cells with Rh-VAD-FMK probe. Subsequently, Rluc 8.6 substrate, coelenterazine h, is added to the cells. The conversion to coelenterazine by Rluc 8.6 generates energy that is transferred to the rhodamine of the Rh-VAD-FMK probe resulting in the BRET effect. The BRET values is an indirect readout of the caspase-3 activation. We have used the BRET-approach of AbRGT for the high-throughput screening of caspase-3 inhibitors (Z-VAD-FMK, cpm-VAD-CHO, Q-VD-OPh,

and E-64). The mBRET values determine the potency of the inhibitors. Based on the mBRET values, we found out the relative potency of the four inhibitors (Q-VD-Oph > Z-VAD-FMK > cpm-VAD-CHO > E-64), where Q-VD-Oph is the most potent and E-64 is the least potent inhibitor of caspase-3.

5.1.1 Advantages of AbRGT

1. The method is simple and straightforward and provides unprecedented specificity for studying the function of active proteases.
2. It does not involve post-processing of cell or tissue lysates as it enables direct visualization of localized protease activity at the sub-cellular scale.
3. The method can be used for inhibitor profiling and can be translated to high-throughput screening of protease inhibitors.
4. The probe required for imaging does not have to be highly selective for the target protease.
5. Most importantly, the approach can be applied to study the function of any protease-of-interest (PoI) in the biological system.

5.1.2 Limitations of AbRGT

1. The method can not be applied to image the function of endogenously expressed proteases and is limited to reporter protein tagged protease that are exogenously expressed in the cells.
2. It involves the overexpression of the reporter protein tagged PoI, and the overexpression of some proteases is known to be lethal in certain cell lines.
3. The method requires the tagging of a fluorescent protein to PoI without altering function.
4. Similar to the ABFP method, it also lacks signal amplification.

5.2 Future directions

5.2.1 *In vivo* imaging of protease function

The BRET-approach of AbRGT provides an avenue to use this method for *in vivo* imaging of small animals. The advantage of the BRET system in the *in vivo* studies is that it offers enhanced sensitivity as autofluorescence and photobleaching associated with fluorophore excitation are absent.^{2,3} To extend the AbRGT approach for the *in vivo* imaging of protease, the luciferase tagged PoI will be stably transfected in the cell line of interest. The stable cells will be injected into the mice. Subsequently, mice will be injected with the ABFP, followed by the luciferin administration. The signal in the BRET channel will be measured as an indirect readout of the specific activation of PoI *in vivo* conditions (Figure 5.1). Alternatively, the FRET-approach of AbRGT can also be used for *in vivo* imaging; it can be done by simply changing GFP to a red fluorescent protein (RFP) and rhodamine to near-infrared fluorescence (NIRF) dye. The longer wavelength of near-infrared fluorophores allows the deeper penetration of light into the tissues and hence minimize the effect of tissue autofluorescence.^{4,5}

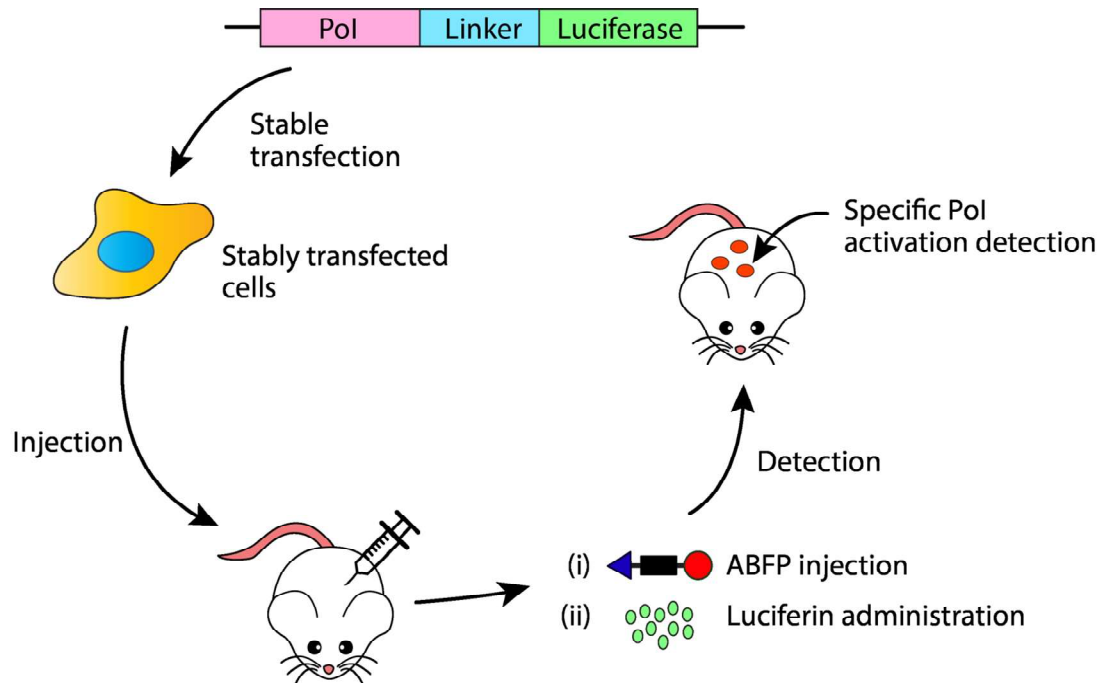


Figure 5.1 Schematic representation of the BRET-approach of AbRGT for in vivo imaging of specific protease activation. PoI (Pink) is tagged to the luciferase gene (green). The PoI tagged luciferase is stably expressed in the cell line of interest. The cells expressing PoI tagged luciferase is injected into the mice. The mice is administered with the ABFP for the labeling of PoI and other proteases of the same family. Subsequently, luciferin is injected into the mice resulting in the BRET effect. The BRET signal is an indirect readout of the specific PoI activation.

5.2.3 Imaging the function of the uncharacterized protease

Considering protease upregulation and downregulation are implicated in various diseases, one could envisage using this technique to image the function of the uncharacterized protease across multiple signaling pathways. For instance, the method can be applied to study the function of the high temperature requirement A2 (HtrA2)/Omi, a serine protease, in the apoptosis pathway. The zymogen form of HtrA2 is a 50 kDa protease localized in the mitochondria. The N-terminal of the HtrA2 zymogen is cleaved off after mitochondrial translocation as a part of the maturation process yielding a 36 kDa mature HtrA2 protease.⁶ HtrA2 is an interesting target to study as it induces apoptosis via both caspase-dependent and caspase-independent pathway. HtrA2 elicits caspase-dependent apoptosis by binding to the inhibitor of apoptotic proteins (IAPs).⁷ Whereas the serine protease activity of HtrA2 results in the induction of apoptosis via the caspase-independent pathway.⁸ However, the mechanism by which HtrA2 induces apoptosis is not fully explored. The function of HtrA2

protease in the apoptosis pathway can be studied using the FRET-approach of AbRGT. To do that, HtrA2 protease will be endogenously tagged to GFP and expressed in the cell line of interest. Subsequently, the cells will be given an appropriate stimulus for apoptotic induction followed by the incubation of cells by a serine protease targeting ABFP, *i.e.*, rhodamine-labeled fluorophosphate probe (Rh-FP, Figure 5.2). Here, the FRET between the GFP-tagged HtrA2 and the Rh-FP probe will be measured as an indirect readout of the HtrA2 activation

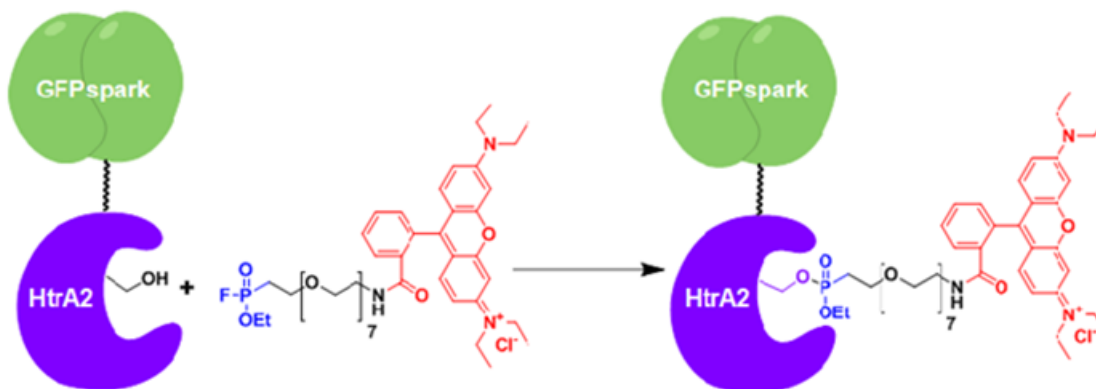


Figure 5.2 Schematic representation of the labeling of HtrA2 tagged GFPspark protein by rhodamine-labeled fluorophosphate probe (Rh-FP). The HtrA2 protease (blue) is tagged to the GFPspark protein (green), incorporating serine at the active site. The HtrA2 GFPspark is incubated with the FP probe. The FP warhead of the FP probe attacks the serine active site residue of the HtrA2 GFPspark protease resulting in the formation of the covalent bond and labeling of the HtrA2 protease FP probe.

5.3 References:

- 1 Albeck, J. G. *et al.* Quantitative analysis of pathways controlling extrinsic apoptosis in single cells. *Mol. Cell*, **30**, 11–25 (2008).
- 2 De A, Jasani A, Arora R, Gambhir SS. Evolution of BRET Biosensors from Live Cell to Tissue-Scale In vivo Imaging. *Front. Endocrinol.* **4**, 131 (2013).
- 3 Wu C. *et al.*, In vivo far-red luminescence imaging of a biomarker based on BRET from Cypridina bioluminescence to an organic dye. *Proc. Natl. Acad. Sci. U.S.A.* **106**, 15599-15603 (2009)
- 4 Hilderbrand SA, Weissleder R. Near-infrared fluorescence: application to in vivo molecular imaging. *Curr Opin. Chem. Biol.* **14**, 71-79 (2010).
- 5 Ntziachristos, V., Bremer, C. & Weissleder, R. Fluorescence imaging with near-infrared light: new technological advances that enable in vivo molecular imaging. *Eur. Radiol.* **13**, 195–208 (2003)
- 6 Suzuki Y, Imai Y, Nakayama H, Takahashi K, Takio K, Takahashi R. A serine protease, HtrA2, is released from the mitochondria interacts with XIAP, inducing cell death. *Mol Cell* **8**, 613–621 (2001).
- 7 Hegde R. *et al.* Identification of Omi/HtrA2 as a mitochondrial apoptotic serine protease that disrupts inhibitor of apoptosis protein-caspase interaction. *J. Biol. Chem.* **277**, 432-438 (2002).
- 8 Verhagen AM. *et al.* HtrA2 promotes cell death through its serine protease activity and its ability to antagonize inhibitor of apoptosis proteins. *J. Biol. Chem.* **277**, 445–454 (2002).

5.4 List of publications and patent

- **Bathla, P.**, and Sandanaraj, B. S. Development of Activity-Based Reporter Gene Technology for Imaging of Protease Activity with an Exquisite Specificity in a Single Live Cell. *ACS chemical biology* **14**, 2276-2285 (2019).
- Sandanaraj, B. S., **Bathla, P.**, Process for Determining enzyme activity in a cell by Activity-based Reporter gene technology (ABRGT). US Patent, 2019 Application number: 16/401906.
- Reddy, M.M., **Bathla, P.**, and Sandanaraj, B.S. A Universal Chemical Method for Rational Design of Protein-based Nanoreactors. *bioRxiv* (2021).